

**A BIOMECHANICS-BASED DELIVERY STRATEGY TO PRIMARY  
IMMUNE CELLS FOR GENERATING CELL THERAPY WITH  
MULTIPLE GENE KNOCKOUT**

A Dissertation  
Presented to  
The Academic Faculty

by

Tong Yu

In Partial Fulfillment of the  
Requirements for the Degree  
Doctor of Philosophy in  
Bioengineering

School of Biomedical Engineering  
Georgia Institute of Technology  
May 2024

**COPYRIGHT © 2024 BY TONG YU**

**A BIOMECHANICS-BASED DELIVERY STRATEGY TO PRIMARY  
IMMUNE CELLS FOR GENERATING CELL THERAPY WITH  
MULTIPLE GENE KNOCKOUT**

Approved by:

Dr. Todd Sulchek, Advisor  
School of Mechanical Engineering  
*Georgia Institute of Technology*

Dr. Sunil Raikar  
Department of Pediatrics  
*Emory University School of  
Medicine*

Dr. Gabe Kwong  
School of Biomedical Engineering  
*Georgia Institute of Technology*

Dr. James Dahlman  
School of Biomedical Engineering  
*Georgia Institute of Technology*

Dr. Wilbur Lam  
School of Biomedical Engineering  
*Georgia Institute of Technology*

Date Approved: [April 24<sup>th</sup>, 2024]

## ACKNOWLEDGMENTS

This thesis journey has been made possible by the exceptional support of an interdisciplinary network of mentors, colleagues, collaborators, and friends. Friends, family, and fur friends have also endowed me with the mental strength to complete this journey. I appreciate my parents' support, both financially and emotionally, and believe without their help, I wouldn't have had the chance to pursue this journey. I express my deepest appreciation to my husband and my daughter, who provide comfort to me whenever I feel overwhelmed.

First and foremost, I extend my deepest gratitude to my thesis advisor, Todd Sulchek, whose guidance over the past six years has been invaluable. Todd has the amazing ability to see through the technical data to find the bigger impact of my project. He taught me to be a problem-finder.

I am grateful for the support of my thesis committee members Dr. Sunil Raikar, Dr. Gabe Kwong, Dr. James Dahlman, and Dr. Wilbur Lam for their help and advice throughout the journey.

I owe a tremendous debt of gratitude to my labmates in the Sulchek lab for their camaraderie: Anna Liu, Peter Shankles, Katherine Young, Nicholas Stone, Alan Liu, Avi Gupta, Carolina Colon, Sam Chen and many others. Together, we learn to approach failures with humor, laughing at them, and thereby making them less intimidating.

Special thanks are due to the dedicated undergraduate researchers, Noah Kramer, Maya Sultan, Sanjay Rajeev, and Emilee Bencivenga, whose contributions and assistance were invaluable in conducting challenging experiments.

This thesis was enriched by amazing collaborators, without whom our research applications would not have been possible. I express my gratitude to Dr. Navi Jhita at Emory University, Dr. Joseph Fraietta and Dr. Bruce Levine at University of Pennsylvania, and Dr. Reginald Tran at Georgia Tech.

Special thanks to the Parker H. Petit Institute for Bioengineering and Bioscience Core facilities staff, including, Sommer Durham, Andrew Shaw, and Erich Williams, and for their invaluable assistance with flow cytometry and microscopy.

Finally, I extend my tremendous appreciation to the Center for Cell Manufacturing Technology (CMA<sup>T</sup>), who funded two projects in this thesis. And I am grateful to be a part of CMA<sup>T</sup> trainee family.

## TABLE OF CONTENTS

<b>ACKNOWLEDGMENTS.....</b>	<b>iii</b>
<b>LIST OF TABLES.....</b>	<b>viii</b>
<b>LIST OF FIGURES .....</b>	<b>ix</b>
<b>LIST OF SYMBOLS AND ABBREVIATIONS.....</b>	<b>xii</b>
<b>SUMMARY .....</b>	<b>xiii</b>
<b>CHAPTER 1. INTRODUCTION AND BACKGROUND .....</b>	<b>1</b>
1.1 Gene Editing in T Cell Therapy .....	1
1.1.1 Allogeneic T Cell Therapy.....	2
1.1.2 Overcoming T Cell Dysfunction.....	4
1.1.3 Expanding CAR T to T cell malignancies .....	6
1.1.4 Potential Adverse Effect .....	7
1.2 Current Delivery Platform .....	8
1.2.1 Biochemical Method.....	9
1.2.2 Electroporation.....	11
1.2.3 Mechanoporation .....	12
1.3 Key Values for Microfluidic Mechanoporation .....	13
1.3.1 Minimal Disruption of Physiology .....	13
1.3.2 Enable Sequential Processing .....	15
1.2.3 Non-stochastic Delivery.....	16
1.4 References .....	16
<b>CHAPTER 2. THESIS OVERVIEW .....</b>	<b>23</b>
2.1 Value Proposition for Cell Volume Exchange for Convective Transfection (VECT) device .....	23
2.2 Aim 1: Using Critical Design Features To Achieve Reproducible And Efficient Delivery.....	25

2.3 Aim 2: Capability to perform Sequential Gene Editing of CAR T Cells using multiplexed CRISPR/Cas9 Delivery.....	25
2.4 Aim 3: Contributions of Fluid and Cell Mechanics to Mechanoporation Delivery 26	
2.5 References.....	27
<b>CHAPTER 3. USING CRITICAL DESIGN FEATURES TO ACHIEVE REPRODUCIBLE AND EFFICIENT DELIVERY .....</b>	<b>28</b>
3.1 Introduction.....	28
3.2 Definition And Methodologies to Manipulate CDEs.....	29
3.2.1 Robust Prototyping Needed for Reproducible Results Under High Pressure.....	30
3.2.2 A microscopy-based method to quantify operating gap size .....	32
3.2.3 New Fabrication Method to Reduce Deformation.....	36
3.2.4 New Material for Rigid Device to Eliminate Deformation.....	41
3.2.5 Optimal Microfluidic Channel Design for Maximum Functional delivery .....	43
3.3 Summary .....	51
3.4 Method .....	53
3.4.1 PDMS-glass Composite Device Fabrication.....	53
3.4.2 Microchannel functionalization .....	54
3.4.3 Channel imaging and data analysis.....	54
3.4.4 Epoxy Device Fabrication.....	55
3.4.5 Transfection of Cells.....	55
3.4.6 Video Analysis for Cell Trajectory and Speed .....	56
3.4.7 Cell Culture.....	56
3.4.8 Statistical Analysis.....	57
3.5 References.....	57
<b>CHAPTER 4. CAPABILITY TO PERFORM SEQUENTIAL GENE EDITING OF CAR T CELLS USING MULTIPLEXED CRISPR/CAS9 DELIVERY .....</b>	<b>59</b>
4.1 Introduction.....	59
4.2 Cas9 Delivery Capability in CAR T cell manufacturing .....	60
4.2.1 Comparison with Electroporation .....	61
4.2.2 VECT is Compatible with Downstream CAR T Manufacturing Processes.....	67
4.2.3 VECT is applicable to patient derived T cells .....	69
4.3 Capability in Sequential Gene Editing.....	71
4.3.1 Process Development for Second Editing.....	72

4.3.2 Chromosome Repair requires 24hr in T cells .....	78
4.3.3 Sequential Editing Improves T cell cytotoxicity.....	83
4.4 Summary .....	87
4.5 Method .....	90
4.5.1 PDMS-glass Composite Device Fabrication.....	90
4.5.2 Epoxy Device Fabrication.....	90
4.5.3 Cell lines .....	90
4.5.5 Expansion of primary T cells .....	91
4.5.6 Primary patient samples .....	91
4.5.7 Microfluidic cell processing setup .....	92
4.5.8 Electroporation.....	93
4.5.9 Flow cytometry quantification of gene knockout .....	93
4.5.10 qPCR.....	94
4.5.11 Generation of CAR encoding lentiviral vector. ....	95
4.5.12 Lentiviral vector transduction of T cells. ....	96
4.5.13 Cytotoxicity assay .....	96
4.5.14 Statistical Analysis.....	97
4.6 References .....	97
<b>CHAPTER 5. CONTRIBUTIONS OF FLUID AND CELL MECHANICS TO MECHANOPORATION DELIVERY.....</b>	<b>100</b>
5.1 Introduction .....	100
5.2 Contributions of Fluid Mechanics and Biomechanics to Delivery .....	102
5.2.1 Strain rate and acceleration both contribute to high delivery.....	103
5.2.2 Cells appear stiffer and relax faster with a high strain rate.....	110
5.2.3 Stiffness is the major contributing factor to high delivery.....	114
5.3 Summary Fluid mechanics and cell mechanics .....	119
5.4 Method .....	122
5.4.1 PDMS-glass Composite Device Fabrication.....	122
5.4.2 Epoxy Device Fabrication.....	122
5.4.3 Video Analysis for Cell Trajectory and Speed .....	123
5.4.4 Atomic force microscopy.....	123
5.4.5 Microfluidic cell processing setup .....	124
5.5.6 Flow cytometry and FACS .....	125
5.5.7 Statistical Analysis.....	125

5.5 References .....	126
<b>CHAPTER 6. CONCLUSIONS AND OUTLOOK.....</b>	<b>127</b>
6.1 Summary of Major Findings .....	127
6.1.1 Aim 1: Using Critical Design Features To Reproducibly Achieve Efficient Delivery .....	127
6.1.2 Aim 2: Capability to perform Sequential Gene Editing of CAR T Cells using multiplexed CRISPR/Cas9 Delivery.....	129
6.1.3 Aim 3: Contributions of Fluid and Cell Mechanics to Mechanoporation Delivery....	132
6.2 Continuing and Future Work.....	133
6.2.1 Long-term cell persistence and repeated challenge assay in sequentially edited T cells .....	133
6.2.2 Gene editing homogeneity by VECT.....	134
6.2.3 Mechanistic study on cell death by VECT.....	135
6.2.4 Application in naïve/unstimulated T cell gene editing .....	135
6.2.5 Study of T cell mechanics at fast strain rate and acceleration regime .....	136
6.3 Conclusions.....	137
6.4 References .....	138

## LIST OF TABLES

Table 5.1 Multivariable regression function and statistics for delivery efficiency.	108
Table 5.2 Multivariable regression statistics for cell viability.	110

## LIST OF FIGURES

Figure 3.1: Cell size analysis shows significant difference in cell diameter between cell line and primary T cells.	32
Figure 3.2: Pressure-flow rate relation in PDMS devices indicating deformation.	33
Figure 3.3: Schematic illustration for the difference between negative and positive imaging method.	34
Figure 3.4: Schematic illustration of conjugation method to link FITC-BSA to PDMS and glass.	35
Figure 3.5: Positive contrast imaging method provides more quantitative channel measure with better accuracy.	36
Figure 3.6 PDMS-glass composite devices improved transfection if fabricated with spin coating method.	38
Figure 3.7 Glass-microchannel distance is a deterministic attribute of transfection success in PDMS-glass composite devices.	39
Figure 3.8 Epoxy device fabrication process through replica molding.	42
Figure 3.9 Epoxy replica molding gave devices without deformation and are able to transfect to unstimulated T cells.	43
Figure 3.10: VECT device design and optimization schematic	46
Figure 3.11: serpentine inlet focuses cells under ridges for compression and improves delivery efficiency.	48
Figure 3.12: optimization of ridge design.	49
Figure 3.13: gutter reduces compression rate but helps reduce shear damage on cells.	51
Figure 4.1: VECT is capable of delivering cas9 at similar efficiency as electroporation.	63

Figure 4.2: optimal cas9 RNP concentration results in comparable CD5 knockout as electroporation.	64
Figure 4.3: VECT edited T cells show similar memory phenotype and superior proliferation compared with electroporation.	67
Figure 4.4: VECT treatment resulted in higher transduction efficiency and CAR-T cell cytotoxicity in multiple donors.	69
Figure 4.5: VECT delivery resulted in surface knockdown of CD5 in B ALL-patient derived T cells.	72
Figure 4.6: Epoxy VECT devices without gutters achieved high delivery and viability in unstimulated/naïve T cells.	74
Figure 4.7: Epoxy VECT devices resulted in TCR knockdown but failed to produce proliferative T cells.	76
Figure 4.8: Processing cryopreserved naïve T cells increases cell apoptosis	77
Figure 4.9: Viability and delivery optimization for 24-hour sequential editing experiment.	78
Figure 4.10: Sequential editing by VECT resulted in similar double KO as batch with reduced or undetectable translocation.	82
Figure 4.11: Proliferation is preserved only in VECT-generated sequential edited groups.	83
Figure 4.12: Batch and sequentially edited T cells were turned into CD19CAR+ therapeutic cells effectively.	85
Figure 4.13: 6hr sequentially edited CAR T cells had superior cytotoxicity against difficult target cells.	88
Figure 5.1 High speed video analysis showed velocities at 3 locations relative to the ridge.	103
Figure 5.1 High speed video analysis showed velocities at 3 locations relative to the ridge.	104
Figure 5.3 Gutter feature reduces compression rate and reduces acceleration.	105

Figure 5.4 high strain rate and acceleration significantly contributed to delivery.	106
Figure 5.5 synergistic effect of high compression and high acceleration led to rapid improvement of delivery.	119
Figure 5.6 acceleration negatively contribute to viability.	110
Figure 5.7 Ericksen's number predicts delivery efficiency for primary T cells.	111
Figure 5.8 high strain rate promote cell stiffening and fast volume recovery.	112
Figure 5.9 Cell stiffness is identified in highly transfectable population.	115
Figure 5.10 Difference in stiffness separate T cells from healthy donors and AML patients by delivery efficacy.	117
Figure 5.11 T cell activation led to decreased cell stiffness and in turn decreased ability for T cells to be transfected.	118
Figure 5.12 Change in fluid mechanics and natural variation T cell mechanics cause differential Ericksen's number and Young's modulus, both are predictors of delivery by VECT.	120

## LIST OF SYMBOLS AND ABBREVIATIONS

CAR	Chimeric antigen receptor
TCR	T-cell receptor
CD19	Cluster of Differentiation 19
TRAC	T-cell receptor alpha constant
B2M	$\beta$ 2 microglobulin
HLA	Human leukocyte antigen
PD-1	Programmed Cell Death Protein 1
CD5	Cluster of differentiation 5
VECT	Volume exchange for convective transfer
CDE	Critical design element
<i>d</i>	Distance between glass and channel
AFM	Atomic force microscopy
KD	Kilodaltons
ND	No device control
PDMS	Polydimethylsiloxane
Er	Ericksen number
T <sub>c</sub>	Cell compression time
T <sub>v</sub>	Cell viscous time constant
E	Young's Modulus
Tau	Relaxation time constant
EP	Electroporation

## SUMMARY

Adaptive T cell therapy has emerged as a promising strategy in cancer treatment, utilizing synthetic receptor modified T cells to specially target tumor antigens. Despite successes, challenges persist, including the need for multiplexed gene editing in production of allogeneic T cell product, expanding application to T cell malignancies, and overcoming T cell dysfunction. These challenges require new technologies that lead to safer and efficient multiplexed gene editing techniques to lead to improved therapies. Currently, multiplexed gene editing is performed in one process step, raising concerns regarding chromosome translocations. This thesis addresses safer and more efficient multiplexed gene editing by leveraging the innovative microfluidic volume exchange for cell transfection (VECT) platform. To achieve efficient and reproducible delivery of gene editing cargo to primary T cells, we propose to understand device and intrinsic cellular attributes that significantly impact delivery outcome. Then, we design optimal devices for sequential gene editing of primary T cells in CAR (Chimeric Antigen Receptor) T engineering pipeline, focusing on the reduction of chromosomal translocation. We hypothesize sequential multiplexed gene editing results in lower chromosomal translocation and improved T cell persistence. This study addresses the goals through 3 aims. Aim 1 focuses on identifying critical design elements (CDEs) for VECT devices, revealing device design and operational factors influencing delivery to primary T cells. Aim 2 demonstrates VECT's capability in functional Cas9 delivery and sequential gene editing of CAR T cells. Aim 3 focuses on intrinsic cell mechanics to reveal cell biomechanics' contributions to delivery efficiency. In completing the study, we

created two easy fabrication methods to reproducibly generate high delivery to T cells, Then, we demonstrated an application of VECT to deliver CRISPR/Cas9 to mediate gene editing in T cells. VECT was shown to be capable of generating highly efficient and viable TCR and B2M knockout T cells in both batch and sequential workflow. Importantly, VECT sequential editing is shown to reduce the frequency of chromosomal translocations. Interestingly, we identified a combined effect of strain rate and acceleration to significantly improve delivery; and identified cell stiffness as an intrinsic determinant of delivery efficiency. Overall, this study underscores VECT's potential in industrial-scale multiplexed gene editing of T cells with improved safety profile.

## **CHAPTER 1. INTRODUCTION AND BACKGROUND**

### **1.1 Gene Editing in T Cell Therapy**

Adaptive T cell therapy entails the use of autologous T-cells from patients to be genetically modified to express a synthetic receptor targeting a specific antigen on tumor cells. Typically, this receptor combines extracellular antigen-binding domains from antibodies (CAR T-cell therapy) or from exogenous T-cell receptor (TCR T-cell therapy) with intracellular signaling components like the T-cell receptor CD3 $\zeta$  chain [1-4]. Additional co-stimulation can be provided by molecules like CD28 or 4-1BB to further enhance T-cell activation and persistence [2, 5]. Such therapies have demonstrated significant success in oncological diseases in achieving sustained long-term remissions, particularly in refractory patients, boosting the complete response rates to 80-97% in specific B-cell malignancies like acute lymphoblastic leukemia (ALL) [6-8]. This clinical efficacy has spurred active investigation into expanding T-cell therapy to various other cancer types, upholding a promising future for cellular immunotherapy against cancer. The first FDA-approved CAR T-cell therapies, Kymriah and Yescarta were released in 2017 for treating B-cell ALL and diffuse large B-cell lymphoma (DLBCL) by targeting CD19. Subsequently, other CD19 CAR T-cell products and the first non-CD19-directed CAR targeting B-cell maturation antigen (BCMA) for multiple myeloma treatment have gained approval.

However, it has not been universally successful, especially beyond hematopoietic malignancies. Factors such as the chemotherapy history, the preexisting senescence of T cells in patients, loss of antigen expression from tumor cells, or hostile tumor microenvironment (TME), can influence the sustained effects of T cells [9, 10].

Additionally, the long lead time and complex manufacturing process present hurdles to accessibility of the therapies due to manufacturing failures and cost [11]

With the maturation of gene editing technologies, especially the advent of RNA-guided endonucleases such as Cas9, it is possible and simple to target specific gene sequences [12]. And more investigators turn to genetic modification methods to overcome these challenges. Allogeneic T cell products, in which cells are sourced from healthy donors, genetically modified to avoid host versus graft responses, and supplied to multiple patients, will not only greatly reduce the cost of manufacturing and shorten the treatment regimen, but also provide higher quality starting materials without T cell dysfunction [13]. Manufacturing process for allogeneic CAR-T and TCR-T cells requires genetic knockout of multiple genes related to foreign antigen presentation and recognition to improve safety and persistency of infused cells (e.g. endogenous TCR and HLA) [14, 15]. Besides its application in allogeneic cell production, gene editing has been applied in negative regulator (e.g., PD1, CD5)[16] knockout to overcome immunosuppressive TME, in epigenetic modification to overcome dysregulated gene expression (e.g. DNMT3) [17], in shared target antigen (e.g., CD5 and CD7) knockout to reduce T cell fratricide when used against T-cell malignancies [18, 19].

### *1.1.1 Allogeneic T Cell Therapy*

Allogeneic T cell therapies are considered a solution to scalable and sustainable production. In a typical allogeneic production pipeline, cells sourced from healthy donors are genome engineered and genetically edited to provide efficacy and

durability, analyzed for quality control, stored in suitable formulation buffer under cryopreservation for weeks to months, and reactivated on-demand for administration into patients. This greatly reduces lead time for treatment and reduces the cost of manufacturing and analytical testing. The manufacturing process of allogenic T cells, however, is more complex than autologous product. It includes an essential step of gene silencing of multiple genes. This multiplexed gene editing step, if not done carefully, can introduce more risk factors such as large chromosome damage to the product. The primary concern gene editing addresses for allogeneic therapies is the risk for graft-versus-host disease (GvHD), wherein the donor T-cells recognize foreign surface human leukocyte antigen (HLA) molecules in the patients receiving the transfer, triggering an immune response. Because the endogenous TCR is responsible for GvHD, genetically deleting TCR from T cells have helped prevent adverse events [20]. In this process, an endonuclease is targeted to the *TRAC* or *TRBC* locus responsible for generating the alpha and beta chain on the TCR [13]. The approach makes an “off-the-shelf” cell product possible, eliminating the need for HLA matching.

On the other hand, administered T cells, if not HLA matched, face the risk of host-mediated rejection upon immune recognition. This rejection can be mediated by preexisting anti-HLA antibodies, leading to rapid clearance of mismatched donor cells; or by cell-mediated responses from host T and natural killer (NK) cells [21]. Lymphodepletion can be administered prior to cell infusion to manage these responses; but leading to an increased risk of complications associated with T-cell immunodeficiency and prolonged cytopenia [22]. Genetically removing HLA molecules through the disruption of the  $\beta 2$  microglobulin (B2M) gene locus can

effectively provide immunosurveillance stealth [23]. Alternative targets have included editing of HLA class II-associated transcription factors [24]. Additionally, responses mediated by natural killer cells against donor T cells with HLA knockout can be addressed through simultaneous knocking in of nonpolymorphic HLA molecules (e.g. HLA-E) [25, 26].

To specifically address cell source material to generate allogeneic products, CAR T-cell therapeutics can be derived from inducible pluripotent stem cells (iPSCs) amenable to genetic modification and differentiation into mature tumor-targeted T-cells. iPSCs are obtained from adult somatic cells by inducing expression of a combination of transcription factors that transform cells into a pluripotent state. To transform them into safe and efficient T cell product, manufacturing requires editing of multiple genes. Like all allogeneic product, these cells require knockout of endogenous TCR and HLA. Additionally, manufacturing may incorporate knock-ins of transgenic TCR or CAR under *TRAC* locus. Proof-of-concept studies have demonstrated successful generation of non-viral CAR T-cells from T lymphocyte-derived iPSCs using cas9 to target the endogenous *TRAC* locus to knock-in a CD19-CAR construct [27] and the method has since been used in clinical trials [28]. This strategy puts regulation and signal transduction of CAR under control of physiological T cell activation.

### *1.1.2 Overcoming T Cell Dysfunction*

Despite the development of successful CD19 CAR T therapies, long-term response rate to CAR T therapies outside treatment of CD19 B cell malignancies, especially in solid tumor treatment remained low and variable across patients. The field has proposed that dysregulation of T cell activation signals, a phenomenon called tonic signaling, and dysregulated metabolism as the two main cause the causes of unsuccessful CAR T-cell therapy [29, 30]. These dysregulated signaling activities can be modulated through genetic or epigenetic manipulation. Sustained cell proliferation and long-term persistence are required for complete disease remission [30, 31]. However, dysfunctional intracellular signaling and metabolism led to rapid exhaustion of T-cells and diminished stem cell memory/central memory differentiation, and premature senescence limited T-cell expansion and persistence.

Additional hurdles arise in the treatment of solid tumors. Adoptive T-cells targeting solid tumors must navigate to tumor sites, overcome tissue barriers, and target a heterogenous tumor population [32]. Even if successful trafficking and infiltration occur, T-cells may succumb to dysfunction within the toxic tumor microenvironment (TME), characterized by metabolic disruptions, inhibitory soluble factors and cytokines, and an abundance of suppressive immune cells or tumor cells expressing ligands for negative immune checkpoint receptors.

Addressing these challenges requires a multifaceted approach, with promising approach including site-specific genetic editing. The advent of easily multiplexable precision genome editing using CRISPR-Cas9 technology offers the opportunity to overcome many biological barriers to successful T-cell therapy for solid tumors. CRISPR-Cas9 editing of T-cells has been done with targeting inhibitory genes (e.g.,

*PDCDI*, encoding PD-1; *LAG3*, encoding LAG-3) and those encoding death receptors such as CD95/Fas to prevent TME-mediated inhibition or apoptosis. Some of these single or combined knockout studies have shown improved durability of T cell therapy responses and enhanced tumor control.

With a deeper understanding of T cell dysfunction as a result of epigenetic regulation of gene transcription, targeting epigenetic-modification genes emerges as a third promising strategy. This method uses modification of genes associated in epigenetic regulations, including the deletion of regulators like TET2, DNMT3, or the insertion of transcription factors such as c-Jun and BATF [33]. Doing so restores the epigenetic landscape of non-exhausted T cells and prolongs their persistence, especially when surviving the TME in solid tumor treatment.

In summary, gene editing techniques targeting inhibitory receptors in T cells offer a promising strategy to overcome T cell dysfunction and enhance the efficacy of T cell therapy against cancer. By disrupting the inhibitory signaling pathways that impair T cell function, gene knockout enables the generation of robust and durable anti-tumor immune responses.

### *1.1.3 Expanding CAR T to T cell malignancies*

Redirecting T cell cytotoxicity towards malignant B cells has been successful, but reprogramming T cells to target malignant T cells without harming normal T cells is challenging. Identifying the antigens that are highly expressed on malignant T cells but not on normal T cells is the first challenge, and removing this target on therapeutic CAR T cells is the second challenge, which limits self-fratricide of CAR T cells. CD5,

CD7, and CD3 are 3 highly expressed antigens on all T cells that are the subject of CAR T therapies targeting T lymphocytes. Without knockout, preclinical studies have shown reduced expansion of CD7-CAR T cells due to fratricide where CAR-T cells show cytotoxicity towards self-population [19, 34, 35]. A knockout in shared antigen, such as CD5 and CD7, overcomes fratricide and allows T cells to expand to a clinically required quantity.

#### *1.1.4 Potential Adverse Effect*

Advancing the CAR T field toward a paradigm of off-the-shelf, ready-to-use products derived from healthy donors or iPSCs requires an efficient and safe ability to perform multiplexed gene editing. However, achieving safe and efficient multiplexed editing is challenging.

The challenges inherent of multiplex gene editing became apparent from the first-in-human trial of multiplex CRISPR-Cas9 edited in which TRAC, TRBC and PDCD1 were deleted in T-cells and supplied with a transgenic TCR specific for tumor-associated antigen NY-ESO-1[36]. Transfer of gene-edited TCR-engineered T-cells into patients resulted in durable engraftment with edits at all three genomic loci. However, the proportion of cells carrying all three desired edits was low and decreased over time. This can be attributed to the random delivery process inherent in current gene delivery techniques such as electroporation and lipid nanoparticles. Moreover, the random delivery process resulted in heterogeneously edited populations of T cells, leading to inconsistent therapeutic outcomes [36].

Additionally, workflows utilizing wild-type Cas9, which edit the genome through generation of double-stranded breaks (DSBs) in the chromosome, have been associated with the generation of chromosomal translocations, raising concerns about genomic stability and potential oncogenic risks. In a follow-up with patients who received gene edited BCMA TCR T cells, researchers found that post-infusion T cells carried translocation between the three chromosomes where edited genes are located. And the proportion of cells with translocation consistently decreased over time. More studies now pointed out that populations with translocations tend to be short-lived and more likely exhausted and can lead to safety challenges if the rearrangements lead to oncogenic state of the cell [36, 37]. With the maturation of CRISPR/Cas9-based gene editing, more Cas9 variants have been tested as replacement of the wild-type cas9. These variants, such as dCas9, Cas9 base-editor, and prime-editor, do not result in DSB and thus eliminates the risks of translocation [38]. They have shown promise in the pre-clinical setting[39, 40]. However, they are not as versatile as wild-type Cas9 in their lack of gene knocking capabilities. Applications that require multiple knockouts and knock-ins, such as knocking-in transgenic CAR in the *TRAC* locus and knocking in HLA-E in *B2M* locus, cannot be achieved without DSBs [41].

Addressing these challenges is crucial for enhancing the safety and reliability of gene-edited T cell therapies, particularly in the context of allogeneic products aimed at broader patient populations. Developing strategies to minimize chromosomal translocations and ensure genomic integrity will be paramount for advancing the clinical translation of gene-edited T cell therapies.

## **1.2 Current Delivery Platform**

### *1.2.1 Biochemical Method*

The biochemical delivery approach to CRISPR/Cas9 technology encompasses the use of biomaterials and biomolecules to form a carrier vehicle. Among these, nanoparticle-based delivery systems stand out as versatile platforms offering unique advantages for gene transfection. Nanoparticles (NPs) are materials with nano-scale dimensions (e.g., 1–100 nm), widely utilized for drug delivery due to their tailored surface properties and size. Specifically, lipid nanoparticle (LNP)-based systems have gained popularity in nonviral CRISPR/Cas9 delivery due to their ability to effectively condense the cargo and facilitate cellular uptake. These systems commonly feature cationic phospholipids, which complex with and condense nuclei acid, improving their cellular uptake. Their ease of formulation makes them ideal for commercial manufacturing. For instance, lipofectamine, a commercially available LNP-based system for gene delivery, has been widely utilized as a gold standard for preclinical CRISPR/Cas9 delivery research, showcasing its effectiveness in various cellular contexts. Despite their promise, challenges remain, including endo-lysosomal sequestration, cellular toxicity, and low efficiency in suspension cells [42, 43], highlighting the need for continued refinement and optimization of LNP-based delivery systems for clinical translation. Recent research has focused on enhancing the properties of LNPs, including improved cell interaction and penetration, endosome escape, and reducing toxicity, to optimize their efficacy.

Peptide-based delivery systems offer another biochemical avenue for CRISPR/Cas9 delivery, leveraging short peptides known as cell-penetrating peptides (CPPs) to facilitate intracellular delivery of therapeutic cargos with reduced immune

or cytotoxic responses. Various studies have explored the potential of CPPs for CRISPR/Cas9 delivery, aiming to optimize gene editing efficiency while minimizing off-target effects. Lostale-Seijo et al. (2017) [44] developed a non-covalent strategy for delivering Cas9 RNPs complexed with an amphipathic CPP (PT24/Cas9 RNP), demonstrating efficient delivery of the Cas9 RNP cargo with low toxicity. Additionally, Del'Guidice et al. (2018) [[45]] utilized an amphiphilic peptide (6His-CM18-PTD4) to deliver functional transcription factors and CRISPR/Cas9 RNPs into hard-to-transfect primary natural killer cells. These studies highlight the potential of peptide-based delivery systems to enhance the efficiency and precision of CRISPR/Cas9 gene editing, offering a promising alternative to traditional nanoparticle-based approaches. However, further research is needed to optimize peptide design and to understand the adverse effect for broader clinical applications of this technology.

In addition to nanoparticle and peptide-based approaches, hydrogel-based delivery systems have emerged as new platforms, offering unique advantages such as stimuli-responsive behavior and sustained release kinetics [46]. Stimulus-responsive hydrogels can transition from a swollen state to a collapsed state in response to external stimuli such as pH, temperature, pressure, or electric fields. Hydrogel-based nanoparticles have been engineered to improve the encapsulation and targeted delivery and controlled release.

Despite their success in delivering small cargos such as Cas9 mRNA and sgRNA, the translation capacity is limited by their low packaging capacity. When it

comes to delivering large plasmid with a homology directed repair (HDR) template, their efficiency is much lower [47].

### *1.2.2 Electroporation*

As an alternative delivery method to biochemical permeabilization, electroporation relies on electrical fields to permeate cell membrane. The core mechanism of electroporation subjects cells to a transient electric field, exerting a high energy density on the cell membrane that results in pore formation, cargo movement, and delivery inside cell cytosol. Compared with nanomaterial-based methods, electroporation serves as a more efficient technique, offering a delicate equilibrium between efficacy and mitigating cellular harm. Modern electroporators, exemplified by MaxCyte, Nucleofector, and Gene Pulsar, have markedly enhanced transfection scalability and effectiveness while minimizing cellular damage. For instance, Lonza's Nucleofector Portfolio enables efficient transfection of challenging cell lines and primary cells with diverse substrates, including DNA vectors and RNA oligonucleotides, achieving transfection efficiencies of up to 90% for select cell types. Conversely, MaxCyte ensures post-transfection cell viabilities exceeding 90% and transfection efficiencies surpassing 90% for various commonly used cell types, all within rapid time frames.

Despite their efficacy, challenges persist in optimizing electroporation buffers and workflows to stave off cellular deterioration. The choice of buffer can greatly impact cell recovery from electroporation. For example, a study showed the tonicity of buffer can result in activation of DNA damage pathway cGAS-STING [48]. Thus,

it would require careful and extensive optimization. In addition, it has been shown that electroporation can result in tonic T cell activation, oxidative stress, reduced spare respiratory capacity, cell exhaustion, and altered T cell metabolism [49]. These damages limit electroporation to one-time-use during the manufacturing process, reducing its workflow flexibility.

### *1.2.3 Mechanoporation*

Mechanoporation is an alternative delivery method for ex vivo cell engineering. They can be paired with microfluidic techniques to achieve streamlined and automated manufacturing process for cell therapies. Particularly, microfluidic mechanoporation technologies have garnered attention for T cell transfection, proving highly applicable to primary immune cells. Efficient transfection of T cells is crucial for generating potent gene-edited engineered T cells. The appeal of microfluidic mechanoporation lies in its straightforward workflow, facilitating a close-looped system and enabling continuous and flexible workflow. These approaches employ mechanical permeabilization of cell membranes, utilizing diverse mechanisms such as nanowires [50], sonoporation [51], and microconstriction- or flow vortex-induced cell deformation [52-55]. In a typical workflow, devices exert mechanical force generated via deformation or shear applied to cells to produce reversible membrane breakage, followed by transport of biomolecules into the cell, either through passive diffusion [49, 55] or active convection [54, 56]. Early microfluidic transfection devices utilized microinjection techniques. The incorporation of pneumatic control systems in recent years made on-chip microinjection more automated [57]. Yet, these devices are currently lower-throughput and difficult to manufacture. A similar design using paralleled microneedles to puncture cells has improved the throughput. Yet it requires

precise alignment of cells and microneedles[58]. Another type of microfluidic based device utilizes a series of horizontal constrictions to generate shear force and disrupt the cell membrane[49, 52, 53]. This approach can be highly efficient, resulting in 80-90% delivery efficiency, though the underlying diffusion-based mechanism is better suited to applications delivering small biomolecules, such as small peptide antigens[59]. An alternative approach relies on large membrane deformation through physical contact[60, 61] or fluidic stretching[62]. Large deformations can result in a convective fluidic transport inside the cell with enhanced delivery of large cargos such as DNA and nanoparticles[47, 63]. A new approach incorporates droplet generation preceding microfluidic transfection to reduce the amount of cargo required[55]. In many cases, one advantage of mechanoporation is the preservation of cell health, which includes viability, proliferation, and a normal cell phenotype[49, 60].

Despite the advantages of microfluidic transfection, challenges remain in clinical translation, including variable delivery outcomes across cell types or donors, susceptibility to channel clogging and potential damage to the cytoskeleton and nucleus during the process [64]. It is hypothesized that cell size and cytoskeletal stiffness dominates the delivery outcome [65]. Therefore, a deeper understanding in the influence of intrinsic cell mechanics on mechanoporation is needed to improve outcome homogeneity and consistency.

### **1.3 Key Values for Microfluidic Mechanoporation**

#### *1.3.1 Minimal Disruption of Physiology*

One of the major concerns for selecting a delivery platform is the impact on cell physiology. An ideal delivery platform should not change the normal transcriptome or metabolome. Although nanomaterials, especially LNPs, have been widely used in ex vivo and in vivo transfection, they present significant limitations due to concerns regarding LNP-induced oxidative stress [66]. For T cells, induced oxidative stress is associated with differentiation into short-lived effector phenotype [67, 68]. Strategies to ameliorate production of ROS, such as codelivery of antioxidative chemicals, should be considered when used in T cell manufacturing.

Electroporation, a commonly employed physical delivery technique, exerts profound effects on gene expression profiles in T cells. Microarray analysis revealed substantial alterations in gene expression following electroporation, particularly in T cells, where numerous genes associated with activation, stress response, and cytokine secretion pathways were dramatically upregulated. Notably, key cytokines such as IL-2, IFN- $\gamma$ , and TNF $\alpha$  exhibited significant increases in secretion following electroporation [49]. Furthermore, the cytokine secretion profiles induced by electroporation bear resemblance to toxicological pathways associated with cytokine release syndrome, a potentially lethal complication observed in engineered cells like chimeric antigen receptor T cells. Even milder electroporation protocols showed significant cytokine misregulation, underscoring the importance of assessing and optimizing delivery methods to minimize adverse effects on cell function and therapeutic outcomes.

In contrast, cells subjected to mechanoporation, namely cell squeezing, stretching, and compression, demonstrated minimal changes in cytokine secretion and in gene expression pattern [49, 69]. Functionally, mechanoporated T cells persisted longer than

electroporated T cells, and showed more efficient control of tumor burden [49]. On the other hand, cells do respond to mechanical signals. Epigenetically, compression and stretching of the nucleus can alter histone modification pattern, making certain genes more accessible [70, 71]. These changes have not been correlated to adverse impact on cell physiology. Overall, these findings point to most valuable feature of mechanoporation – minimal disruption of cell physiology.

### *1.3.2 Enable Sequential Processing*

The aforementioned chromosomal translocation issue associated with multiplexed gene editing in one-shot has been noted in clinical translation of engineered T cell therapies [36]. Translocation events have been hypothesized to negatively impact T cell persistence in vivo. Introducing individual gene edits sequentially with sufficient time to repair DSBs in between is proven to reduce translocation rate [72]. However, due to the cytotoxic effect from many delivery platforms, cells can only endure a limited number of deliveries, preventing efficient workflow shift into sequential multiplex editing. For example, a single electroporation has resulted in 40% loss in viability and a low proliferative lag phase in cell growth [36].

The plasticity of the cell membrane and cytoskeleton ensures the survival of cells after repeated rounds of compressive or tensile stress[70]. Additionally, T cells regularly go through narrow endothelial barriers to extravasate circulation into cite of infection, during which their cytoskeleton experience large strain [73]. Hence, T cells are naturally adapted to surviving large deformation or repeated force exertion. This makes mechanoporation an ideal platform for multi-step and sequential gene editing. Indeed, cell

viability and proliferation remained relatively unchanged after several treatments compared with a single mechanoporation [54].

### *1.2.3 Non-stochastic Delivery*

Biochemical membrane permeabilization and electroporation exhibit a non-selective approach to membrane permeabilization, resulting in the indiscriminate uptake of molecules across a diverse range of cell phenotypes. The stochastic nature of these methods leads to the heterogeneous delivery and editing of populations, with varying degrees of efficiency and accuracy. Consequently, the resulting cell populations often display a mixture of edited and unedited cells, hindering the attainment of homogenous populations required for clinical applications.

Mechanoporation exhibits selectivity in delivering molecules to specific cell types with favorable biomechanical properties, as elucidated by recent investigations. In a study assessing the impact of cell mechanics on permeabilization extent, different cell types exhibiting varying stiffness were tested in a cell-squeeze device. RPE-1 and HeLa K cells, despite having similar diameters, displayed distinct elasticity profiles, with RPE-1 cells exhibiting lower stiffness compared to HeLa K cells. This variation in elasticity correlated with differences in delivery efficiency, where RPE-1 cells demonstrated higher efficiency in molecular loading compared to the stiffer HeLa K cells [65]. This observation underscores the dependence of mechanoporation success on the intrinsic cell cytoskeleton. This poses a possibility for mechanoporation devices to be a non-stochastic platform that can result in efficient homogenous editing.

## **1.4 References**

- [1] June, C.H., et al., CAR T cell immunotherapy for human cancer. *Science*, 2018. 359(6382): p. 1361-1365.
- [2] Grupp, S.A., et al., Chimeric antigen receptor-modified T cells for acute lymphoid leukemia. *N Engl J Med*, 2013. 368(16): p. 1509-1518.
- [3] Baulu, E., et al., TCR-engineered T cell therapy in solid tumors: State of the art and perspectives. *Sci Adv*, 2023. 9(7): p. eadf3700.
- [4] Sun, Y., et al., Evolution of CD8(+) T Cell Receptor (TCR) Engineered Therapies for the Treatment of Cancer. *Cells*, 2021. 10(9).
- [5] Ali, S.A., et al., T cells expressing an anti-B-cell maturation antigen chimeric antigen receptor cause remissions of multiple myeloma. *Blood*, 2016. 128(13): p. 1688-700.
- [6] Melenhorst, J.J., et al., Decade-long leukaemia remissions with persistence of CD4(+) CAR T cells. *Nature*, 2022. 602(7897): p. 503-509.
- [7] Maude, S.L., et al., Tisagenlecleucel in Children and Young Adults with B-Cell Lymphoblastic Leukemia. *N Engl J Med*, 2018. 378(5): p. 439-448.
- [8] Johnson, P.C. and J.S. Abramson, Engineered T Cells: CAR T Cell Therapy and Beyond. *Curr Oncol Rep*, 2022. 24(1): p. 23-31.
- [9] Hou, A.J., L.C. Chen, and Y.Y. Chen, Navigating CAR-T cells through the solid-tumour microenvironment. *Nat Rev Drug Discov*, 2021. 20(7): p. 531-550.
- [10] Marofi, F., et al., CAR T cells in solid tumors: challenges and opportunities. *Stem Cell Res Ther*, 2021. 12(1): p. 81.
- [11] Aijaz, A., et al., Biomanufacturing for clinically advanced cell therapies. *Nature Biomedical Engineering*, 2018. 2(6): p. 362-376.
- [12] Jinek, M., et al., RNA-programmed genome editing in human cells. *Elife*, 2013. 2.
- [13] Depil, S., et al., 'Off-the-shelf' allogeneic CAR T cells: development and challenges. *Nature Reviews Drug Discovery*, 2020.
- [14] Torikai, H., et al., A foundation for universal T-cell based immunotherapy: T cells engineered to express a CD19-specific chimeric-antigen-receptor and eliminate expression of endogenous TCR. *Blood*, 2012. 119(24): p. 5697-705.

- [15] Chang, C.W., et al., Generation of Multiplexed Engineered, Off-the-Shelf CAR T Cells Uniformly Carrying Multiple Anti-Tumor Modalities to Prevent Tumor Relapse. *Blood*, 2020. 136.
- [16] Rupp, L.J., et al., CRISPR/Cas9-mediated PD-1 disruption enhances anti-tumor efficacy of human chimeric antigen receptor T cells. *Sci Rep*, 2017. 7(1): p. 737.
- [17] Prinzing, B., et al., Deleting DNMT3A in CAR T cells prevents exhaustion and enhances antitumor activity. *Sci Transl Med*, 2021. 13(620): p. eabh0272.
- [18] Silva, D., et al., CD7-Edited T Cells Expressing a CD7-Specific CAR for the Therapy of T-Cell Malignancies. *Molecular Therapy*, 2017. 25(5): p. 130-130.
- [19] Raikar, S.S., et al., Development of chimeric antigen receptors targeting T-cell malignancies using two structurally different anti-CD5 antigen binding domains in NK and CRISPR-edited T cell lines. *Oncoimmunology*, 2018. 7(3): p. e1407898.
- [20] Brudno, J.N., et al., Allogeneic T Cells That Express an Anti-CD19 Chimeric Antigen Receptor Induce Remissions of B-Cell Malignancies That Progress After Allogeneic Hematopoietic Stem-Cell Transplantation Without Causing Graft-Versus-Host Disease. *J Clin Oncol*, 2016. 34(10): p. 1112-21.
- [21] Loney, C. and E. Breman, Allogeneic CAR-T Therapy Technologies: Has the Promise Been Met? *Cells*, 2024. 13(2).
- [22] Neelapu, S.S., et al., ALPHA Study: ALLO-501 Produced Deep and Durable Responses in Patients with Relapsed/Refractory Non-Hodgkin's Lymphoma Comparable to Autologous CAR T. *Blood*, 2021. 138.
- [23] Hu, X., et al., Hypoimmune anti-CD19 chimeric antigen receptor T cells provide lasting tumor control in fully immunocompetent allogeneic humanized mice. *Nat Commun*, 2023. 14(1): p. 2020.
- [24] Rossi, M., et al., Efficient shRNA-based knockdown of multiple target genes for cell therapy using a chimeric miRNA cluster platform. *Mol Ther Nucleic Acids*, 2023. 34: p. 102038.
- [25] Gornalusse, G.G., et al., HLA-E-expressing pluripotent stem cells escape allogeneic responses and lysis by NK cells. *Nat Biotechnol*, 2017. 35(8): p. 765-772.
- [26] Jo, S., et al., Endowing universal CAR T-cell with immune-evasive properties using TALEN-gene editing. *Nat Commun*, 2022. 13(1): p. 3453.

- [27] Themeli, M., et al., Generation of tumor-targeted human T lymphocytes from induced pluripotent stem cells for cancer therapy. *Nat Biotechnol*, 2013. 31(10): p. 928-33.
- [28] Chang, C.W., et al., FT819: Translation of Off-the-Shelf TCR-Less Trac-1XX CAR-T Cells in Support of First-of-Kind Phase I Clinical Trial. *Blood*, 2019. 134.
- [29] Kouro, T., H. Himuro, and T. Sasada, Exhaustion of CAR T cells: potential causes and solutions. *Journal of Translational Medicine*, 2022. 20(1).
- [30] Fraietta, J.A., et al., Determinants of response and resistance to CD19 chimeric antigen receptor (CAR) T cell therapy of chronic lymphocytic leukemia. *Nature Medicine*, 2018. 24(5): p. 563-+.
- [31] Chong, E.A., et al., CAR T cell viability release testing and clinical outcomes: is there a lower limit? *Blood*, 2019. 134(21): p. 1873-1875.
- [32] Wagner, J., et al., CAR T Cell Therapy for Solid Tumors: Bright Future or Dark Reality? *Molecular Therapy*, 2020. 28(11): p. 2320-2339.
- [33] Xiong, D., L. Zhang, and Z.J. Sun, Targeting the epigenome to reinvigorate T cells for cancer immunotherapy. *Mil Med Res*, 2023. 10(1): p. 59.
- [34] Mamonkin, M., et al., Reversible Transgene Expression Reduces Fratricide and Permits 4-1BB Costimulation of CAR T Cells Directed to T-cell Malignancies. *Cancer Immunol Res*, 2018. 6(1): p. 47-58.
- [35] Gomes-Silva, D., et al., CD7-edited T cells expressing a CD7-specific CAR for the therapy of T-cell malignancies. *Blood*, 2017. 130(3): p. 285-296.
- [36] Stadtmauer, E.A., et al., CRISPR-engineered T cells in patients with refractory cancer. *Science*, 2020.
- [37] Chang, C.R., et al., Ultra-high efficiency T cell reprogramming at multiple loci with SEED-Selection. *bioRxiv*, 2024.
- [38] Tsuchida, C.A., et al., Mitigation of chromosome loss in clinical CRISPR-Cas9-engineered T cells. *Cell*, 2023. 186(21): p. 4567-+.
- [39] Webber, B.R., et al., Highly efficient multiplex human T cell engineering without double-strand breaks using Cas9 base editors. *Nature Communications*, 2019. 10.
- [40] Georgiadis, C., et al., Base-edited CAR T cells for combinational therapy against T cell malignancies. *Leukemia*, 2021. 35(12): p. 3466-3481.

- [41] Jo, S., et al., Endowing universal CAR T-cell with immune-evasive properties using TALEN-gene editing. *Nature Communications*, 2022. 13(1).
- [42] Rezalotfi, A., et al., Challenges of CRISPR-Based Gene Editing in Primary T Cells. *International Journal of Molecular Sciences*, 2022. 23(3).
- [43] Sinclair, F., et al., Recent advances in the delivery and applications of nonviral CRISPR/Cas9 gene editing. *Drug Delivery and Translational Research*, 2023.
- [44] Lostalé-Seijo, I., et al., Peptide/Cas9 nanostructures for ribonucleoprotein cell membrane transport and gene edition. *Chemical Science*, 2017. 8(12): p. 7923-7931.
- [45] Del Guidice, T., et al., Membrane permeabilizing amphiphilic peptide delivers recombinant transcription factor and CRISPR-Cas9/Cpf1 ribonucleoproteins in hard-to-modify cells. *Plos One*, 2018. 13(4).
- [46] Iqbal, Z., et al., Biomaterial-assisted targeted and controlled delivery of CRISPR/Cas9 for precise gene editing. *Biomaterials Science*, 2023. 11(11): p. 3762-3783.
- [47] Bohrer, L.R., et al., CGMP compliant microfluidic transfection of induced pluripotent stem cells for CRISPR-mediated genome editing. *Stem Cells*, 2023.
- [48] An, J., et al., Enhancement of the viability of T cells electroporated with DNA via osmotic dampening of the DNA-sensing cGAS-STING pathway. *Nature Biomedical Engineering*, 2024. 8(2): p. 149-+.
- [49] DiTommaso, T., et al., Cell engineering with microfluidic squeezing preserves functionality of primary immune cells in vivo. *Proceedings of the National Academy of Sciences of the United States of America*, 2018. 115(46): p. E10907-E10914.
- [50] Shalek, A.K., et al., Vertical silicon nanowires as a universal platform for delivering biomolecules into living cells. *Proceedings of the National Academy of Sciences of the United States of America*, 2010. 107(5): p. 1870-1875.
- [51] Belling, J.N., et al., Acoustofluidic sonoporation for gene delivery to human hematopoietic stem and progenitor cells. *Proceedings of the National Academy of Sciences of the United States of America*, 2020. 117(20): p. 10976-10982.
- [52] Williams, A.R., S. Bao, and D.L. Miller, Filtroporation: A simple, reliable technique for transfection and macromolecular loading of cells in suspension. *Biotechnol Bioeng*, 1999. 65(3): p. 341-6.
- [53] Sharei, A., et al., Ex Vivo Cytosolic Delivery of Functional Macromolecules to Immune Cells. *Plos One*, 2015. 10(4).

- [54] Liu, A., et al., Microfluidic generation of transient cell volume exchange for convectively driven intracellular delivery of large macromolecules. *Mater Today (Kidlington)*, 2018. 21(7): p. 703-712.
- [55] Joo, B., et al., Highly Efficient Transfection of Human Primary T Lymphocytes Using Droplet-Enabled Mechanoporation. *ACS Nano*, 2021.
- [56] Kang, G., et al., Intracellular Nanomaterial Delivery via Spiral Hydroporation. *Acs Nano*, 2020. 14(3): p. 3048-3058.
- [57] Adamo, A., et al., Microfluidic jet injection for delivering macromolecules into cells. *J Micromech Microeng*, 2013. 23.
- [58] Dixit, H.G., et al., Massively-Parallelized, Deterministic Mechanoporation for Intracellular Delivery. *Nano Lett*, 2020. 20(2): p. 860-867.
- [59] Booty, M.G., et al., Microfluidic Squeezing Enables MHC Class I Antigen Presentation by Diverse Immune Cells to Elicit CD8(+) T Cell Responses with Antitumor Activity. *Journal of Immunology*, 2022. 208(4): p. 929-940.
- [60] Liu, A., et al., Cell Mechanical and Physiological Behavior in the Regime of Rapid Mechanical Compressions that Lead to Cell Volume Change, in *Small*. 2019. p. e1903857.
- [61] Deng, Y.X., et al., Intracellular Delivery of Nanomaterials via an Inertial Microfluidic Cell Hydroporator. *Nano Letters*, 2018. 18(4): p. 2705-2710.
- [62] Hur, J., et al., Microfluidic Cell Stretching for Highly Effective Gene Delivery into Hard-to-Transfect Primary Cells. *ACS Nano*, 2020.
- [63] Kiru, L., et al., In vivo imaging of nanoparticle-labeled CAR T cells. *Proceedings of the National Academy of Sciences*, 2022. 119(6): p. e2102363119.
- [64] Kim, H., et al., Expanding CAR-T cell immunotherapy horizons through microfluidics. *Lab Chip*, 2024.
- [65] Uvizl, A., et al., Efficient and gentle delivery of molecules into cells with different elasticity via Progressive Mechanoporation. *Lab on a Chip*, 2021. 21(12): p. 2437-2452.
- [66] Manke, A., L.Y. Wang, and Y. Rojanasakul, Mechanisms of Nanoparticle-Induced Oxidative Stress and Toxicity. *Biomed Research International*, 2013. 2013.

- [67] Wu, H., et al., Mitochondrial dysfunction promotes the transition of precursor to terminally exhausted T cells through HIF-1 $\alpha$ -mediated glycolytic reprogramming. *Nature Communications*, 2023. 14(1).
- [68] Huang, Y., et al., Rewiring mitochondrial metabolism to counteract exhaustion of CAR-T cells. *Journal of Hematology & Oncology*, 2022. 15(1).
- [69] Hur, J., et al., Genetically Stable and Scalable Nanoengineering of Human Primary T Cells via Cell Mechanoporation. *Nano Letters*, 2023.
- [70] Nava, M.M., et al., Heterochromatin-Driven Nuclear Softening Protects the Genome against Mechanical Stress-Induced Damage. *Cell*, 2020. 181(4): p. 800-+.
- [71] Tajik, A., et al., Transcription upregulation via force-induced direct stretching of chromatin. *Nat Mater*, 2016. 15(12): p. 1287-1296.
- [72] Horii, T., et al., Efficient generation of conditional knockout mice via sequential introduction of lox sites. *Scientific Reports*, 2017. 7.
- [73] Burkhardt, J.K., E. Carrizosa, and M.H. Shaffer, The actin cytoskeleton in T cell activation. *Annual Review of Immunology*, 2008. 26: p. 233-259

## CHAPTER 2. THESIS OVERVIEW

### 2.1 Value Proposition for Cell Volume Exchange for Convective Transfection (VECT) device

The Sulchek lab has successfully demonstrated a novel non-viral approach for macromolecular delivery through microfluidic volume exchange for cell transfection (VECT). The VECT approach uses microfluidic flow through a series of ridges that deform flowing cells as they pass. The device facilitates reagent delivery using a convective mechanoporation process, where cells undergo a series of rapid and large intensity compressions to transiently open membrane pores and induce active transport of extracellular fluid with suspended molecules and particles into the cell interior. Unlike other shear-based mechanoporation devices, VECT enabled delivery of large molecules, including nanoparticles, large macromolecules (>2 MDa), and plasmid (~10K bp) with high efficiency (~90%), without sacrificing efficiency. This capability made VECT a promising platform to replace viral transduction at delivering large transgene for gene engineering and gene editing.

Another highlight of VECT is the low adverse effect on cell physiology. Treated cell remain highly viable (90+%). Most importantly, VECT showed no interruption of nuclear envelope or genetic integrity, resulted in no disruption of normal cell proliferation, and maintained normal expression in survival-related genes [1]. Shear-based mechanoporation devices can have unwanted coupling of high delivery efficiency to low cell viability. This could be attributed to that efficient membrane permeabilization by shear force requires sufficient interaction time in the range of 100 $\mu$ s. On the other hands, VECT has demonstrated increased efficiency without

harming cell viability. This is proposed to be due the short compression time cells experience under VECT compression (on the scale of 10 $\mu$ s). These make VECT an ideal platform for therapeutic cell engineering. Currently, VECT is capable of processing  $>2 \times 10^6$  cells/min in a single channel. VECT can be easily scaled-up via channel parallelization. As a microfluidic device, VECT can be readily automated and integrated into other cell culture systems. This reduces human labor, ensuring a simple and flexible workflow.

We have used the approach to deliver a variety of nanoparticle tracers and labels as well as transgene products into cells. Volume exchange depends on intrinsic cell biomechanics [1-3] and leads to better delivery of large cargo compared to a stochastic process like diffusion. In principle, VECT generates a more homogeneously edited population. In a previous study, we showed that compared to electroporation, VECT preserved cell nuclear integrity and resulted in less cGAS activity [1]. The high cell viability after VECT treatment permits sequential delivery of multiple cas9 RNPs that potentially eliminates chromosomal rearrangement. We propose to innovate and apply optimized VECT device to perform multiplexed gene editing of primary T cells with subsequent studies on the impact of gene editing workflow on chromosomal stability and cell potency, and on the application of biomechanics to favorably transfect T cells. This work will contribute significantly not only to the understanding of how different gene editing workflows impact genomic stability and how biomechanics affect cargo transport, but it also will provide a promising new platform that can generate more effective and safer engineered T cell products that will benefit cancer patients broadly.

## **2.2 Aim 1: Using Critical Design Features To Achieve Reproducible And Efficient Delivery**

In this aim, we focus on understanding the Critical Design Features (CDE) for optimal delivery to T cells. Based on prior findings of sufficient strain rate as the main requirement for convective delivery, we hypothesize that device fabrication, design and operational parameters that impact strain rate will be the CDEs. We then hypothesize controlling a single or multiple CDEs enables **consistent** and **efficient** delivery to primary T cells. Specific parameters to be tested include fabrication methods and microchannel design, including existence of focusing features and clearing zones termed gutters, compression number, duration, and post-compression recovery time. Optimization outcome will be based on result reproducibility, delivery efficiency using 500KD FITC-dextran, post-processing viability, and cargo concentration. Additionally, we propose to use high-speed video analysis to understand the cell, fluid, and microstructure interaction in each design for a thorough mechanistic understanding. Expected results include the development of a reliable microfluidic device with high T cell editing efficiency, viability, memory phenotype, and normal proliferation. Potential challenges related to cell size variation will be addressed through alternative approaches such as using unstimulated T cells or size-based cell sorting to ensure uniform distribution.

## **2.3 Aim 2: Capability to perform Sequential Gene Editing of CAR T Cells using multiplexed CRISPR/Cas9 Delivery**

In this aim, we will demonstrate functional delivery and gene knockout using the optimal device designed from aim 1. To demonstrate impact, we will compare all results

to the current gold-standard method electroporation that is a clinically established method for RNP delivery. We hypothesize that T cell function, including proliferation, activation, phenotype, and cytotoxicity upon CAR functionalization, will be equivalent to the no device control groups and improved compared to electroporation.

We also hypothesize that the improved cell health after processing that T cells will survive two consecutive VECT processing steps, enabling us to introduce sgTCR and sgB2M RNP sequentially. The benefit of a sequential process will be a decrease of negative outcomes associated with multiple double strand breaks to the genome. The study will focus on assessing knockout efficiency, genomic stability, chromosomal translocation events, and T cell memory phenotype. By utilizing a qPCR translocation assays, the study will evaluate DSB repair kinetics and chromosomal translocation at different time points post-editing. Furthermore, CAR-T cell potency will be evaluated through killing assays using CD19+ Nalm6 and Raji cells. Expected results include a lower translocation rate in the sequential delivery group compared to batch delivery that results in better memory formation and more efficient tumor elimination.

#### **2.4 Aim 3: Contributions of Fluid and Cell Mechanics to Mechanoporation Delivery**

In aim 3, we investigate the correlation between T cell biomechanics, fluid mechanics, and transfection efficiency with the goal to manipulate device and process design for improved delivery by VECT. We hypothesize through changing device design and operational conditions, we alter forces exerted on cells to along with convective delivery. Cells are naturally heterogenous in their mechanics. Some cells likely experience more forces under the same external condition due to a different mechanical property. Hence, we hypothesize that there exist a group of cells with mechanics suitable for efficient

delivery by VECT. Both external (device features and flow profile) and internal variations work together to predict cell transfectability. This study will utilize high-speed video analysis and atomic force microscopy (AFM) coupled with fluorescent cargo delivery to assess whether changes in T cell mechanics, for example through activation, to affect the delivery outcome. First, we will evaluate fluid-cell and micro-constriction-cell interaction using high-speed video analysis in various constriction designs to elucidate a set of relevant fluid dynamic features affecting delivery outcome. we will evaluate biomechanical characteristics, including cell and nucleus size, stiffness, and viscoelastic relaxation time, using imaging-based method and AFM. Finally, we will fluorescent dextran delivery to correlate outcomes to biomechanics and fluid mechanics. Modifications in cell mechanics will also be conducted through pharmacological treatments to confirm the correlation.

## 2.5 References

- [1]. Liu, A., et al., Cell Mechanical and Physiological Behavior in the Regime of Rapid Mechanical Compressions that Lead to Cell Volume Change, in *Small*. 2019. p. e1903857.
- [2]. Uvizl, A., et al., Efficient and gentle delivery of molecules into cells with different elasticity via Progressive Mechanoporation. *Lab on a Chip*, 2021. **21**(12): p. 2437-2452.
- [3]. Kizer, M.E., et al., Hydroporator: a hydrodynamic cell membrane perforator for high-throughput vector-free nanomaterial intracellular delivery and DNA origami biostability evaluation. *Lab on a Chip*, 2019. **19**(10): p. 1747-1754.

## **CHAPTER 3. USING CRITICAL DESIGN FEATURES TO ACHIEVE REPRODUCIBLE AND EFFICIENT DELIVERY**

### **3.1 Introduction**

Development of reliable and efficient manufacturing processes capable of consistently producing high-quality cell transfection is central to the success of translocation of mechanoporation to clinical use. Consistent with this perspective, prototyping of mechanoporation devices should include consideration of device robustness and data reproducibility. In microfluidic devices, small deviations during fabrication and operation can have profound impact on the balance of physical factors, causing cells to experience different forces and to deviate from predicted behavior [1]. Therefore, understanding the source of result variation is necessary for robust device usage. They must achieve consistent performance across multiple production runs and batches. This necessitates stringent control over device fabrication, operational parameters, and quality assurance measures to minimize batch-to-batch variation and ensure reproducible outcomes.

Central to the reliable operation of microfluidic devices is the concept of critical design features. CDEs encompass specific characteristics that are “function or feature of an engineered system that is necessary to consistently manufacture products with the desired quality attributes” [2]. In the context of microfluidic transfection devices, quality attributes can mean transfection efficiency, resulting viability, cell phenotype, and cell function. CDEs related to these parameters can include flow rate, constriction size, constriction duration, device surface chemical modification. Understanding CDEs ensures optimal and reproducible result for mechanoporation.

Previously, research has shown that operational flow rate and constriction size are design features that critically impact device performance for processing K562 and Jurkat cell lines [3]. Yet, a list of VECT device critical design features has never been comprehensively studied for primary T cells.

In this chapter, we explore the significance of CDEs in the context of VECT transfection outcome in primary T cells. We discuss the challenges associated with testing, understanding, and maintaining these design features in VECT devices and outline strategies for optimizing fabrication techniques. Second, we tackle what device design features may aid processing of T cells. Finally, we test operational protocols to mitigate variability and ensure edited T cell quality. By focusing on CDEs, we aim to provide insights into the key factors influencing the performance of microfluidic mechanoporation devices broadly to facilitate their translation into reliable and scalable manufacturing processes for cell-based therapies.

### **3.2 Definition And Methodologies to Manipulate CDEs**

In this section, we aim to define parameters that significantly impact VECT performance by delivering a fluorescently-conjugated dextran molecule and examining the delivery efficiency, cell viability, delivered concentration, and reproducibility across various operating processes. We aim to comprehensively understand the impact of varying fabrication process, operating parameters, and device design, and define a list of factors impacting delivery outcome and device robustness, as well as developing a simple analytical method for quantifying the most essential feature.

To examine device reliability, we developed a microscopy-based method for quantifying operating gap size that overcomes the limitations of traditional approaches using fluorescent solution to flow inside a microchannel. Furthermore, we pioneered a new fabrication method utilizing castable epoxy material to reduce deformation and enhance reliability. Additionally, we explore alternative materials such as reinforced PDMS and epoxy-based devices to eliminate deformation under high pressure.

By addressing these issues head-on, we strive to establish a robust framework for achieving reproducible and reliable mechanoporation outcomes. Through our multidimensional approach, we aim to define CDEs that will not only optimize device robustness and performance but also pave the way for advancements in mechanoporation technology with broader translational implications

### *3.2.1 Robust Prototyping Needed for Reproducible Results Under High Pressure*

VECT was found to achieve high delivery to Jurkat, a T cell derived cell line [cite, AL paper]. Yet, when the same design and operating parameters were tested on primary T cells, they failed to produce consistently good results (data shown in Figure 3.6 B “Plain PDMS device”). We observed a major difference between the cell lines and primary human T cells is their biomechanics, including cell stiffness and size. As shown in Figure 3.1, Jurkat cells are much larger, with an average  $13.5 \pm 2.44\mu\text{m}$  cell diameter; whereas T cells, even after 24-hr activation with anti-CD3/anti-CD28 dynabeads, have a smaller cell diameter of  $8.99 \pm 0.83\mu\text{m}$ . Unstimulated T cells are even smaller than activated T cells, with an average diameter of  $7.21 \pm 0.40\mu\text{m}$  Thus

clearly the 4-6 $\mu\text{m}$  difference in cell diameter would require a smaller constriction size or faster cell velocity to compress cells with the same strain rate.

However, it is not simple to make devices to synergistically achieve small constriction size and fast operational velocity during rapid prototyping phase.

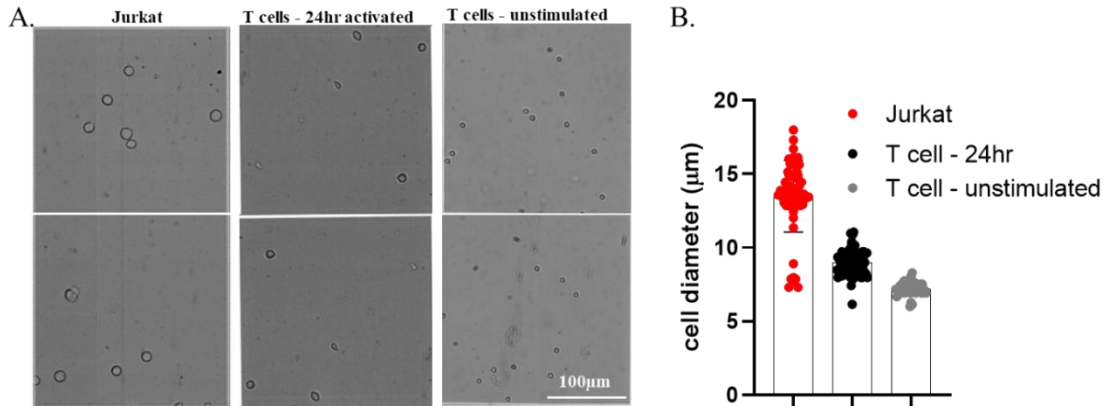


**Figure 3.1: Cell size analysis shows significant difference in cell diameter between cell line and primary T cells.** A) Images of Jurkat T cells (left) and primary T cells, activated for 24 hours (middle) or unstimulated (right) B. cell size calculated from images indicated Jurkat cells are significantly larger than primary T cells, both activated or unstimulated,  $p < 0.0001$ . 24-hour stimulated T cells are significantly bigger than unstimulated T cells,  $p < 0.001$ . Stat test: one-way ANOVA.  $N = 80-100$ . Error bar = SD.

Conventionally, microfluidic devices for mechanoporation have been fabricated using Poly(dimethyl siloxane) (PDMS), an elastic polymer favored for its low cost and ease of fabrication. Nonetheless, PDMS devices are prone to deformation and changes in geometry under high pressures, which can significantly affect cell interactions within the microchannels [4, 5]. Indeed, when we tested flow rate in VECT devices with pressure ranging from 1-8 bar, the result indicated that PDMS devices could only tolerate pressure up to 4 bar before delamination. Moreover, the pressure-flow rate relation was linear below 3bar, indicating channel deformation at higher pressure

(Figure 3.2). As mechanoporation relies on interactions between cells and microchannels, a small deformation can greatly alter the force on cells.

From these observations, we hypothesize that operating gap size post deformation is one of the CDEs for VECT devices.

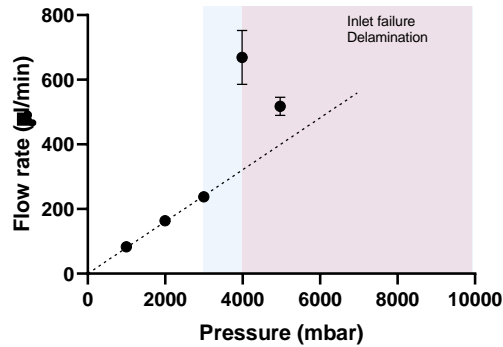


**Figure 3.2: Pressure-flow rate relation in PDMS devices indicating deformation.** A nonlinear pressure-flow rate relation above 3bar indicates channel buckling. Above 4 bar, the inlet starts to leak and devices delaminate. Blue region: nonlinear flow. Red region: device failure. N=3. Error bar = SD.

### 3.2.2 A microscopy-based method to quantify operating gap size

Understanding the operating channel geometry of devices is important to understand its influence on delivery efficiency and other desired cellular responses. As a part of our effort to identify, quantify, and control CDEs for VECT, we would like to precisely quantify the channel geometry under relevant pressure conditions within our microfluidic mechanoporation devices. However, accurately measuring channel geometry has proven challenging with the previously described fluorescent imaging method [4]. Due to fluorescent spill over into other z-stack layers, accurately delineating the edge of the device becomes difficult, impeding the precise measurement of deformation.

In this section, we introduce a microscopy-based method using positive fluorescent contrast to quantify the operating gap size within microfluidic mechanoporation devices. We begin by discussing the limitations of existing imaging techniques, particularly negative contrast imaging, in which a fluorescent fluid is flowed through the channel while imaging with a confocal fluorescent microscope. This method has been commonly employed for channel deformation studies [5, 6]. Negative contrast imaging relies on fluorescent agents to highlight the interior of channels (Figure 3.3, top), yet its accuracy is hindered by dependencies on microscopy settings. For example, increasing exposure time caused increased signal intensity outside the imaging focal planes, leading to overestimate of channel height. The brightness and the cutoff of fluorescent signal can be altered based on the exposure and signal gain value, leading to variability in measurements.

To address these limitations, we developed a positive contrast imaging method, with fluorescent molecules outlining the exterior of the microchannel (Figure 3.3, bottom). By fitting the data to a double Gaussian function, we were able to calculate the channel height as the distance between the two Gaussian peaks, minimizing reliance on instrument settings and enhancing measurement precision.

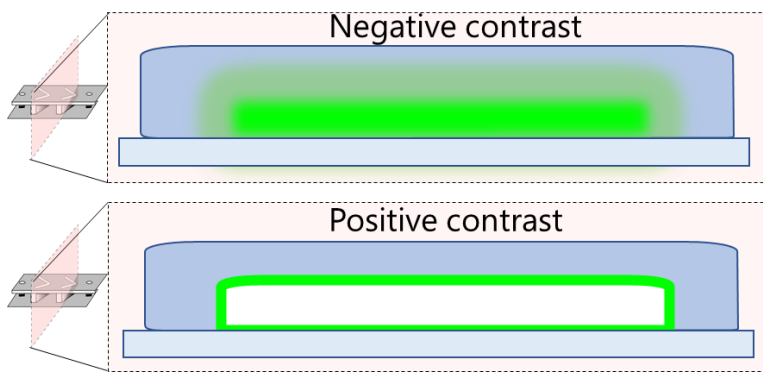


**Figure 3.3: Schematic illustration for the difference between negative and positive imaging method.**

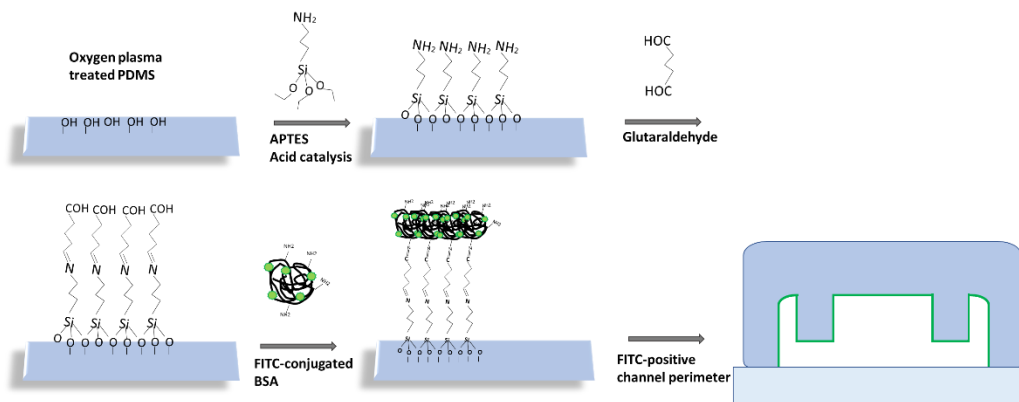


**Figure 3.4: Schematic illustration of conjugation method to link FITC-BSA to PDMS and glass.** After conjugation, devices are outlined with fluorescent signals around the perimeter for positive contrast imaging.

We first developed a chemical conjugation method to covalently link fluorescein-bovine serum albumin (FITC-BSA) to PDMS. Briefly, we functionalized PDMS with amine groups using (3-Aminopropyl)triethoxysilane (APTES); then linked glutaraldehyde to the amine groups; and finally, using the free aldehyde groups, covalently linked FITC-BSA to PDMS (Figure 3.4). The devices were imaged using a fluorescent confocal microscopy perpendicular to the direction of flow at various pressures (Figure 3.5). After image acquisition, we plotted fluorescent intensity from the top of microchannel to the glass, at the middle of the channel to measure maximum deformation. For negative contrast images, we fitted the curve to a Gaussian function and used  $\pm 1, 2,$  and  $3$  standard deviations ( $\sigma$ ) from the mean as the channel height (Figure 3.5 A). For positive contrast images, we fitted the curve to 2 Gaussian functions and used the distance between the 2 means as the channel height (Figure 3.5 B). To validate the efficacy of our positive contrast imaging method, we compared the measured channel heights obtained through negative contrast imaging, positive contrast imaging, and profilometry performed on the silicon wafer on the same

microfluidic channels. Profilometry data indicated a mean height of  $26.92 \pm 0.174 \mu\text{m}$ , while the new positive contrast method resulted in  $22.97 \pm 1.365 \mu\text{m}$  resting channel height, and negative contrast method resulted in  $21.36 \pm 0.451 \mu\text{m}$ ,  $42.72 \pm 0.901 \mu\text{m}$ , and  $64.08 \pm 1.352 \mu\text{m}$  resting channel height based on  $\pm 1\sigma$ ,  $\pm 2\sigma$ , and  $\pm 3\sigma$  cutoff (Figure 3.5 C). All measurements from negative contrast method were statically different from profilometry data. Because the result from  $\pm 1\sigma$  cutoff is the closest to profilometry result, we used it for later deformation analysis.

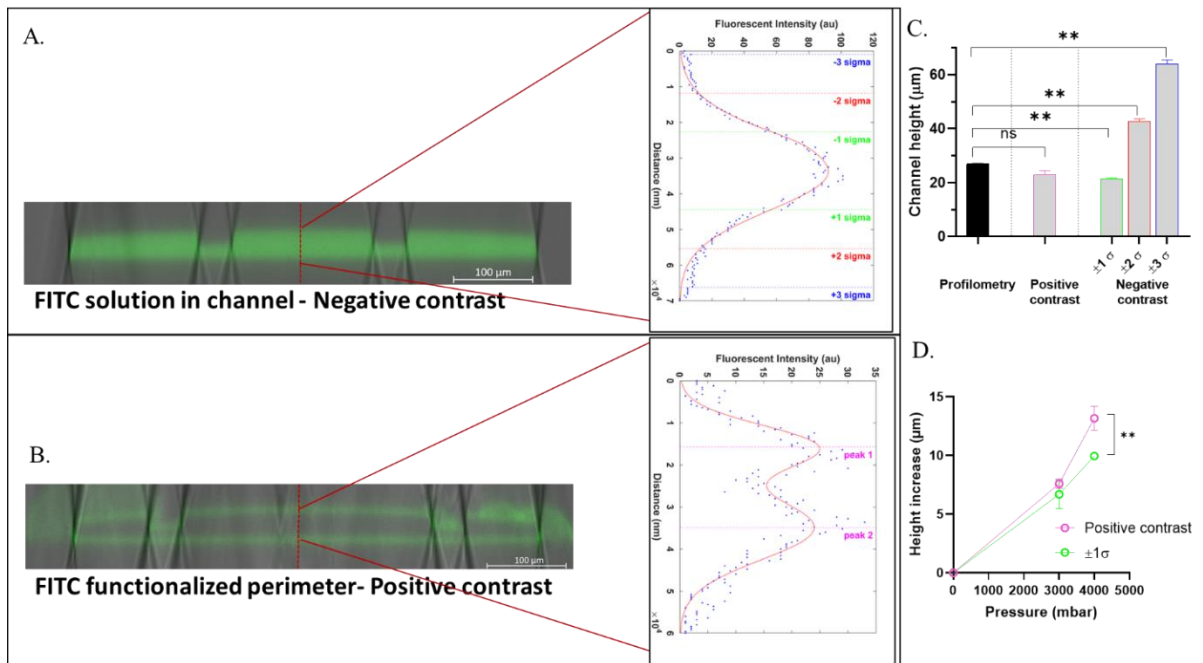


**Figure 3.5: Positive contrast imaging method provides more quantitative channel measure with better accuracy.** A) schematic and image of a VECT device cross-section imaged by negative contrast method. Fluorescent intensity is plotted along the red line and data modeled as a single Gaussian curve with  $R^2=0.9880$ . Channel height is measured as distance across 68%, 95%, and 99.7% of the curve ( $\pm 1$ ,  $\pm 2$ , and  $\pm 3 \sigma$ ). B) schematic and image of a VECT device cross-section imaged by positive contrast method. Fluorescent intensity is plotted as double Gaussian curves with  $R^2=0.9294$ . Channel height is measured as distance between the two peaks. C) channel height measured from profilometry on silicon wafer, positive contrast, and negative contrast imaging of PDMS devices are compared. D) channel deformation under two flow rate is plotted based on positive contrast and the most accurate negative contrast method. \*  $P < 0.05$ . \*\*  $P < 0.01$ . Stat test: one-way ANOVA.  $N=3$ . Error bar=SD.

We then investigated the degree of channel deformation under flow conditions. At 3 bar pressure, both methods indicated similar degree of channel height increase of  $7.60 \pm 0.40 \mu\text{m}$  and  $6.69 \pm 1.21 \mu\text{m}$ . At 4 bar pressure, however, the negative contrast method indicated  $9.96 \pm 0.14 \mu\text{m}$  height increase, while the new negative contrast method resulted in significantly higher increase of  $13.17 \pm 1.01 \mu\text{m}$  (Figure 3.5 D). Because the positive contrast method gave statistically the same height readout as the standard profilometry method, we believed the deformation result measure by it was more accurate than the negative contrast method at  $\pm 1\sigma$  cutoff. This suggests that previously used negative contrast method tended to underestimate microchannel displacement especially under high deformation condition.

Overall, our results indicated that positive contrast imaging yielded measurements comparable to silicon profilometry. In addition, positive contrast is more robust, providing images with quantifiable fluorescent boundaries for robust data processing, without manual determination by users. Due to these reasons, we conclude that positive imaging method is more reliable in dynamic microfluidic systems where large channel geometry may change during operation.

### *3.2.3 New Fabrication Method to Reduce Deformation*

After confirming deformation with the imaging method, we explored other more rigid materials for fabrication. Commercially, most microfluidic devices are fabricated with plastic such as polystyrene and poly methyl methacrylate (PMMA) using hot embossing. Yet, this method is costly for small batches of devices and has a long lead

time, making it unsuitable for rapid prototyping in a research laboratory. Alternatively, researchers have attempted to make hybrid device of PDMS on a stiff substrate. For example, using PDMS-glass composite material, it has been shown the resulting devices had much channel buckling [6].

We first fabricated composite devices by pouring a small amount of mixed PDMS on a silicon wafer with manual rotation until the wafer is covered by PDMS. Then we cured on a hot plate. Afterwards, we added rectangular glass to cover the microchannel, leaving only the inlet and outlet uncovered. Finally, we poured PDMS to form the bulk body of the devices (Figure 3.6 A, “Manually equilibrate”). We used devices with pre-deformation gap size of 3  $\mu\text{m}$  and performed delivery at 4 bar to achieve a 200  $\mu\text{L}/\text{min}$  flow rate. This hybrid device did improve delivery efficiency compared to PDMS devices. Yet, it also showed variability across batches, with a mean delivery efficiency of 20.17% and a coefficient of variation (CV) of 91.70% (Figure 3.6 B). We therefore devised other fabrication methods in which we pour

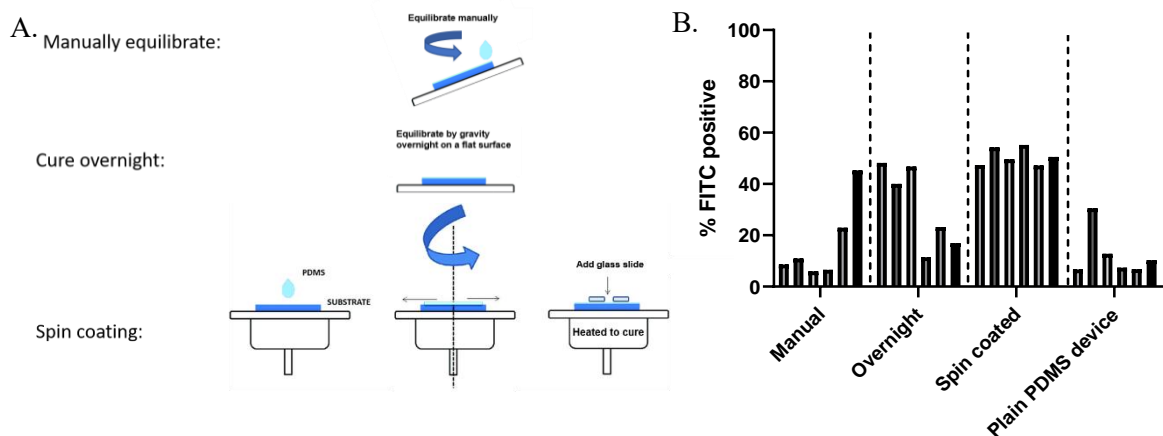


**Figure 3.6 PDMS-glass composite devices improved transfection if fabricated with spin coating method.** A) illustration of the 3 methods used to make hybrid devices. B) delivery data consistency across 3 hybrid fabrication methods, compared with plain PDMS devices.

PDMS and to equilibrate to a more uniform thickness overnight (Figure 3.6 A, “Cured overnight”), or used a spin coater to control the initial PDMS layer thickness (Figure 3.6 A, “Spin coating”). Comparing efficiency and consistency, we found that spin coating gave the highest delivery efficiency to primary T cells activated for 24 hours,

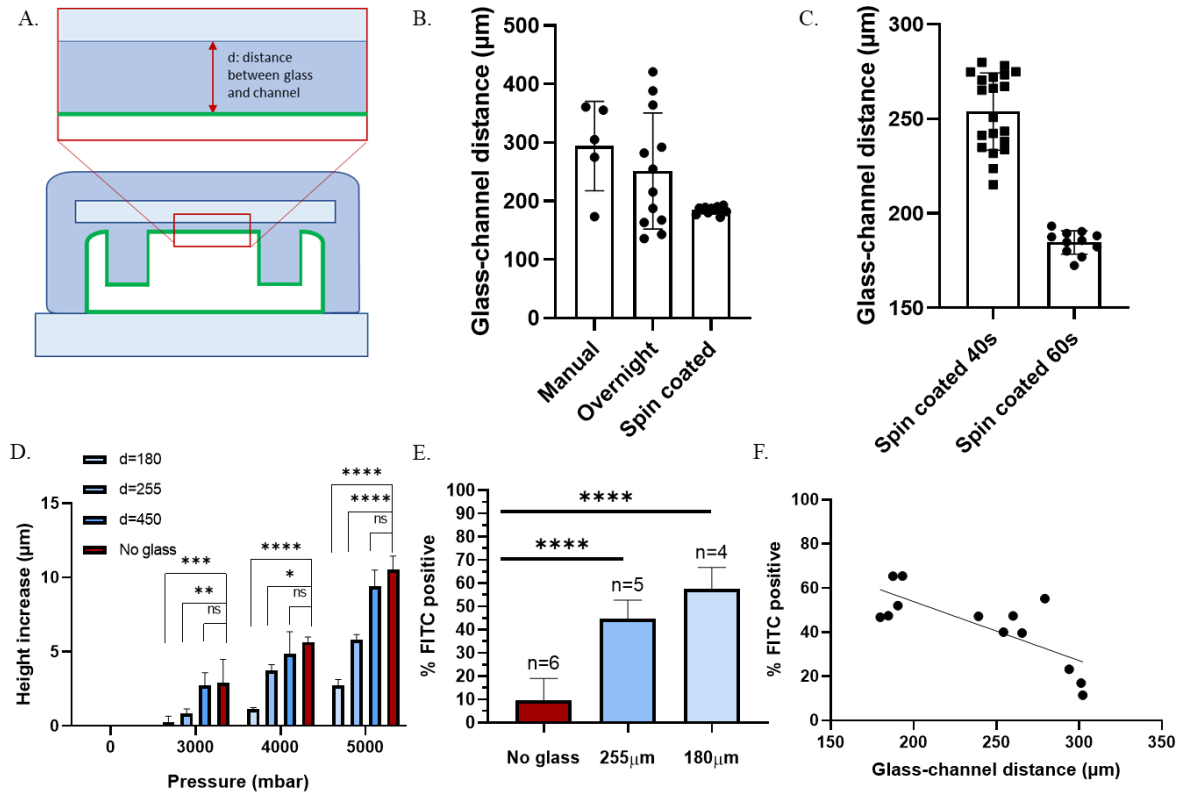


**Figure 3.7 Glass-microchannel distance is a deterministic attribute of transfection success in PDMS-glass composite devices.** A) illustration of glass-microchannel distance,  $d$ . B)  $d$  distribution from the 3 methods used to make PDMS-glass hybrid devices. C) Spin coating parameter, namely the time of spinning, can change  $d$ . D) smaller  $d$  devices are more efficient at controlling deformation.  $N=3$ . E) smaller  $d$  devices are more efficient at delivery to Jurkat. See graph for number of replicas. F) a clear negative relation between  $d$  and transfection efficiency.  $R^2 = 0.76$ ,  $p = 0.0025$ . D: Stat = two-way ANOVA. E: Stat = one-way ANOVA. Error bar=SD.

with an average efficiency of 48.00% and a CV of 11.87% across 6 devices. Overnight equilibration showed only slight improvement compared with an average efficiency of 31.11% and CV of 51.12% across 6 devices (Figure 3.6 B).

Spin coating, compared to manual and overnight equilibration methods for PDMS-glass device fabrication, yielded much more consistently manufactured devices, which led to significantly improved delivery outcomes. The major difference between the methods is the uniformity of the initial PDMS layer. Spin coating results in more uniform layer thickness. This observation prompted us to hypothesize that the glass-channel distance ( $d$ ) (Figure 3.7 A) is a crucial CDE, and it determines how much the device deforms under the same pressure. If a fabrication method resulted in uneven PDMS thickness, then device across the same mold will yield inconsistent result.

To test this hypothesis, we measured  $d$  using a bright-field microscopy. We measured the z-location of the focal plane of the inserted glass slide and of the top of the microchannel, and take the difference to be the distance between glass and microchannel. Our data indicated a significantly more consistent  $d$  generated from spin coating than from overnight equilibration (Figure 3.7 B).

Next, we focused on controlling the glass-channel distance ( $d$ ) in PDMS-glass devices through precise manipulation of the spin-coating parameters during PDMS film deposition (Figure 3.7 C). Through systematic experimentation, we fabricated PDMS-glass devices with varying  $d$  values (455  $\mu\text{m}$ , 250  $\mu\text{m}$ , and 180  $\mu\text{m}$ ) and subjected these devices to channel pressures of 3, 4, and 5 bar. Our results showed a direct relationship between channel deformation and  $d$ , with minimal deformation observed in channels with  $d = 180 \mu\text{m}$ . Conversely, when the glass was positioned too far from the channel ( $d = 455 \mu\text{m}$ ), its capacity to reinforce the channel was compromised, leading to increased deformation (Figure 3.7 D). This underscored the

critical role of reproducible reinforcement in overall device performance, highlighting the need for meticulous control over this parameter in microfluidic mechanoporation device fabrication.

To assess the impact of deformation on transfection efficiency, we conducted transfection experiments using Jurkat T cells (average diameter 14 $\mu$ m) at 5 bar pressure in 5.6  $\mu$ m gap VECT devices with  $d$  values of 255  $\mu$ m and 180  $\mu$ m. Remarkably, we observed enhanced transfection in devices with smaller  $d$  (57.58% vs. 47.82%, Figure 3.7 E). A linear regression with combined data revealed a significant negative correlation between  $d$  and delivery efficiency (Figure 3.7 F) with a p-value of 0.0025. The regression gave a linear relation of delivery efficiency =  $-0.2528*d + 101.6$  and a Y intercept of 401.7  $\mu$ m. This can be interpreted as every 1  $\mu$ m deformation reduces delivery by 0.25%. With no deformation, this device in theory can achieve 100% transfection efficiency. And with a  $d$  over 400  $\mu$ m, there is no delivery. This interpretation is consistent with prior observation that at  $d=450$   $\mu$ m glass composite devices had the same degree of deformation as plain PDMS devices. This study shed light on the correlation between deformation limitation and improved device functionality, confirming the reinforcement distance as a crucial CDE for the composite devices.

### 3.2.4 New Material for Rigid Device to Eliminate Deformation

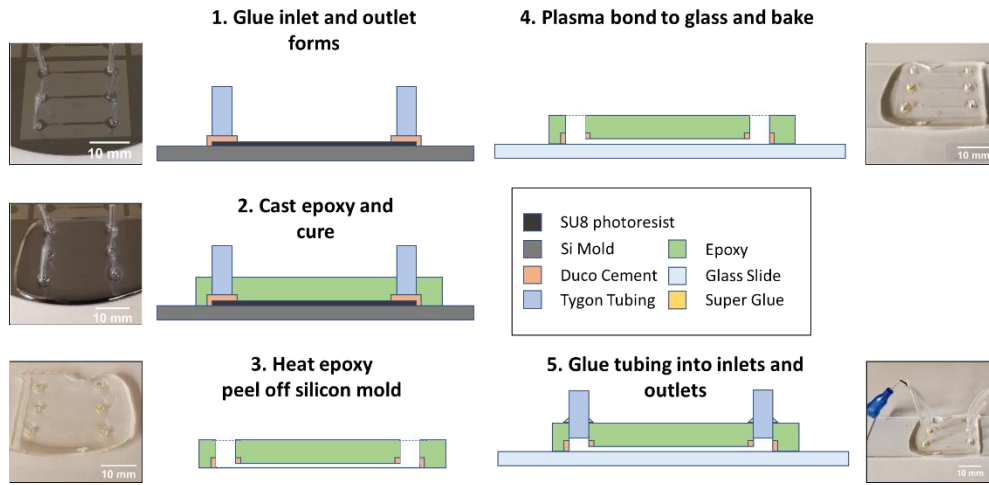


**Figure 3.8 Epoxy device fabrication process through replica molding.**

As an alternative to PDMS-glass devices with stronger material properties, new fabrication materials were needed for transfecting smaller primary cells effectively. Even the most efficient PDMS-glass device exhibited positive deformation at high pressures and small gap sizes needed to induce compression or volume exchange in unstimulated primary T cells with diameters between 7-8  $\mu\text{m}$ . Recognizing this limitation, we explored alternative materials with higher stiffness and the same replica molding compatibility [7].

We tested an epoxy-based material for replica molding on silicon-SU8 wafer. The epoxy chosen exhibited a material Young's modulus of 2 ~ 5 GPa, 1000-fold higher than PDMS of 1 MPa [8]. Briefly, epoxy and cross-linking agent was mixed and poured over the microchannel on the mold with preformed inlet and outlet ports,

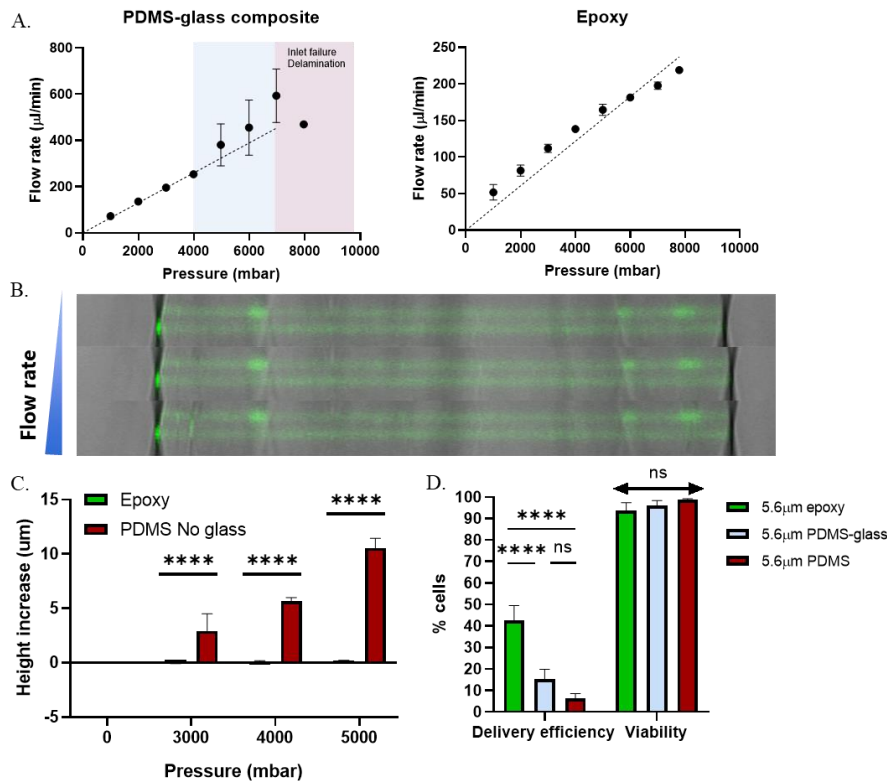


**Figure 3.9 Epoxy replica molding gave devices without deformation and are able to transfect to unstimulated T cells.** A) pressure-flow rate plot in PDMS-glass composite and epoxy devices. Blue region: nonlinear flow. Red region: device failure. B) positive contrast fluorescent imaging showing no deformation in epoxy devices. C) epoxy devices showed nearly zero height increase at 0-5000 mbar pressure. D) epoxy devices resulted in 3-fold higher delivery than PDMS-glass devices, and 7-fold higher delivery than PDMS devices to unstimulated T cells; viability of T cells remained the same. Stat = one-way ANOVA. N=3. Error bar=SD.

cured for 24 hours, heated to soften the cured epoxy, and bonded to glass slide after plasma treatment (Figure 3.8). Compared with plain PDMS or PDMS-glass composite devices, epoxy devices have a linear pressure-flow rate relation, indicating

no deformation. And they can tolerate 8 bar pressure, the limit of the pressure controller we used, without delaminating or leaking (Figure 3.9 A).

Using the same imaging method, we determined that epoxy devices showed no deformation at all tested pressure (3-5 bar), confirming the rigid nature of the material (Figure 3.9 B and C). We then tested delivery capability in unstimulated T cells, which had an average diameter of 8  $\mu\text{m}$ . We thus chose a 5.6 $\mu\text{m}$  gap device to exert 30% strain, and used 5 bar pressure to achieve an estimated flow rate of 200 $\mu\text{L}/\text{min}$ . Indeed, epoxy devices gave the highest delivery efficiency of 500KD FITC-dextran, with an average efficiency of 42.53%, comparing to 15.2% in PDMS-glass composite devices and 6.47% in PDMS devices (Figure 3.9 D). Epoxy devices, at least at 30% strain, did not significantly reduce T cell viability assessed by propidium iodide (PI) (Figure 3.9 D), with over 90% of cells remaining viable post-mechanoporation. This finding substantiated the notion that mechanoporation techniques could preserve cell viability compared to conventional methods such as electroporation, further emphasizing the potential of epoxy-based devices in facilitating efficient transfection of primary cells while maintaining cellular integrity.

### *3.2.5 Optimal Microfluidic Channel Design for Maximum Functional delivery*

After establishing a fabrication method that provides consistent critical features for fabrication and delivery outcome, we fabricated multiple designs of the VECT devices with an aim to transfect 24-hour activated T cells. These variations included: constriction gap size, cell velocity/operating pressure, inlet cell focusing feature,

clearing zones termed gutters, compression number, duration, and post-compression recovery time.

As marked in Figure 3.10 A, we tested three design features of the VECT device. First, we evaluated a serpentine focusing structure connecting the inlet and channel. The serpentine region was designed to use the Dean force to focus cells to the middle of the channel to increase the number of cells compressed by the ridge constrictions<sup>36</sup>. We reasoned that small T cells required a small ridge gap which increased the flow resistance and directed a high volumetric flow through the gutter region. Next, different arrangements of chevron ridges were tested including ridge spacing, width, and number of ridges. Within the compression channel, the ridge layout, including width, count, and spacing, are hypothesized to impact cargo delivery to cells based upon resulting cycles of volume exchange. Finally, we evaluated the effect of the gutter regions that flank the chevron ridges, which were originally included to vent cell aggregates and improve volumetric flow. We tested how the gutters alter the flow pattern and can in principle reduce cell transfection efficiency. Variations in design of serpentine, ridge layout, and gutter were optimized by evaluating the delivery of a fluorescently conjugated dextran (500,000 Dalton, similar to the molar weight of RNP) with flow cytometry. We used percentage delivery, cell viability immediately after processing, and intracellular cargo concentration to comprehensively quantify the efficiency of each design (Figure 3.10 B).

The compression gap and flow rate were optimized to T cell biomechanical responses. We measured the T cell diameter on various days prior to and post activation in two healthy donors (Figure 3.10 C). The result indicates cells expanded

in size post activation from 8.0  $\mu\text{m}$  to 9.3  $\mu\text{m}$  ( $8.9 \pm 0.8$  donor 1 and  $9.6 \pm 1.3$  donor 2) 24-hour post activation. Cells further expand to 12  $\mu\text{m}$  on day 2 that persisted

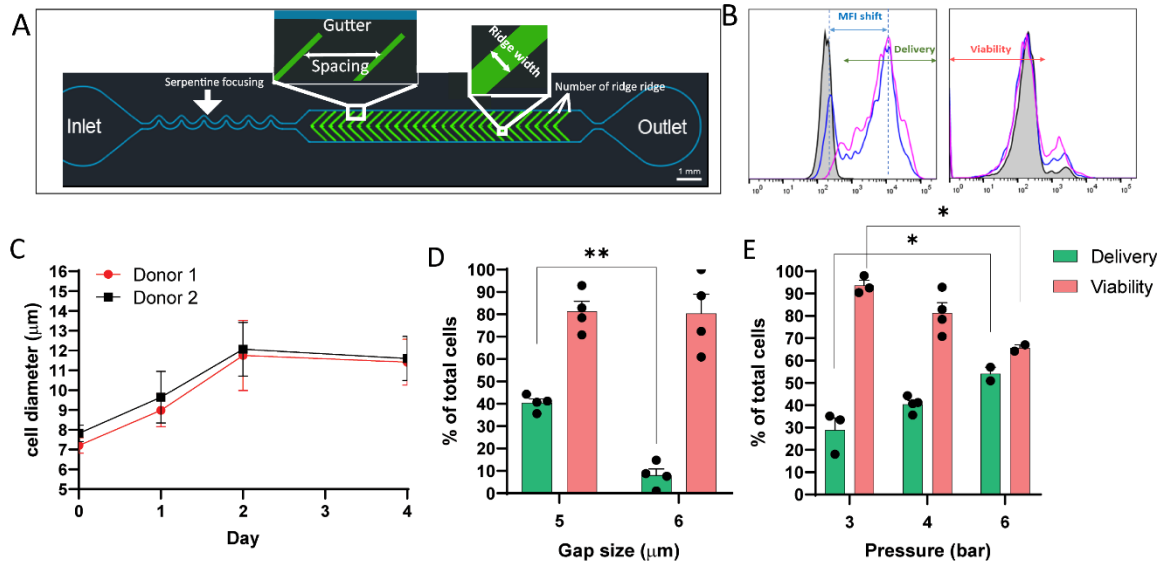


**Figure 3.10: VECT device design and optimization schematic.** A) a device schematic showing three features optimized in this study. B) exemplary flow cytometry histograms of FITC and 7-AAD. Arrows indicate gating strategies used to quantify delivery efficiency (percentage of FITC positive population), mean fluorescent intensity (MFI) shift (fluorescent intensity ratio of positive and negative population), and cell viability (percentage of 7-AAD negative population). C) T cell size from two donors on day 0-4 post activation is measured by bright field microscopy. T cells from donor 2 activated for 24 hours is used for the following optimization experiment. D and E) Delivery efficiency and viability of T cells processed in 4.5 or 5.5  $\mu\text{m}$ -gap device, and under 3, 4, or 6 bar pressure. D: Stat = t-test. E: Stat = one-way ANOVA. \* p-value < 0.05, \*\* p-value < 0.01. Error bar=SD.

throughout expansion. We decided to choose the 24-hour activated T cells instead of 48-hour to reduce ex vivo culture time and boost T cell product potency [cite]. Since their sizes are larger, we used the previously described PDMS-glass composite fabrication method instead of epoxy devices.

We tested 5  $\mu\text{m}$  and 6  $\mu\text{m}$  gap (post deformation gap) devices to compress the cells corresponding to strain of 0.48 and 0.35 (Figure 3.10 D). We found that the 5  $\mu\text{m}$  gap resulted in improved delivery with an average of 40% transfection efficiency

and >80% viability, compared to a 10% delivery for the 6  $\mu\text{m}$  gap. This observation is consistent with the finding that a strain of 0.5 is sufficient to produce volume exchange [9]. Next, we optimized the flow rate under various pressures (Figure 3.10 E). We observed that increased delivery corresponded with increasing pressure. However, we also found a decrease of cell viability with pressure. Since the viability dropped by 20% when pressure changes from 4 to 6 bar whereas the delivery efficiency increased by 10%, further experiments were conducted with 5  $\mu\text{m}$  gap operated under 4 bar pressure.

The serpentine inlet was added to counteract the high flow resistance from the small ridge gaps by focusing cells to the middle of the channel. The focusing was evaluated with devices that have 12 sets of 10  $\mu\text{m}$ -wide ridges with 440  $\mu\text{m}$  spacing between each ridge. Three designs were tested: a serpentine with small radius of curvature (80  $\mu\text{m}$ ) denoted as “high focusing efficiency”, a serpentine with large radius of curvature (120  $\mu\text{m}$ ) denoted as “low focusing efficiency”, and no serpentine neck (Figure 3.11 A). We evaluated the capacity of the serpentine to ensure cells passed under the ridges and avoid flow into gutters. Using high-speed video microscopy, we tracked the position of cells, and visualized the cell paths relative to the ridges. From the cell trajectory maps, we see that both types of serpentine focus cells to be uniformly compressed under the first ridge. With no serpentine, we observed 39.8% of the cells flowed into the gutter of the first ridge and were not compressed (Figure 3.11 A and B). We found that the percentage of cells compressed by ridges is significantly lower in the no focusing inlet device compared to both serpentine designs (99.5 $\pm$ 0.79% and 98.7 $\pm$ 0.63% in high and low efficiency

serpentine) (Figure 3.11 B). It was also observed that the FITC-dextran delivery efficiency with a serpentine channel averaged 40-45%, while in devices without a serpentine we observed only 10% FITC positive population (Figure 3.11 C). In experiments going forward, we decided to use the high focusing efficiency inlet due to a higher resulting MFI shift.

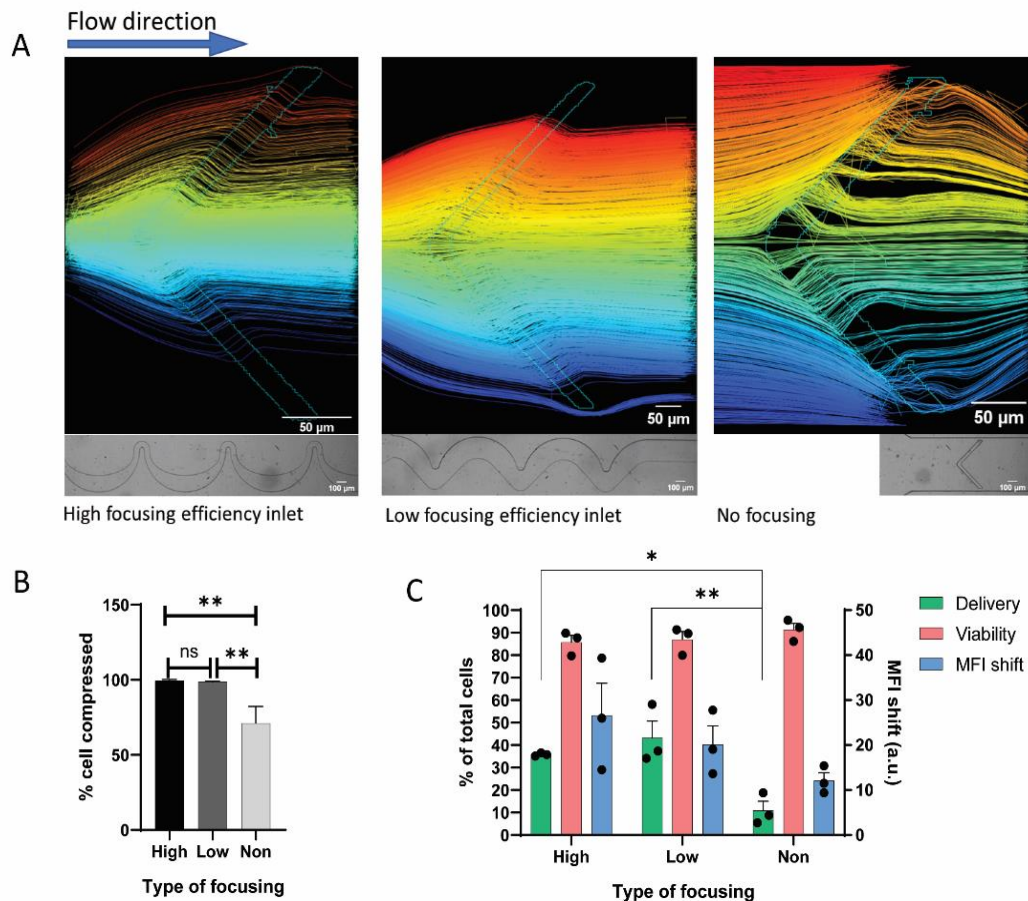


**Figure 3.11: serpentine inlet focuses cells under ridges for compression and improves delivery efficiency.** A) cell trajectories upon interaction with the first ridge is plotted for devices with three types of serpentine channels shown in the bright field microscopy image. Color indicates Y-position of trajectories. B) Focusing efficiency, calculated as the percentage of trajectories under the first ridge, is plotted. N = 3 for each type of focusing. \* p-value < 0.05, \*\* p-value < 0.01. C) Delivery efficiency, viability, and MFI shift of T cells processed in devices with three serpentine inlet types. Stat= one-way ANOVA. Error bar=SD.

Next, the ridge arrangement was optimized by evaluating the ridge width, spacing, and count. We designed devices with 10, 20, and 40  $\mu\text{m}$  wide ridge, with the understanding that ridge width affects both the flow resistance as well as the imposed shear force acting on cells [10, 11]. Although there was no statistical significance associated with the differences, the 10  $\mu\text{m}$ -ridge device results in 14% higher delivery percentage compared with the other two designs ( $45.3 \pm 2.5\%$  compared with

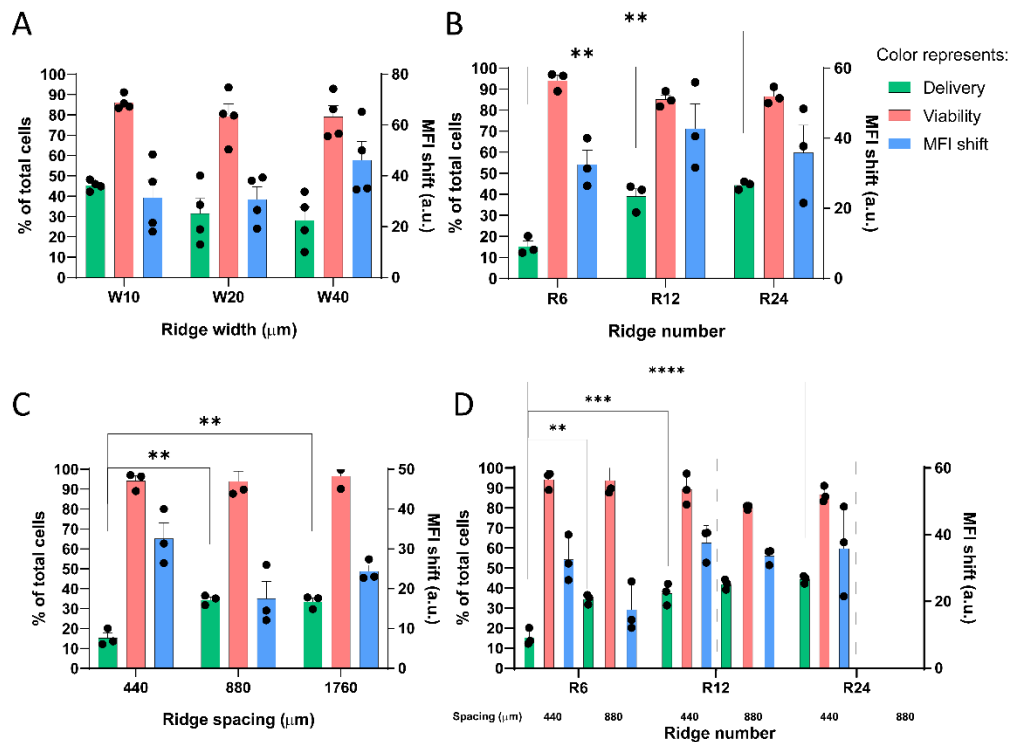


**Figure 3.12: optimization of ridge design.** A) Delivery efficiency, viability, and MFI shift of T cells processed in devices with 10, 20, or 40  $\mu\text{m}$  wide ridge. B) Delivery efficiency, viability, and MFI shift of T cells processed in devices with 6, 12, or 24 ridges. C) Delivery efficiency, viability, and MFI shift of T cells processed in devices with 440, 880, or 1760  $\mu\text{m}$  spacing. D) Combined effect of spacing and ridge number. Stat = one-way ANOVA. Error bar=SD. \*\* p-value < 0.01, \*\*\* p-value < 0.001, \*\*\*\* p-value < 0.0001

31.5  $\pm$  14.8% and 21.9  $\pm$  13.0%) (Figure 3.12 A). This design also has a more consistent performance across 4 replicates. Viability and delivery concentration show no significant difference. We chose to use 10  $\mu\text{m}$ -ridge design in further experiments.

We next optimized the number of ridges. We fabricated devices with 6, 12, and 24 ridges, each with a 440  $\mu\text{m}$  spacing. The data indicate that for this spacing, 12 is the minimal number of ridges required for maximal delivery (Figure 3.12 B). The 6-ridge device only resulted in 10% delivery, while the other two types resulted in significantly higher (40%) delivery efficiency. No difference in viability or cargo concentration was seen.

The last parameter we optimized was the ridge spacing. Ridge spacing of 440, 880, and 1760  $\mu\text{m}$  were tested (Figure 3.12 C). The variations of spacing were tested with the 6-ridge device to accommodate the large spacing which resulted in a long channel length and high flow resistance. To maintain similar flow velocity with previous experiments, we used 3 bar instead of 4 bar pressure used with the 6-ridge devices. We observed that the 880  $\mu\text{m}$ -spacing resulted in significantly higher delivery efficiency compared with 440  $\mu\text{m}$  and was similar to the delivery observed with 1760  $\mu\text{m}$  spacing. As spacing increased, cells were allowed more time in volume recovery between ridges. From the data, we conclude 880  $\mu\text{m}$  spacing, which provides  $\sim 1$  ms cell recovery time between ridges, is sufficient for cells to recover to its pre-compression volume.

To study the combined effect of ridge count and spacing on delivery, we plotted delivery outcome in 6-, 12-, and 24-ridge device with 440  $\mu\text{m}$  and 880  $\mu\text{m}$  spacing (Figure 3.12 D). With 6 ridges, large spacing is results in maximum delivery. However, in 12- and 24-ridge devices, 440  $\mu\text{m}$  spacing is sufficient for optimal delivery. The result suggests the number of ridges is more impactful than the ridge spacing, provided sufficient volume recovery time is reached.

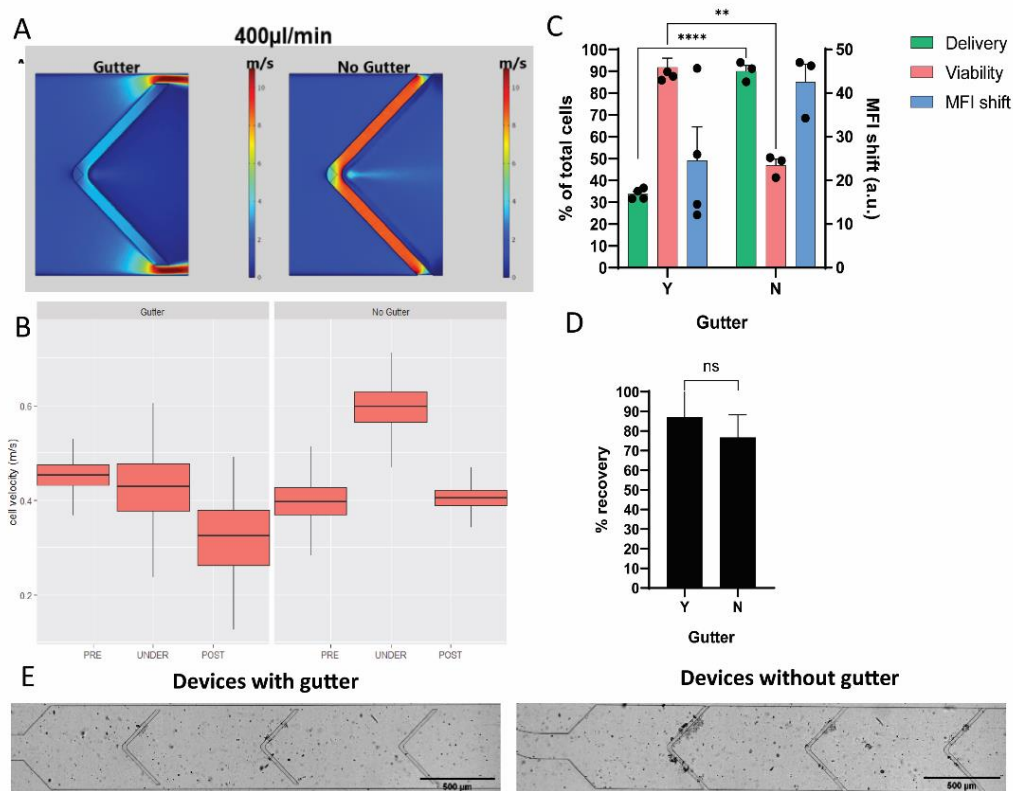


**Figure 3.13: gutter reduces compression rate but helps reduce shear damage on cells.** A) COMSOL simulation of cell velocity inside device with or without gutter under constant flow rate. B) Velocity of cells from high-speed videos are plotted over three locations inside the channel: before cells encounter the ridge (PRE), under the ridge (UNDER), and after cells exist the ridge (POST) in devices with or without gutter. A total of 6000 cells are tracked and plotted. C) Delivery efficiency, viability, and MFI shift of T cells processed in devices with and without gutter. \*\* p-value < 0.01. \*\*\*\* p-value < 0.0001. D) Percentage of cells recovered at the outlet is plotted as the ratio of cell count in 100 $\mu$ L device-processed T cells to cell count in 100 $\mu$ L non-processed control. E) bright field microscopy image showing channels after cell passage. N=3. Stat = t-test. Error bar=SD.

Finally, we tested the effect of having a gutter. Serpentine devices with a 6-ridges and 880  $\mu$ m ridge spacing were produced with and without gutters and operated with 3 bar pressure. We had previously hypothesized that the gutter altered the flow pattern providing a path of least flow resistance to help clear cell aggregates. The altered flow pattern is supported by COMSOL simulations, in which the gutter region has much higher flow rate than the under-ridge region (data not shown). However,

because of the reduced flow rate, the device with the gutter also results in a slower cell compression rate than that in the device without gutter (Figure 3.13 A). To confirm this finding, we took videos of cells in each type of design and calculated the average velocity before, under, and after a ridge compression. The results show that while the before and after ridge velocity remains similar (0.4 m/s), the under-ridge velocity in no-gutter design is 1.5-fold higher than the velocity in the gutter design (Figure 3.13 B). This device was also observed to yield a significantly higher delivery efficiency of  $90.13 \pm 4.50\%$  and higher but not significantly different intracellular concentration (Figure 3.13 C). However, the viability was reduced by 50% after processing under these conditions. Because of this finding, we did not use this design for gene editing, though by examining how this design could be made more gentle could greatly increase the transfection efficiency in future studies. We also did not observe a lower cell recovery in no-gutter devices (Figure 3.13 D). Images of the ridges after passage of 200,000 cells confirmed the majority of the channel is unobstructed albeit the presence of small cell aggregates at the first ridge in the no-gutter design (Fig, 3.13 E).

### **3.3 Summary**

In the pursuit of efficient intracellular delivery through microfluidic mechanoporation devices, understanding and controlling Critical Design Elements are paramount. This chapter delves into several key aspects crucial for achieving reproducible and high-performance microfluidic devices.

Robust Prototyping for Reproducibility under High Pressure: The necessity of robust prototyping methodologies is explored, particularly in the context of high-

pressure conditions. Elastomer deformation under pressure is identified as a critical factor affecting cell-microchannel interaction and subsequent delivery efficiency. An analytical method enabling easy quantification of deformation is highlighted as instrumental in accelerating optimization processes.

**Microscopy-Based Method to Quantify Operating Gap Size:** A novel microscopy-based approach is introduced for precisely quantifying the operating gap size within microfluidic devices. We proved that this method gives more accurate measure of deformation compared to a previously described, negative contrast method. It facilitates accurate assessment and control of deformation, thereby enhancing device performance and reproducibility.

**New Fabrication Method to Reduce Deformation:** Addressing the challenge of deformation, a new fabrication method is proposed to mitigate this issue. We identified the glass-channel distance as one of the most important CDEs for this specific hybrid device associated with their ability to control channel deformation, as well as fabrication strategies to control CDE variability. Spin coating is identified as the optimal technique for PDMS-glass hybrid devices fabrication and results in successful transfection of activated primary T cells.

**New Material for Rigid Device to Eliminate Deformation:** In cases where hybrid devices still result in excessive deformation, a rigid device fabrication method utilizing thermal plastic epoxy is suggested. This approach offers the advantage of replica molding and effectively eliminates deformation, leading to improved intracellular delivery efficiency to small, unstimulated primary T cells.

Optimal Microfluidic Design for Maximum Functional Delivery: Building upon more consistent and repeatable results, this subsection focuses on identifying CDEs in microfluidic channel structure. Features such as serpentine patterns for cell focusing, clog clearing zones for viability enhancement, and specific ridge configurations are elucidated to optimize delivery efficiency. By considering both delivery efficiency and cell viability, we chose the device design to include a serpentine inlet, 12 10  $\mu\text{m}$ -wide ridges spaced 880  $\mu\text{m}$  apart, and parallel gutters to process the 24-hour activated T cells.

In summary, this chapter underscores the critical role of meticulous design and fabrication in achieving reliable and efficient microfluidic mechanoporation devices. By addressing key challenges and leveraging insights into CDEs, advancements in intracellular delivery capabilities are facilitated, promising significant implications in various biomedical applications.

### **3.4 Method**

#### *3.4.1 PDMS-glass Composite Device Fabrication*

4ml 10:1 PDMS: linker was mixed and spin-coated on wafer on the Laurell WS650 spin coater at 200 rpm for 60 seconds. The film (180-200 $\mu\text{m}$  thick) was cured at 80°C for 3 mins. Glass slides were cut into rectangular pieces to completely cover the microchannel. The glass pieces were plasma cleaned in an air plasma cleaner and placed over PDMS-covered channels. Additional 30ml PDMS was poured and cured at 80 °C for 1hr. Cured devices were cut, punched at inlet and outlet, and plasma

bonded to glass slides. Spin speed and time were altered to spin thin films of 180, 255, and 450 $\mu\text{m}$  thickness. For 180 $\mu\text{m}$ , 200 rpm for 60-90 seconds; for 255 $\mu\text{m}$ , 200 rpm for 45 seconds; for 450 $\mu\text{m}$ , 100 rpm for 60 seconds.

#### *3.4.2 Microchannel functionalization*

Microfluidic devices were plasma treated and injected with (3-Aminopropyl)triethoxysilane (APTES) in ethanol (1:2 volume APTES: ethanol) for 5 mins, followed by 33% acetic acid wash for 5 mins. Treated microchannels were cleaned with an empty syringe to pump out remaining chemicals and degassed in vacuum chamber for 10 mins. Functionalized devices were allowed to dry overnight. Dried devices then reacted with 3% glutaraldehyde for 30 mins under a chemical fume hood, and subsequently washed with DI water and then reacted with 0.1% FITC conjugated bovine serum albumin (FITC-BSA) for 10mins. All steps were performed at room temperature.

#### *3.4.3 Channel imaging and data analysis*

Devices were imaged with a Zeiss LSM 700 confocal microscopy using a 488nm laser with 20 $\mu\text{m}$  pinhole. To image the cross-sections of channels, a Z-stack scanning program along the width of the channel was used. For positive contrast imaging, water was injected into FITC-BSA functionalized channel at various pressure. For negative contrast imaging, 0.1% FITC-BSA solution was injected into the channel as the contrast agent. Images were processed by Zen to obtain fluorescent

intensity data along the vertical line in the middle of the channel cross-section, which was then fitted in MATLAB as a double (for positive contrast method) Gaussian or single (negative contrast method) Gaussian curve.

#### *3.4.4 Epoxy Device Fabrication*

Tubing (1/16" inner, 1/8" outer diameter) was cut into 1 cm pieces and glued to inlets and outlets using Duco Cement. SuperClear epoxy was mixed at 1:1 volume and vacuum degassed. Mixture was poured and left to cure overnight at room temperature. The epoxy-covered wafer was heated at 80°C for 10 minutes until the cured epoxy became soft. The epoxy could therefore be carefully lifted from the wafer and subsequently cut into individual chips while retaining the molded shape. Tubing and remaining Duco cement was then removed from the inlets and outlets. Devices were plasma bonded with glass slides and baked at 80°C oven for 20 mins. Clean tubing was super glued into the inlets and left to dry for >2 hours [12].

#### *3.4.5 Transfection of Cells*

Delivery of dextran tracer was done as in a prior study [cite 9]. Briefly, devices were passivated in 1% Pluronic for >1hr. Jurkat, 24hr-activated, or unstimulated primary T cells were resuspended in Gibco OptiMEM to a density of  $5 \times 10^6$  cells/ml. 0.3mg/ml 2,000K Dalton FITC-dextran was added to cells. A pressure controller from ElveFlow was used to pump cells at a pressure ranging from 3 to 5 bar in PDMS and PDMS-glass hybrid devices or 5 bar in epoxy devices. After transfection, cells were washed twice in phosphate buffered saline (PBS) after 5 min recovery in solution

containing calcium. Transfection result was analyzed in a BD Accuri CSampler flow cytometer. 7-AAD was used to assess viability.

#### *3.4.6 Video Analysis for Cell Trajectory and Speed*

To measure the cell trajectory and speed in presence and absence of serpentine focusing features and gutters, we took measurements of the cell tracks from video data. Imaging was done with the VECT device on the stage of an inverted bright-field microscope (Eclipse Ti, Nikon, Japan), with a high-speed camera attachment (Phantom v7.3, Vision Research, NJ, USA). Cells were pushed through gap compression at 1 – 4bar pressure. Videos of cells were taken at 300-pixel by 300-pixel region at high speed ( $>10,000$  fps) at the first compression ridge. 20,000 – 30,000 frames were analyzed using FIJI/ImageJ TrackMate program [13]. We calibrated the length scales of each image based on known ridge dimensions, which enabled us to translate the number of pixels into an area measurement. We also converted cell velocity from  $\text{frame}^{-1}$  to  $\text{s}^{-1}$  using frame rate obtained from. Focusing efficiency was calculated by quantifying the percentage of cells that had an average track Y position within the range of the ridge Y position.

#### *3.4.7 Cell Culture*

The Jurkat cell line was obtained from American Type Culture Collection (ATCC, Manassas, VA). The primary culture media for the Jurkat was RPMI (Corning, Manassas, VA) with 10% fetal bovine serum (FBS) and 1% penicillin/streptomycin.

Primary T cells were isolated from PBMC in the Sulchek lab. PBMCs from healthy consenting donors was purchased from AllCells (Alameda, CA) and cryopreserved. Upon thaw, T cells were isolated with EasySep Human T cell isolation kit (STEM CELL technologies, Vancouver, Canada) and stimulated with Dynabead Human T-Activator CD3/CD28 (Thermo Fisher Scientific, Waltham, MA) in a 1:1 ratio, according to the manufacturer protocol. T cells were expanded in X-VIVO 15 media (Lonza, Switzerland) with 10% Fetal Bovine Serum (Corning, MA), 1% penicillin/streptomycin/amphotericin B (Lonza, Greenwood, SC), 1% GlutaMAX (Gibco, Thermo Fisher Scientific, Waltham, MA) and 100 ng/mL IL-2 (PeproTech, Rocky Hill, NJ). Cells were maintained at a concentration of  $\sim 1.5 \times 10^6$  cells mL<sup>-1</sup> and incubated at 37°C with 5% CO<sub>2</sub>. 24-hour after stimulation, Dynabeads were removed by pipetting and brief incubation on DynaMag magnet before conducting a delivery experiment. For extended expansion post cell processing, the culture media was changed every 72 hours and T cells were diluted to  $1.5 \times 10^6$  cells mL<sup>-1</sup> after each media exchange. T cells were reactivated every 6 days from the last activation with a 24-hour Dynabead stimulation. Unstimulated T cells were cultured in the same media without addition of Dynabeads.

#### *3.4.8 Statistical Analysis*

GraphPad Prism and Microsoft Excel were used to perform statistical analysis and generate plots. Tests include One-way ANOVA, t-test, and linear regression, with or without modulation for data set with unequal variance. All tests used an alpha value of 0.05.

### **3.5 References**

[1] Halldorsson, S., et al., Advantages and challenges of microfluidic cell culture in polydimethylsiloxane devices. *Biosens Bioelectron*, 2015. 63: p. 218-231.

- [2] Food and H.H.S. Drug Administration, International Conference on Harmonisation; guidance on Q8(R1) Pharmaceutical Development; addition of annex; availability. Notice. Fed Regist, 2009. 74(109): p. 27325-6.
- [3] Liu, A., et al., Microfluidic generation of transient cell volume exchange for convectively driven intracellular delivery of large macromolecules. *Mater Today (Kidlington)*, 2018. 21(7): p. 703-712.
- [4] Gervais, T., et al., Flow-induced deformation of shallow microfluidic channels. *Lab Chip*, 2006. 6(4): p. 500-7.
- [5] Wang, X.J. and I.C. Christov, Theory of the flow-induced deformation of shallow compliant microchannels with thick walls. *Proceedings of the Royal Society a-Mathematical Physical and Engineering Sciences*, 2019. 475(2231).
- [6] Inglis, D.W., A method for reducing pressure-induced deformation in silicone microfluidics. *Biomicrofluidics*, 2010. 4(2).
- [7] Sonstevold, L., et al., Biocompatible bonding of a rigid off-stoichiometry thiol-ene-epoxy polymer microfluidic cartridge to a biofunctionalized silicon biosensor. *Journal of Micromechanics and Microengineering*, 2022. 32(7).
- [8] Pustan, M., et al., AFM Characterization of Temperature Effect on the SU-8 Mechanical and Tribological Properties. *Polymers (Basel)*, 2022. 14(5).
- [9] Liu, A., et al., Cell Mechanical and Physiological Behavior in the Regime of Rapid Mechanical Compressions that Lead to Cell Volume Change, in *Small*. 2019. p. e1903857.
- [10] Sharei, A., et al., A vector-free microfluidic platform for intracellular delivery. *Proceedings of the National Academy of Sciences of the United States of America*, 2013. 110(6): p. 2082-2087.
- [11] Nikfar, M., et al., Numerical simulation of intracellular drug delivery via rapid squeezing. *Biomicrofluidics*, 2021. 15(4): p. 044102.
- [12] Yu, T., et al., Fabrication and Characterization of a Rigid Microfluidic Mechanoporation Device with High Pressure Tolerance and High Cell Transfection. *2022 Ieee 35th International Conference on Micro Electro Mechanical Systems Conference (Mems)*, 2022: p. 329-332.
- [13] Tinevez, J.Y., et al., TrackMate: An open and extensible platform for single-particle tracking. *Methods*, 2017. 115: p. 80-90

# CHAPTER 4. CAPABILITY TO PERFORM SEQUENTIAL GENE EDITING OF CAR T CELLS USING MULTIPLEXED CRISPR/CAS9 DELIVERY

## 4.1 Introduction

As cell therapies continue to revolutionize cancer treatment by better addressing challenges such as timing, toxicity, and graft versus host disease, the necessity for multiple genetic edits in both preclinical and clinical development becomes increasingly urgent. However, existing cell engineering techniques often fall short in efficiently processing highly functional and viable cell products required for next-generation therapies. Multiple gene edits are typically performed in one step which significantly increases the risk of chromosomal translocation [1, 2]. The conventional methods such as of lipid nanoparticles, while effective, presents limitations in cargo size, hindering the delivery of larger genetic constructs essential for multiple edits. On the other hand, alternative approaches like electroporation can compromise cell viability and proliferation, posing challenges in cell therapy manufacturing. Most importantly, adverse impacts on cell physiology present a major hurdle to achieving sequential gene editing, which has been shown to reduce the translocation rate [3]. Current manufacturing of genetically manipulated T cells already requires 10-14 days of *ex vivo* cell expansion to reach the desired number of T cells for a single dose. Further reducing cell viability or proliferation due to multiple transfections would further lengthen the time to reach the dose, adding additional cost to the already expensive manufacturing process. In addition, prolonged culture condition can lead to T cell senescence, reducing in vivo efficiency [4, 5].

In light of these limitations, this chapter introduces a novel approach of sequentially introducing multiple gene edits to avoid formation of multiple DSBs. We hypothesized that sequential introduction of target gene edits, if given sufficient time to repair individual DSBs, can reduce translocation and prolong CAR T cell persistence. This study aims to explore the potential of cell VECT in facilitating sequential gene editing of CAR T cells, a pivotal advancement in enhancing the efficacy and safety of cell-based immunotherapies.

We investigate the functional delivery capability of gene reprogramming molecules by VECT. This study aims to achieve several objectives. Firstly, we demonstrate the feasibility of functional delivery of gene reprogramming molecules using VECT by prioritizing CD5 editing as a means to generate fratricide-free CAR T-cell products against T-cell leukemia. Secondly, through single CD5 knockout experiments, we explore the impact of VECT on T-cell physiology, including viability, proliferation, and memory phenotype. Thirdly, we assess whether VECT-treated cells retain the capacity to be transduced into cytotoxic CAR-T cells. Finally, utilizing TRAC and B2M as targets, we showcase sequential editing and its effects on population heterogeneity, translocation, memory, cytotoxic efficiency, and potential mechanisms of cell damage induced by sequential VECT. Through these aims, we aim to shed light on the transformative potential of VECT in enhancing gene editing efficiency and optimizing cell-based immunotherapies.

#### **4.2 Cas9 Delivery Capability in CAR T cell manufacturing**

Microfluidics is a pathway to improve the manufacturing precision of gene modified cells. However, to date, it remains to be demonstrated that microfluidic

treatment preserves the functionality of T cell products in a complete CAR T workflow. In this section, we used microfluidics to perform CRISPR/Cas9 gene editing of CD5, a negative T-cell regulator, followed by the insertion of a chimeric antigen receptor (CAR) transgene via lentiviral vector transduction to generate CAR T cells targeted against the B cell antigen CD19. CD5 was selected as the target molecule for knockout due to its role in negatively regulate CAR T proliferation and application in generating CD5 CAR T product that targets malignant T cells. CD5 knockout was demonstrated to improve T cell proliferation rate and duration of persistence and has also been used to generate fratricide-free anti-CD5 CAR T cells.

In this section, primary T cells were processed with VECT microfluidics to perform CRISPR-based knockout of the CD5 locus. Processed cells were then used in a retro-viral transduction assay by conventional incubation method to produce CAR T cells. We compared manufacturing-relevant parameters after VECT processing, such as editing and transduction efficiency, memory markers, proliferation, cell quantity, and product cytotoxicity to ablate cancer cells. Then we make conclusions on next steps.

#### *4.2.1 Comparison with Electroporation*

In our exploration of Cas9 delivery efficacy within CAR T cell manufacturing, we undertook a comprehensive comparison between our VECT method and the conventional electroporation technique (EP). Employing the optimized device from Chapter 3, we first tested the delivery efficiency of a GFP-Cas9 protein without assessing the knockout efficiency to deconvolute delivery from functional editing. At

50  $\mu\text{g}/\text{mL}$  cas9 concentration, VECT generated similar delivery efficiency (Figure 4.1), 59.5% compared to 59.7% by EP. GFP-conjugated cas9 did not result in functional knockout, possibly due to the GFP interfering with the nuclease function. To conclude, we have demonstrated VECT's ability to delivery protein to primary T cells at similar efficiency as electroporation. We then tested functional gene editing using a wild-type Cas9.

We delivered Cas9 and guide RNA (gRNA) ribonucleoprotein (RNP) targeted against CD5, a pivotal negative regulator of T cell function. To assess the functional knockout of CD5 expression, quantified as the percentage of CD5-negative population, we systematically escalated dosing concentrations until reaching a discernible plateau. Among the various doses examined, the gene knockout efficiency exhibited a notable peak at 10  $\mu\text{g}/100\mu\text{L}$ , (5, 10, and 15  $\mu\text{g}$  protein/ $100\mu\text{L}$  cells) achieving an average efficacy of 55.8% and 62.7% on day 5 and 10 post-editing, respectively, utilizing the VECT methodology. In comparison, the gene knockout efficiency through

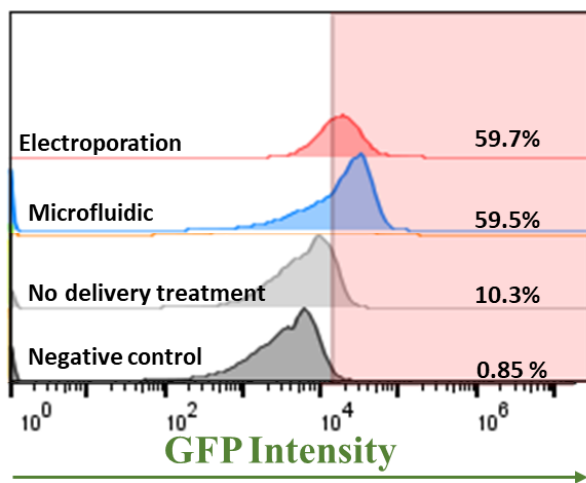


**Figure 4.1: VECT is capable of delivering cas9 at similar efficiency as electroporation.** GFP level in 24-hour activated T cell, quantified 24 hours after delivery of 500 $\mu\text{g}/\text{mL}$  GFP-Cas9 by electroporation, VECT, incubation, and negative control.

electroporation exhibited its zenith at 5  $\mu\text{g}/100\mu\text{L}$ , reaching 77.1% and 77.3% on day 5 and 10, respectively (Figure 4.2).

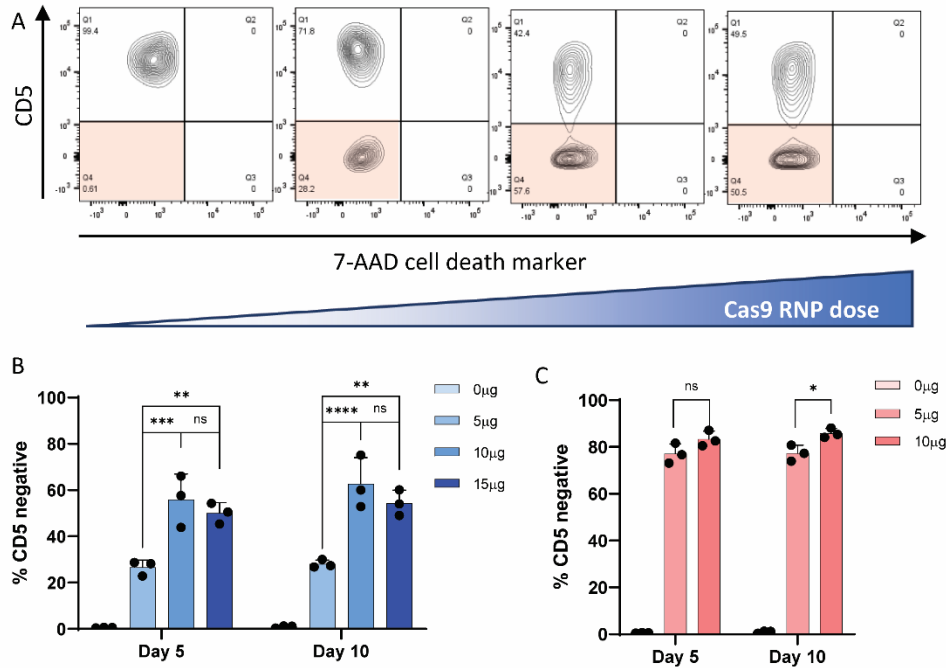


**Figure 4.2: optimal cas9 RNP concentration results in comparable CD5 knockout as electroporation.** A) Exemplary flow cytometry contour plots with CD5 expression on the y-axis showing increasing knockout efficiency with increasing RNP concentration. B) a summary of CD5 knockout efficiency 5 and 10 days post VECT treatment with 0, 5, 10, and 15 $\mu\text{g}$  sgCD5 cas9 RNP. C) a summary of CD5 knockout efficiency 5 and 10 days post electroporation treatment with 0, 5, and 10 $\mu\text{g}$  sgCD5 cas9 RNP. N=3. Stat = one-way ANOVA. Error bar=SD. \*\* p-value < 0.01, \*\*\* p-value < 0.001, \*\*\*\* p-value < 0.0001

Understanding the physiological effects of Cas9 delivery methods on T cells is paramount to ensuring the integrity and functionality of engineered CAR T cells. Therefore, we investigated how the delivery mechanisms and RNP dose, specifically VECT and electroporation, influence key aspects of T cell physiology [22, 40]. Our analysis yielded intriguing insights, revealing no discernible reduction in the stem memory T cell composition at heightened Cas9 concentrations for either VECT or

electroporation, as opposed to unprocessed control cells (Figure 4.3 A and B). About 58% of cells remained CCR7+CD45RA+, a marker of long-lasting memory phenotype [6], after VECT, and 61% after electroporation. Negative control group showed 55% stem memory phenotype, showing no statistical difference. Throughout a 5- and 10-day expansion period, the composition of the stem memory population remained unaltered across negative control, VECT, and electroporation cohorts, thereby indicating that the rapid compressions intrinsic to VECT did not encumber T cell memory formation (Figure 4.3 B). This resilience to alteration in memory T cell composition highlights the compatibility of both VECT and electroporation with the preservation of T cell subpopulations crucial for sustained anti-tumor responses. This observation not only corroborates existing research showing cell-squeeze maintained T cell phenotype and preserved normal gene expression [7, 8], but also reaffirms the potential of these delivery methods to uphold the memory phenotype essential for durable CAR T cell therapies.

Therefore, we chose to use 10  $\mu\text{g}/100\mu\text{L}$  cas9 in VECT and in electroporation for further experiments. After 5- and 10-day expansion, the resulting composition of stem memory population remains unchanged between negative control, VECT, and electroporation, showing that rapid compressions does not impair T cell memory formation. We recorded T cell viability and proliferation (Figure 4.3 C and D) up to 10 days after gene editing. VECT treated T cells show similar viability as the negative control cells, while electroporation treated T cells experience reduced viability that remained lower at all time points compared to both VECT and control groups. As observed in some studies [8, 9], electroporated T cells can experience slower

expansion. In these studies, we observed an expansion of only 20-fold over 10 days. In comparison, the VECT treated cells expand at similar rate as control cells which were significantly more robust than that of electroporated cells, with an expansion of 80-fold over 10 days. Taking into account both the editing efficiency and proliferation rate, we calculated the number of live and edited T cells on day 10, normalized it to number of treated cells, and used this ratio as the cell yield. On day 10, VECT treated T cells give a yield of 50-fold while electroporation treated cells have a yield of 10-fold (Figure 4.3 E). The VECT device workflow was able to generate 5-fold more edited cells per input cell over 10-day expansion. This increased yield can possibly be attributed to increased quality and viability after processing. The benefits of an increased yield include faster time to generate a dose, decrease cost, and an overall reduced ex vivo manufacturing time leading to improved quality of T cell product.

In summary, the VECT device workflow outperformed electroporation comprehensively, yielding a significantly higher quantum of edited cells per input cell over a 10-day expansion interval. While both VECT and electroporation preserve memory T cell composition, VECT emerges as a superior choice for maintaining cellular viability and supporting robust proliferation. This augmented yield not only augments operational efficiency but also holds potential application for manufacturing

timelines and associated costs, thereby unequivocally contributing to the elevation of CAR T cell product quality and efficacy.

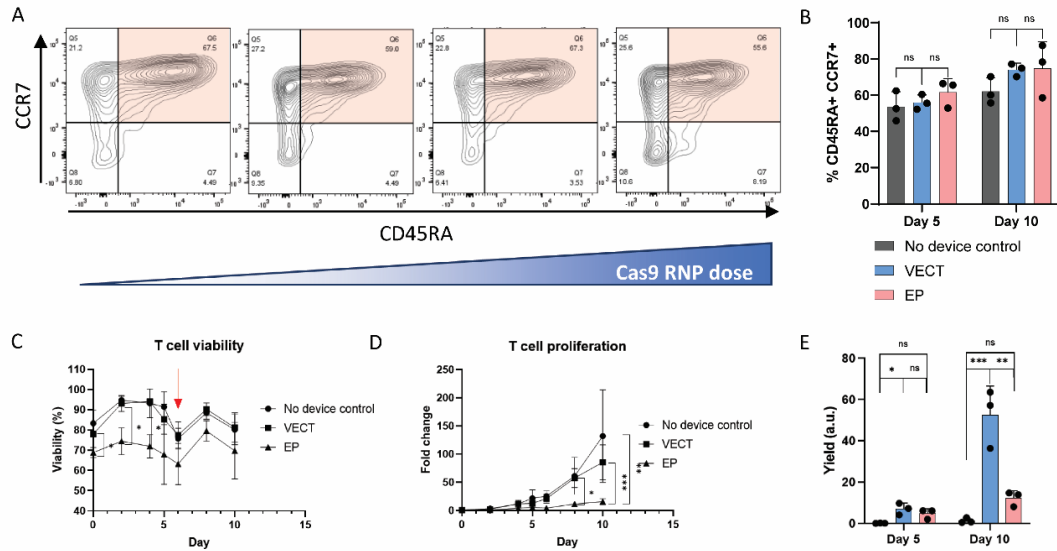


**Figure 4.3: VECT edited T cells show similar memory phenotype and superior proliferation compared with electroporation.** A) exemplary flow cytometry contour plots with CD45RA expression on the x-axis and CCR7 expression on the y-axis showing similar percentage of stem memory phenotype among VECT treated T cells. The stem memory phenotype is defined as CD45RA<sup>+</sup> CCR7<sup>+</sup> as shown in the red box. B) a summary plot of the proportion of stem memory phenotype among T cells treated by VECT or by electroporation 5 and 10 days post editing. C) T cell viability on day 0-10 post editing. Red arrow indicates time point for the second activation D) T cell proliferation plotted as fold change in cell count among T cells treated by VECT or by electroporation 5 and 10 days post editing. E) yield of CD5 edited T cell treated by VECT or by electroporation. Yield is defined as the number of live, CD5 negative cells on day 5 or 10 post editing normalized to the number of live cells pre-editing. N=3 from a single donor. Stat = one-way ANOVA. Error bar=SD. \* p-value < 0.05, \*\* p-value < 0.01, \*\*\* p-value < 0.001

#### *4.2.2 VECT is Compatible with Downstream CAR T Manufacturing Processes*

The successful generation of cytotoxic CD5- CD19 CAR+ T cells represents a significant milestone in CAR T cell manufacturing, highlighting the adaptability of the VECT workflow to downstream processes. Leveraging the optimized VECT methodology, we evaluated compatibility with viral transduction, a critical step in producing therapeutic CAR T cells. Our study, to our knowledge, is a pioneering effort in demonstrating the feasibility of integrating microfluidic mechanoporation into a CAR T cell manufacturing workflow, demonstrating the versatility and potential of VECT in advancing cellular immunotherapy.

Figure 4.4 illustrates the incorporation of the gene editing step 24 hours after T cell activation and 24 hours before viral transduction to yield CD19 CAR T cells carrying CD5 knockout. Utilizing six replicates from distinct donors, we quantified CD5 knockout efficiency and CD19 CAR transduction efficiency (Figure 7B-D). Our gating strategy, depicted in Supplement Fig. 2, facilitated the analysis of CD5 expression levels in the absence of VECT processing. Notably, microfluidics-processed cells exhibited an average knockout efficiency of 49.6% across six donors, coupled with a transduction efficiency of 35.7%, surpassing the transduction efficiency of unprocessed cells (31.3%) (Fig. 7D). Although donor-specific variations were observed, with the highest delivery and transduction efficiency recorded in donor 1 (64% and 42%, respectively), the overall results underscored the compatibility of VECT with downstream viral transduction processes.

Furthermore, our cytotoxicity assay, conducted by coculturing VECT-treated and untreated T cells with CD19+ 697 B cell leukemia cells, revealed promising results. At varying ratios of T cells to leukemia cells (1:3, 1:1, and 3:1), CD19 CAR transduced cells demonstrated higher target cell death compared to GFP-transduced T cells, indicative of CD19 CAR-specific cytotoxicity (Fig. 7E). Importantly, no statistical significance was observed in target cell death rates between VECT-treated

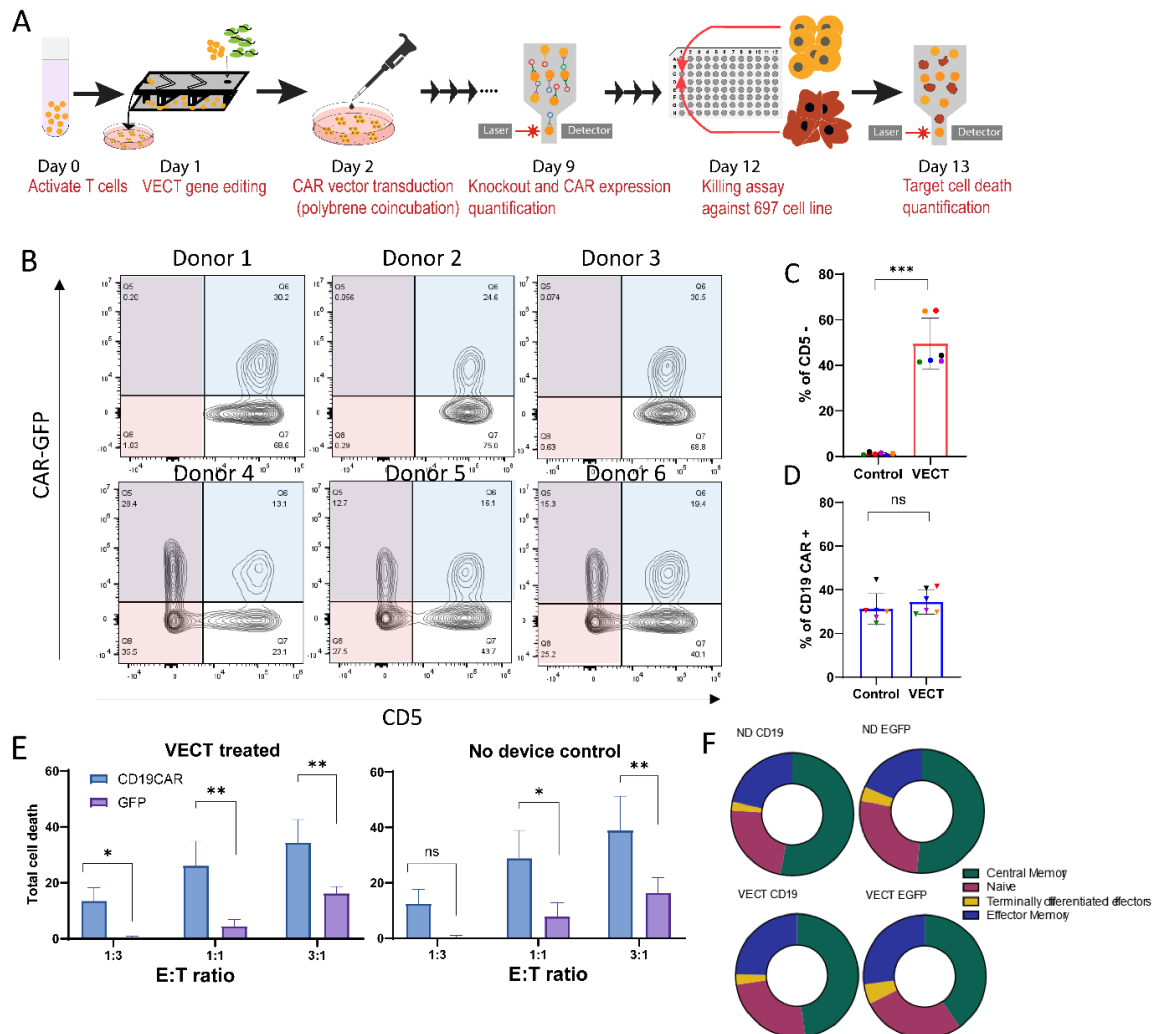


**Figure 4.4: VECT treatment resulted in higher transduction efficiency and CAR-T cell cytotoxicity in multiple donors.** A) Schematic drawing showing the time line of gene editing, CD19 CAR transduction, and cytotoxicity assay. B) exemplary flow cytometry contour plots with CD5 expression on the x-axis and CD19 CAR – GFP expression on the y-axis. CD5 – population is shown in red box. GFP expression level is used to gate CD19 CAR + population, which is shown in blue box. C,D) Bar plot of knockout efficiency (C) and transduction efficiency (D) across six healthy donors. Colors indicate individual donors. E) Cytotoxicity result based on a 24-hour killing assay of CD19 CAR transduced T cells against CD19 positive 697 pre-B cell leukemia cell line at 1:3, 1:1, and 3:1 effector to target ratio (E:T ratio). The percentage of dead target cells are measured with 7-AAD and annexin V in a co-culture with non-edited T cells and microfluidic-treated CD5 knockout T cells. To ensure the observed cytotoxicity is a result of interaction between CD19 and CAR, the cytotoxicity result is compared to that of a population transduced with GFP vector only. A 2-way ANOVA with Welch's test is run to determine statistical significance between CD19CAR and GFP groups in VECT and no device control separately. Additional 2-way ANOVA was run between CD19CAR transduced cells between VECT and no device control at all E:T ratio. No statistical significance was detected. F) Cell phenotype among control (ND) and microfluidic-treated (VECT) population in CD19 CAR or mock transduced groups. The proportion of naïve, central memory, effector memory, and terminally differentiated populations are plotted.

and untreated control groups across all ratios, reaffirming that VECT processing did not compromise the T cell capacity to eliminate target cells (Fig. 7E, blue bars in VECT and control group) (Fig. 7F).

These findings collectively underscore the compatibility and efficacy of VECT in facilitating downstream CAR T cell manufacturing processes. By seamlessly integrating microfluidic mechanoporation with viral transduction, VECT enables the generation of functional, cytotoxic CD5- CD19 CAR+ T cells, heralding a promising advancement in the field of cellular immunotherapy.

#### *4.2.3 VECT is applicable to patient derived T cells*

We repeated the gene editing process on T cells derived from diagnostic specimens derived from B cell ALL patients. 24 hours following T cell activation, patient derived T cells were processed by VECT devices previously optimized for T cells from healthy donors, receiving 10  $\mu\text{g}/100 \mu\text{L}$  sgCD5 cas9 RNP. We assessed knockout efficiency on day 4 instead of day 9 post activation to avoid exerting stress from prolonged culturing. CD5 expression was examined by flow cytometry (Figure 4.5 A). Across the 3 patient donors, the average knockout efficiency was  $30.90\% \pm 11.0\%$  (Figure 4.5 B, left). This editing efficiency was significantly lower compared to that achieved in healthy donor T cells ( $59.88\% \pm 10.15\%$ ) (Figure 4.5 B, right,  $p=0.02$ ). To understand the cause, we analyzed cell size and cell stiffness post activation. Patient derived cells grew to  $8.95 \pm 1.36 \mu\text{m}$ , while healthy donor T cells grew to  $9.84 \pm 1.25 \mu\text{m}$  in diameter (Figure 4.5 C,  $p<0.001$ ). The nearly  $1 \mu\text{m}$  difference would lead to  $\sim 10\%$  reduction in strain and possibly insufficient compression. The patient cell stiffness was also found to be significantly softer than health donor groups (Figure 4.5 D,  $p<0.0001$ ). Patient derived cells also show a much higher relaxation rate (Figure 4.5 E,  $p<0.0001$ ). This mechanical difference can be an additional contributor to their harder-to-transfect property as we observed a lower CD5 editing efficiency for softer cell types in both the healthy-derived and patient-derived specimens. Overall, the VECT process was able to deliver gene modifying cargo to patient derived T cells, albeit the optimal design should be reevaluated to better suit the underlying cell biomechanics.

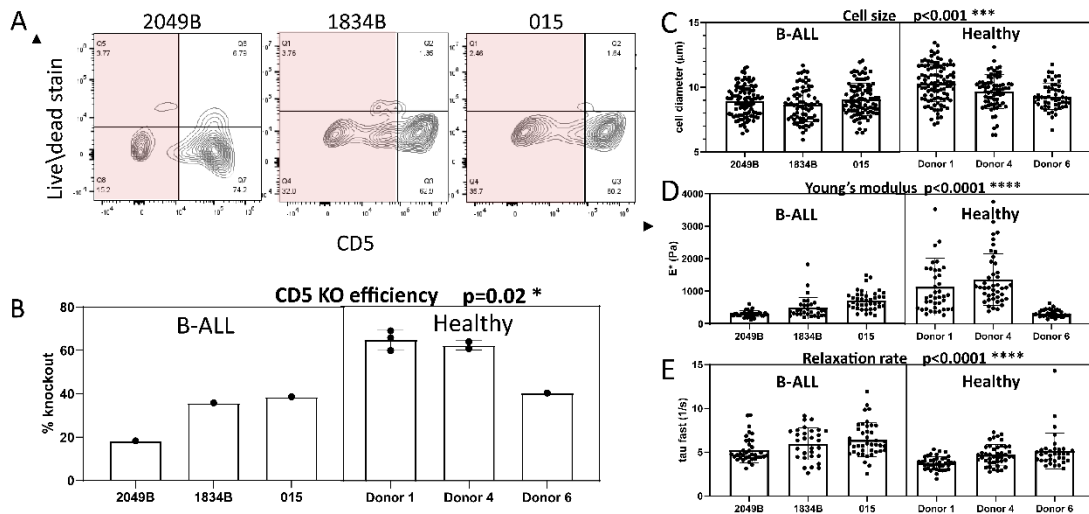


**Figure 4.5: VECT delivery resulted in surface knockdown of CD5 in B ALL-patient derived T cells.** A) exemplary flow cytometry contour plots with CD5 expression on the x-axis and live-dead stain on the y-axis. CD5 – population is shown in red box. B, C, D) Bar plot of knockout efficiency (B), cell size 24-hours post activation (C), Young’s modulus (D), and viscous relaxation rate (E) in 3 patient-derived and 3 healthy donor-derived T cells. A t test is run on each data set between B-ALL and healthy donor. p-value is reported above each plot. Stat = nonparametric one-way ANOVA. Error bar=SD.

### 4.3 Capability in Sequential Gene Editing

With the validation of cell VECT for permanent gene editing, we next sought to evaluate this delivery platform for multiplexed gene editing. Multiplexed gene editing requires the delivery of multiple gene editing reagents to target different gene editing sites. Techniques for multiplexed gene editing are of great interest in many cell engineering use cases, particularly in cell therapies. Many cell therapies currently in preclinical and clinical development use multiple gene edits to target disease indications that cannot be effectively targeted by cell therapies that were created using a single gene edit. A powerful example is in the development of off-the-shelf allogeneic T cell therapy in which T cells made from iPSCs go through TCR and B2M knockout and CAR knock-in [10].

Multiplexed editing in cell therapies is motivated by the high demand for allogeneic cell therapies. The current dependence of clinical cell therapies on autologous cells poses a substantial cost, logistical, and manufacturing burden [11-13]. Furthermore, many patients are not able to provide usable T-cells for autologous treatment due to advanced disease state or negative effects of chemotherapy, making these patients ineligible for life-saving cell therapies [13]. To achieve desired safety and efficacy, this product may require knockout of TCR, HLA, and PD-1. The implementation of multiplexed gene editing for cell therapy manufacturing facilitates a wide range of new cell therapy use cases and treatment targets.

In this section, we aimed to perform permanent gene knockout of the TRAC locus and the B2M locus, a combination that would enable the development of an allogeneic T-cell therapy free of GvHD risks. We used the cell VECT platform for sequential and one-step delivery of CRISPR-Cas9 RNPs targeting *TRAC* and *B2M*. We will develop the optimal workflow for primary T cells, test the impact of consecutive VECT treatment on T cell proliferation, and test if sequential editing can reduce translocation and improves T cell persistence.

#### *4.3.1 Process Development for Second Editing*

In Chapter 3, we demonstrated successful delivery to unstimulated T cells and 24-hour stimulated T cells. In this section, we aim to test gene editing in both T cells and develop a suitable workflow for VECT sequential delivery. We first tried delivery and gene editing in unstimulated/naïve T cells. Workflow on unstimulated T cells is desired for its potential to reduce manufacturing lead time, reduce cell senescence,

and reduce genome toxicity [5, 14]. We used the epoxy device fabrication method demonstrated in Chapter 3, and tested a device with 4.5  $\mu\text{m}$  constriction gap, with 6 or 12 ridges, 880 or 1760 $\mu\text{m}$  spacing. Since gutter was shown to impact the delivery most drastically, we tested the effect of gutter on naïve T cells. Figure 4.6 showed the resulting delivery efficiency, viability and MFI shift at 5bar operating pressure. The number of ridges and ridge spacing showed no significant impact on transfection results. All four variations resulted in 20-30% delivery, 80-90% viability, and 20-30-fold MFI shift. Surprisingly, in devices without gutter, we achieved both high delivery and high viability at 5 bar, with an average delivery efficiency of  $68.95\pm 21.02\%$  and  $84.58\pm 10.75\%$  live, non-necrotic population. MFI shift, as an indirect measure of cargo concentration, was the highest among no gutter designs, with an average fold-shift of  $32.68\pm 13.74$  fold (Figure 4.6 C). We then proceed to knockout TCR with this device.

Using the same condition, we achieved  $27.6\pm 7.12\%$  surface TCR knockdown (Figure 4.7 A and B). T cell viability remained high immediately after processing

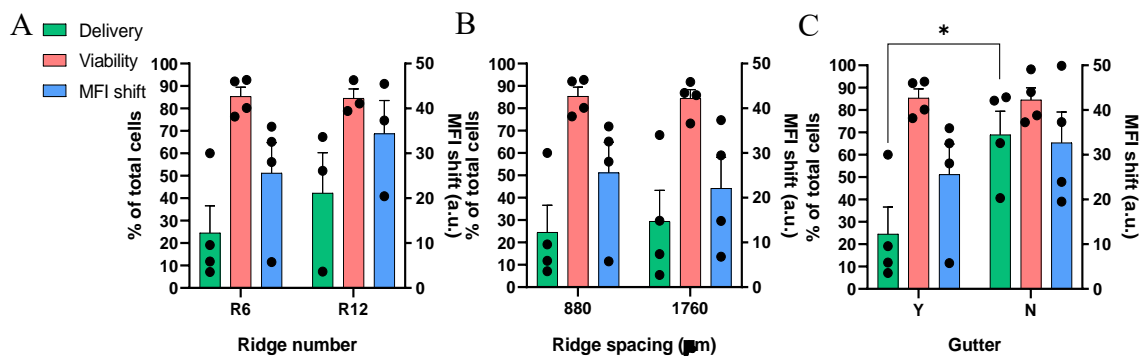


**Figure 4.6: Epoxy VECT devices without gutters achieved high delivery and viability in unstimulated/naïve T cells.** A, B, C) Bar plot of FITC-dextran delivery, viability and MFI shift achieved in 4.5 $\mu\text{m}$  constriction devices with variation in number of ridges (A), spacing between ridges (B), and presence or absence of gutter (C). N= 3-4. One-way ANOVA is used as Statistical test. Error bar=SD. \* P<0.05. No statistical difference is detected in resulting cell necrosis.

(Figure 4.7 D, 75.87% VECT, 88.50% No device control). However, after T cells were activated for 48 hours, viability dropped to 50.87% with only 35.56% cells expressing high CD69, an activation marker (Figure 4.7 C and D). T cell proliferation remained low throughout 5 days, with only a 1.45-fold growth compared to a 4-fold growth rate among the control population (Figure 4.7 E). Obviously, these T cells were not suitable for downstream therapeutic use. This suggested that using non-necrotic viability immediately after VECT treatment might not correctly predict long-term viability. Therefore, we quantified both apoptosis and necrosis after VECT treatment with the reasoning that cells at early apoptosis stages usually become fully dead with compromised membrane function in 24 hours [15]. Our findings indicated that although apparent cell necrosis remained low, treated T cells turned apoptotic in a pressure and flow rate dependent manner, with an inverse relation with strain-rate (Figure 4.8 A and B). At 4.5 $\mu$ m constriction at 5 bar, the truly viable cells dropped to below 40% (Figure 4.8 B).

In these experiments, we used cryopreserved T cells. Therefore, we asked the question whether cryopreservation or the post-thaw conditions caused the cell membrane to be more fragile, increasing sensitivity to mechanical compression [cite]. We then repeated the same VECT treatment on freshly isolated naïve T cells. Again, we used 4.5 $\mu$ m constriction gap and 5 bar operating pressure. Looking at their non-necrotic, non-apoptotic viability, fresh T cells had significantly higher viability ( $67.67\pm 10.85\%$  fresh vs.  $34.50\pm 6.94\%$  cryopreserved,  $p=0.011$ ) with similar degree of delivery (Figure 4.8 C). This supported our hypothesis that a combination of

cryopreservation and mechanoporation may combine to exacerbate negative impact on cell viability.

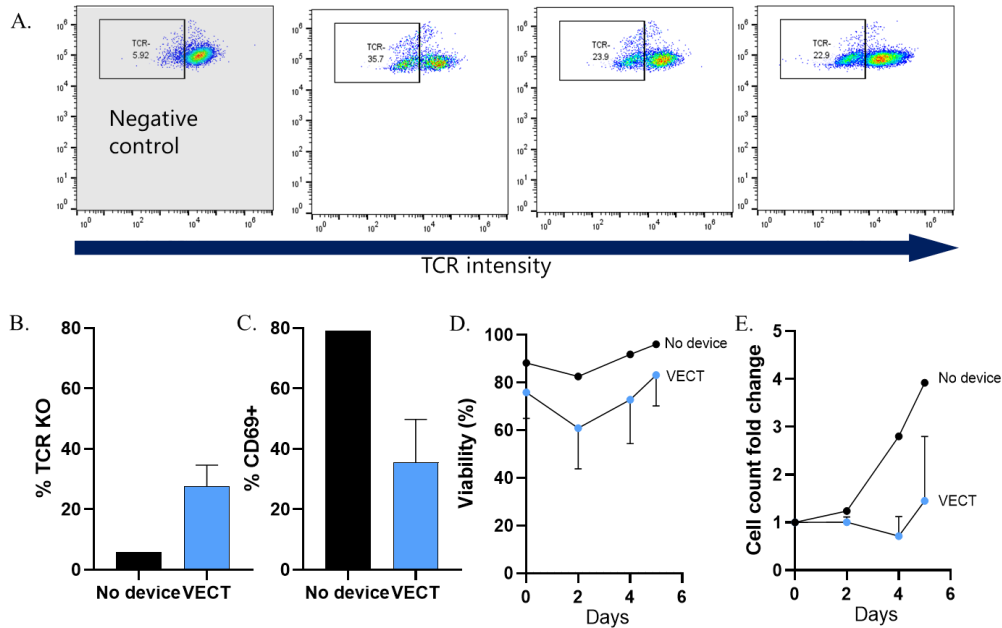


**Figure 4.7: Epoxy VECT devices resulted in TCR knockdown but failed to produce proliferative T cells.** A) exemplary flow cytometry plot showing surface TCR expression level. B) Average TCR knockdown level in no device control and VECT treated groups. VECT: N = 3 devices. C) CD69 expression level, indicating degree of cell activation 48-hours after Dynabeads were added to cell culture. D) T cell viability quantified by necrosis stain. E) T cell fold change over 5 days post editing. N=1 for no device; N=3 for VECT. Error bar=SD.

So far, we have shown that VECT is capable to modify genes of unstimulated T cells. Although switching to freshly isolated T cells improved cell viability, the logistics associated with using freshly isolated T cells prevented us to pursue this route in the current study. Hence, we planned to pursue sequential gene editing in 24-hour activated T cells.

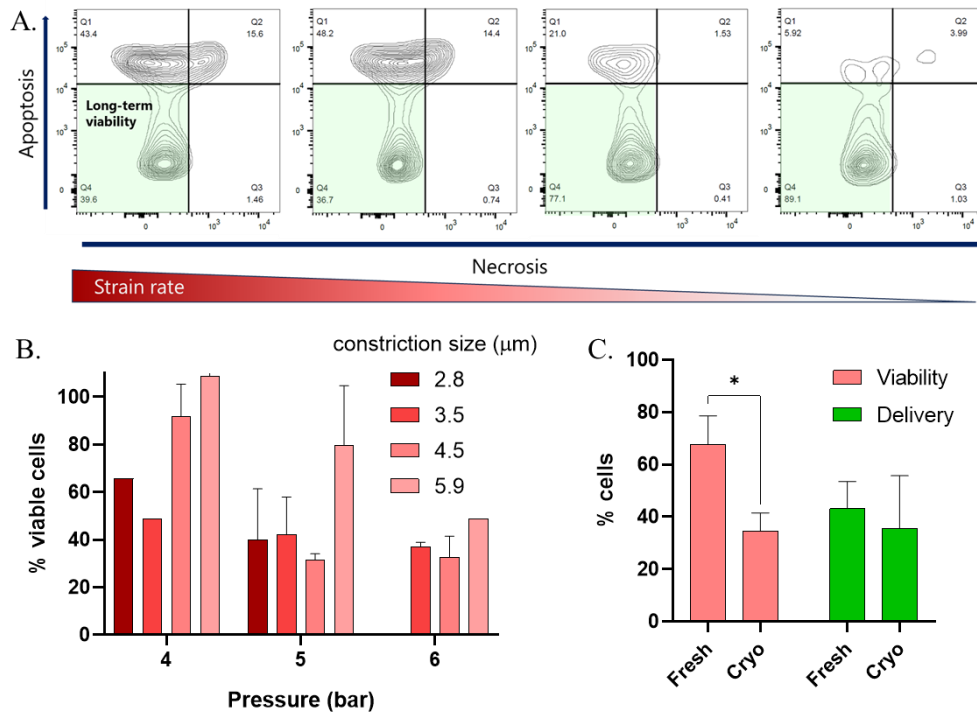


**Figure 4.8: Processing cryopreserved naïve T cells increases cell apoptosis.** A) Contour plot showing gating strategy for non-necrotic and non-apoptotic population with long-term viability (shaded in green). B) Percentage cells under the “long-term viability” population, at 4, 5, and 6 bar pressure and 2.8-5.9 $\mu$ m gap. C) Comparison of long-term viability and delivery of 500KD FITC-dextran to cryopreserved and freshly isolated T cells from the same donor. N= 1-3. T-test is used on viability and delivery separately. Error bar=SD. \*:  $p < 0.05$ .

It was shown that time for DSB repair takes 2-24 hours across various cell lines [16]. We hypothesized that 2-24-hour separation between *TRAC* and *B2M* editing can reduce translocation. Yet, this posed another problem: T cells expand in size after activation, from about 9.8 to 11.6  $\mu$ m from 24- to 48-hour post activation (see Figure 3.10). In a 24-hour recovery workflow, devices need to be optimized for performing the 2<sup>nd</sup> edit. From the finding in Chapter 3, we decided to test devices with 6 and 12 ridges with 880  $\mu$ m, and test variation of gutters. We first eliminated devices resulting in a normalized viability below 80% (Figure 4.9 B, dashed line marks 80% viability).

Considering both delivery efficiency and long-term viability, we calculated a yield of true viability adjusted by delivery efficiency, which is the product of viability, measured as non-necrotic and non-apoptotic, and delivery (Figure 4.9 A, B and C). The result indicated that a 6-ridge, 880 $\mu\text{m}$  spacing, no gutter, 3.5  $\mu\text{m}$  constriction gap is optimal for the 2<sup>nd</sup> editing, with an average adjusted delivery efficiency of 49.01%. Overall, no gutter design (NG) outperformed the other 2 designs at all gap and flow rates. And 6 $\mu\text{m}$  gap (corresponding to 0.5 strain) outperformed 7 $\mu\text{m}$  at the same pressure, except when using 12-ridge design. Delivery plateaued at the medium pressure tested (4 bar for 12-ridge devices and at 3bar for 6-ridge no gutter devices).

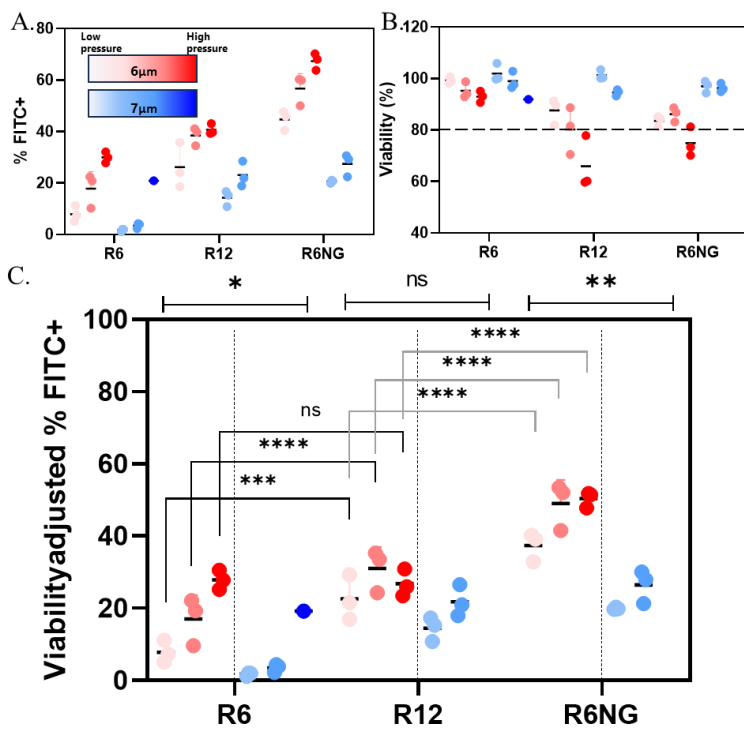


**Figure 4.9: Viability and delivery optimization for 24-hour sequential editing experiment.** A) 500KD FITC dextran delivery efficiency in 6-ridge, 12-ridge- 6-ridge no gutter designs. B) long-term viability in the 3 design types. Dashed line indicates 80% viable cells, used a cutoff to eliminate low viability devices. C) Viability-adjusted delivery in the 3 design types. 6 and 7 $\mu\text{m}$  constrictions (0.5 and 0.4 strain) were tested across 3 pressures. For R6 and R12 devices, we tested 3, 4, and 5 bar; for R6NG, we tested 2, 3, and 4 bar. Stat test: two-way ANOVA. \*  $p < 0.05$ ; \*\*  $p < 0.01$ ; \*\*\*  $p < 0.001$ ; \*\*\*\*  $p < 0.0001$

### 4.3.2 Chromosome Repair requires 24hr in T cells

After establishing the workflow and devices to be used in sequential editing, we performed knockout of *TRAC* and *B2M* in one-step and sequentially with 2, 6, and 24 hours DSB repair time. Additionally, we performed one trial of sequential editing with a 48-hour separation to serve as a negative control for translocations. We achieved between 50-65% single gene knockout efficiency quantified by antibody stain (Figure 4.10 A, red and blue shaded region). No statistical difference is found between single gene knockout efficiency between batch, 2-hour, 6-hour, or 24-hour sequentially edited groups (Figure 4.10 B, red and blue bar). We did note a drastic decrease in efficiency in 48-hour sequential case, likely due to lack of device and operational optimization for T cells 72-hours post activation. The more important parameter is double knockout efficiency; for allogeneic applications, the purity of TCR-HLA-population should be as high as possible. We quantified double knockout efficiency from flow cytometry quantification (Figure 4.10 A, purple shaded region). Once again, no statistical difference was found between batch, 2-hour, or 6-hour sequentially edited groups (Figure 4.10 B, purple bar, 41.63%, 35.61%, 30.0% batch, 2-hour, 6-hour respectively). Yet, we found that 24-hour sequential editing resulted in significantly lower double negative population compared with the batch group (26.68%,  $p=0.0074$ ). We next sought to show the heterogeneity by looking at deviation of double editing efficiency from those generated by a random diffusion. Using an independent probabilistic model, double knockout efficiency should be the product of two single editing efficiency. If experimental double editing efficiency significantly exceeds this calculated value, it could be attributed to a non-random

delivery mechanism. Interestingly, batch-edited population had a higher, but not statistically significant, double editing rate than calculated one (Figure 4.10, B, “experimental” and “theoretical”). On average, experimental double editing efficiency exceeded theoretical number by 12% in batch generated T cells; in all sequential groups, experimental efficiency only exceeded the theoretical number by 1-3%. We conclude that delivery and activity of Cas9 may not be independent events for a cell.

We then looked at the feasibility of using electroporation to perform sequential editing. Using the same dose and a high viability protocol, we achieved 50-60% double knockout across batch, 2-hour, 6-hour, and 24-hour sequential groups (Figure 4.10, C). Interestingly, we did not observe the same degree of increased double editing efficiency compared to that calculated from random diffusion. On average, experimental efficiency exceeded theoretical value by only 1-5% across all groups (Figure 4.10, C, purple bar and gray bar). Although we hypothesized sequential editing could reduce translocation, we acknowledge that batch editing has the potential to improve heterogeneity and production of the desired double knockout population.

The key question is whether sequential editing can reduce or eliminate translocation, and how much time is needed for DSB repair in activated T cells. We ran a probe-based qPCR to quantify the bulk translocation efficiency. Without translocation, the two primers on different chromosomes will not result in exponential amplification. Only when translocation brings two chromosomes together will there be a signal of exponential amplification (Figure 4.10 D). Both TRAC (chromosome 14)-chromosome 15 translocation (termed TCR-B2M in Figure 4.10 E) and B2M

(chromosome 15)-chromosome 14 translocation (termed B2M-TCR in Figure 4.10 E) were quantified and summed as total translocation rate. Batch editing of two genes caused around 1.1% total translocation in both VECT and EP groups; with only 2-hour separation, translocation was reduced to 0.5-0.6%, an estimated 40% reduction (Figure 4.10 E and F). Additional 4 hours separation further reduced translocation by about 60%. 24-hour separation is shown to reduce translocation by 100%. Hence, we concluded that 24-hour is necessary for T cells to completely repair DSB.

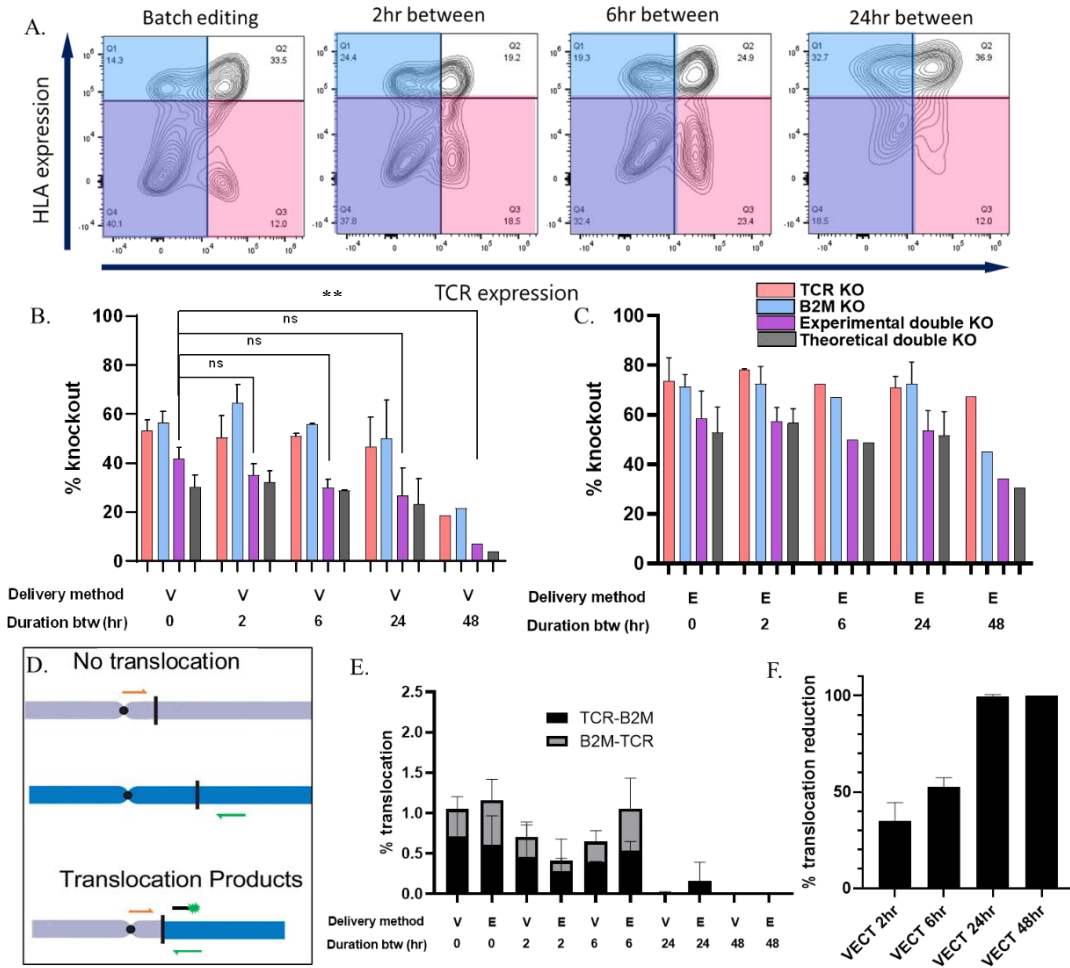


**Figure 4.10: Sequential editing by VECT resulted in similar double KO as batch with reduced or undetectable translocation.** A) exemplary flow cytometry contour plots showing TCR and HLA knockout on x- and y-axis among batch, 2-hour, 6-hour, and 24-hour sequentially edited cells. Red: HLA KO. Blue: TCR KO. Purple: double KO. B and C) bar plot of efficiency for single and double gene knockout, and theoretical double KO calculated as % TCR- × % HLA- by VECT (B) or by EP (C). D) illustration of the mechanism of qPCR to quantify translocation. Single primer on each chromosome does not lead to exponential increase in PCR product; only when translocation brings two chromosomes together will the primers form a flanking pair and give out fluorescent signals. E) Translocation rate among batch- and sequential- populations by VECT and EP. F) translocation reduction calculated as  $\frac{\% \text{translocation (Batch)} - \% \text{translocation (Sequential)}}{\% \text{translocation (Batch)}} * 100\%$ . N=1-4 from a single donor. E and F: qPCR technical replicate = 2. Biological replicate = 3. Stat test= two-way ANOVA. Error bar=SD.

The ability to preserve cell proliferative viability is key to integrating a sequential editing workflow. Next, we assessed T cell proliferation post sequential editing. After VECT treatment, T cells proliferated normally as no device and batch edited groups in 2-hr and 6-hr sequentially treated group, expanding 40-fold in the control group, and 35-38-fold in batch, 2hr, and 6hr edited groups over 15 days (Figure 4.11 top). The 24hr VECT edited group, however, experienced a lag in growth until day 6 when T cells were reactivated. Electroporation, like we hypothesized, showed a much lower fold expansion. Batch electroporated and 2-hour electroporated groups remained proliferative, similar to VECT counterparts. 6-hour and 24-hour electroporated groups had only limited fold change, both had below 10-fold expansion over 12 days (Figure 4.11 bottom).

Our data showed that 6-hour DSB recovery should be considered for functional assessment for their ability to reduce translocation while maintaining editing

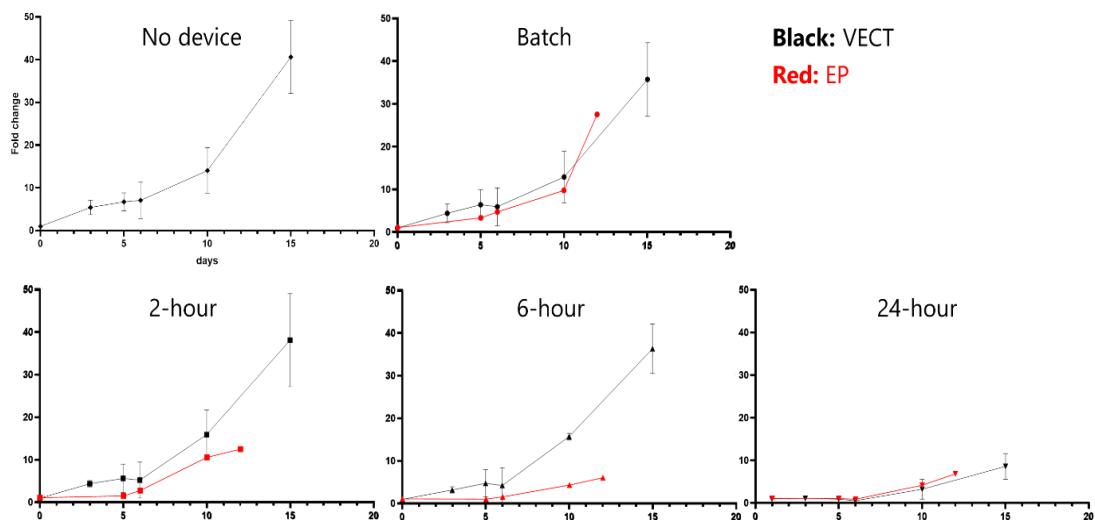


**Figure 4.11: Proliferation is preserved only in VECT-generated sequential edited groups.** Cell proliferation was represented as fold change over the number of cells recovered after device processing. Black lines show data form VECT-treated cells; red lines show data from EP-treated cells. EP: N=1; VECT: N=3. Error bar=SD.

efficiency and proliferative viability. Only VECT is capable of generating proliferative 6-hour sequential edited populations, emphasizing the previously reported limitation of electroporation. Because the ability of T cell populations and turn such T cells into CD19 CAR-T cells and assessed functional killing efficiency.

#### *4.3.3 Sequential Editing Improves T cell cytotoxicity*

Finally, we tested the hypothesis that translocation was a significant cause for diminished CAR T memory phenotype and potency. To do this, we performed the first completely microfluidic approach to transfection and transduction. We first evaluated the kinetics of transduction and CAR expression efficiency of using a microfluidic facilitated approach [17]. Briefly, the transduction device concentrates viral particles to enhance contact between virus and cells, facilitating viral entry and improving transduction efficiency. We tested the kinetics of transduction at multiplicity of infection (MOI) of 1, 5, and 10. In contrast to transduction in a well-plate used in the CD5 KO CD19 CAR production, transduction in this microfluidic device quickly reach a maximum efficiency between 80-90% even at an MOI of 1. (Figure 4.12 A). This transduction efficiency is 10% higher than calculated efficiency under a Poisson probability of MOI of 1. Using the Poisson equation  $P(X=x) = \frac{e^{-\lambda} \lambda^x}{x!}$ , at MOI of 1, transduction success should be 63%. This highlights the improved viral-cell interaction efficiency in this microfluidic device. Of course, how the viral titer was calculated and the cell line/primary T cell form which it was normalized also plays a role in obtaining a high transduction efficiency, but it is outside the scope of this thesis. transduction success should be 63%. This highlights the improved viral-cell interaction efficiency in this microfluidic device. Of course, how the viral titer was

calculated and the cell line/primary T cell form which it was normalized also plays a role in obtaining a high transduction efficiency, but it is outside the scope of this thesis.

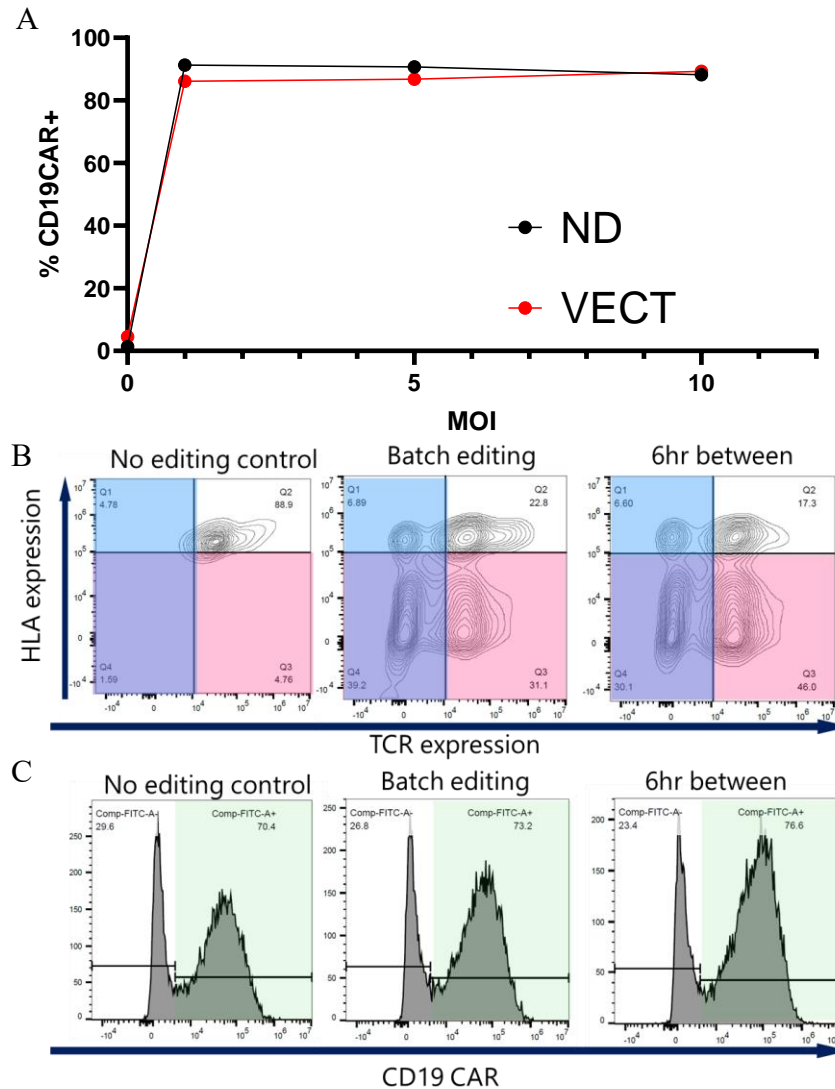


**Figure 4.12: Batch and sequentially edited T cells were turned into CD19CAR+ therapeutic cells effectively.** A) transduction efficiency of VECT (6hr sequential) “VECT” and no device control “ND” across 0-10 MOI in the microfluidic transduction device. B) flow cytometry contour plot of TCR single KO (blue), B2M single knockout (red), and double knockout (purple). C) CD19 CAR expression rate in no device control, batch edited, and 6hr sequentially edited T cells. N=1 for each group.

We tested if a sequential VECT process negatively impacted transduction. Transduction efficiency was very similar among 6-hour sequentially treated T cells and no VECT device control T cells. For downstream potency assessment, we used MOI of 5 to ensure maximum transduction efficiency. We then used VECT to perform batch- and 6 hr-sequential editing. Knockout was quantified on day 9. The results indicated 46% TCR KO, 70% B2M KO, and 39.2% double KO among the batch-edited population; and 37% TCR KO, 76% B2M KO, and 30.1 double KO% among 6 hr-sequential edited T cells (Figure 4.12 B). We again achieved high transduction efficiency across all experimental groups with 70.4%, 73.2%, and 76.6% CD19 CAR expression in no VECT device control, batch-, and 6 hr-sequential editing.

After establishing the efficiency of combining VECT and this transduction device, we tested their ability to eliminate CD19+ cancer cells. Similar to that illustrated in Figure 4.4 A, T cells were mixed with Nalm6 or Raji cells at 1:1 or 3:1 ratio for 24 hours. Target cell death was quantified via flow cytometry with apoptosis marker annexin V and necrosis marker 7-AAD.

As expected, un-transduced T cells (Figure 4.13 A “Mock”) showed low baseline killing against Nalm6 cell line, while transduced cells at all E:T ratios showed high cytotoxicity (Figure 4.13 A, “1:1 N” and “3:1 N”). Cytotoxicity saturated even at 1:1 ratio, as we saw no improvement in target cell death at 3:1 ratio. The three groups, no editing, batch-, and 6hr-sequential edited, did not show statistically different cytotoxicity with 90.0%, 92.0% and 91.9% target cell death respectively. Consistent with the increased cytotoxicity activity, the T cells in the coculture also had increased cell death. Among 1:1 ratio cultured with Nalm6 cells,

20-25% transduced T cells were apoptotic or necrotic, while below 5% un-transduced T cells were dead (Figure 4.13 B). Increased T cell apoptosis and exhaustion usually accompanies the T cell activation and cytotoxic killing process [18]. However, when tested against Raji cells, cytotoxicity is significantly lower, with only 25-72% target cell death rate in 1:1 culture ratio and 60%-85% death in 3:1 culture ratio (Figure 4.13 A). Interestingly, the most efficient target elimination came from 6hr-sequential edited group. Even among un-transduced, 6hr-sequential edited T cells resulted in 43% and 72% target cell elimination. Transducing into CD19 CAR enhanced cytotoxicity slightly but significantly to 72% and 85%. Because of the nonspecific nature of the cytotoxicity, we hypothesized that sequential editing enhanced cytokine secretion. However, further studies of cytokine secretion after coculture with target cells are needed to conclude the mechanism of enhancement. The T cell death rate was slightly higher in culture with Raji cells compared to in coculture with Nalm6 cells. But overall, T cells remain 70-90% viable across all groups. We noticed morphological differences between Nalm6 and Raji cells. Raji notably form large cell aggregates (Figure 4.13 C). Clumps can provide protection to the target cells from getting in contact with CAR T cells. The 6hr-sequentially edited T cells generated superior cytotoxicity without sacrificing effector cell viability, even against a more difficult target cell line. Prior studies showed T cell carrying large chromosome abnormality tend to be short-lived [19], suggesting abnormal physiology among batch-edited CAR T cells. This observation provides evidence of the advantage of sequential multiplex editing.

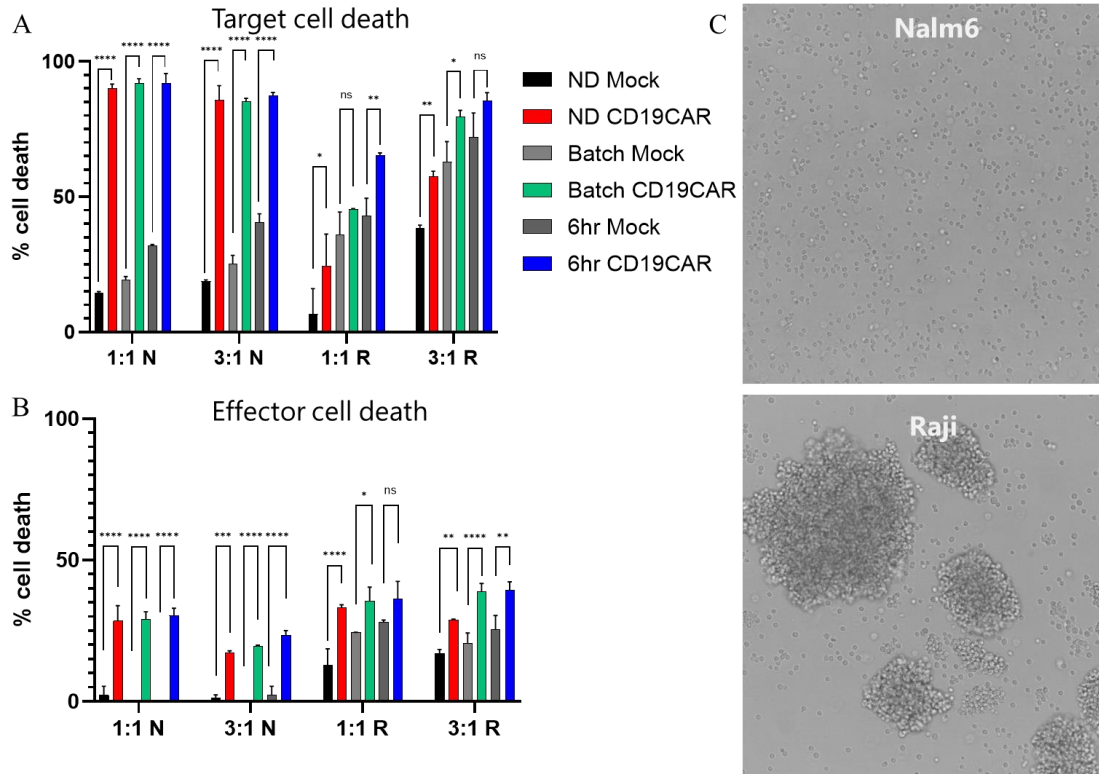


**Figure 4.13: 6hr sequentially edited CAR T cells had superior cytotoxicity against difficult target cells.** A) cytotoxicity quantified as target cell death, which is defined as 1-(% apoptosis- and necrosis-) normalized to viability of target cells cultured without effector cells. B) cell death rate of effector cells defined as 1-(% apoptosis- and necrosis-) normalized to viability of effector cells cultured alone. C) Bright filed image of Nalm6 and Raji cells showing different morphology. N = 2. Stat test = two-way ANOVA. Error bar = SD.

#### 4.4 Summary

Chapter 4 of the thesis explores the cell VECT approach to achieve efficient and non-disruptive delivery of gene editing in CAR T cell therapy manufacturing. We discussed the challenges in existing cell engineering techniques, such as viral transduction and electroporation, which often compromise cell viability and functionality, and bring risks of genome toxicity. These limitations hinder the sequential gene editing necessary for reducing chromosomal translocation and improving CAR T cell persistence.

In the section "Cas9 Delivery Capability in CAR T cell manufacturing," the thesis investigates the capability of microfluidics-based CRISPR/Cas9 gene editing using the VECT method compared to conventional electroporation. The study demonstrates similar delivery efficiency between VECT and electroporation, with VECT showing superior cell viability and proliferation rates. Moreover, VECT-treated cells exhibit enhanced expansion potential, resulting in a higher yield of edited cells over a 10-day expansion period.

In "Comparison with Electroporation," the compatibility of VECT with downstream CAR T manufacturing processes, including viral transduction, is highlighted. The study shows successful generation of functional CAR T cells with CD5 knockout using VECT, affirming its adaptability and efficacy in CAR T cell production. Most importantly, the T cell memory phenotype, which are associated with in vivo CAR T persistence and patient response, was not reduced compared with the negative control. These findings highlight VECT's potential to improve CAR T product as an alternative to EP and viral vectors.

In "VECT is Compatible with Downstream CAR T Manufacturing Processes," the thesis extends the application of VECT to patient-derived T cells, albeit with lower editing efficiency compared to healthy donor T cells. The study identifies mechanical differences between patient-derived and healthy donor T cells, suggesting the need for optimization to better suit patient-specific biomechanics.

In "Capability in Sequential Gene Editing," the chapter presents an alternative multiplexed gene editing workflow by showing the capability of VECT for sequential

gene editing, focusing on targeting multiple loci to develop allogeneic T-cell therapies. In "Process Development for Second Editing," we evaluated the best process parameters for sequential editing, including the choice of T cell activation and the choice of cell source (cryopreserved or freshly isolated), and optimized devices for the second editing based on the stage post activation.

In "Chromosome Repair Requires 24hr in T cells", this study explores the duration of DSB repair, and identified that a 24-hour separation between sequential edits eliminates reduces translocation below the detection limit by qPCR (0.0001%); and 6-hour separation reduces chromosomal translocation while maintaining editing efficiency and cell viability. This thesis then evaluates the impact of sequential editing on T cell proliferation and functionality. In contrast, sequential EP resulted in significantly reduced T cell proliferation, especially in 6hr- and 24hr-seperation. It clearly shows the enabling capacity of VECT for novel gene editing workflow.

Finally, in "Sequential Editing Improves T cell cytotoxicity", we show the sequentially edited T cells can be transduced into functional CD19 CAR T cells at high CAR-expression efficiency. CAR T cells turned from sequentially edited T cells have superior cytotoxicity against a difficult cell line. From this observation, we propose that sequentially edited CAR T cells have the potential to perform better against solid tumor.

In conclusion, Chapter 4 underscores the transformative potential of VECT in enhancing gene editing efficiency and optimizing cell-based immunotherapies, paving the way for safer and more effective treatments in the field of cancer therapy.

## 4.5 Method

### 4.5.1 PDMS-glass Composite Device Fabrication

4 ml 10:1 PDMS: linker was mixed and spin-coated on wafer on the Laurell WS650 spin coater at 200 rpm for 90 seconds. The film (150-180  $\mu\text{m}$  thick) was cured at 80°C for 3 mins. Glass slides were cut into rectangular pieces to completely cover the microchannel. The glass pieces were plasma cleaned in an air plasma cleaner and placed over PDMS-covered channels. Additional 30 ml PDMS was poured and cured at 80 °C for 1hr. Cured devices were cut, punched at inlet and outlet, and plasma bonded to glass slides.

### 4.5.2 Epoxy Device Fabrication

Tubing (1/16" inner, 1/8" outer diameter) was cut into 1 cm pieces and glued to inlets and outlets using Duco Cement. SuperClear epoxy was mixed at 1:1 volume and vacuum degassed. Mixture was poured and left to cure overnight at room temperature. The epoxy-covered wafer was heated at 80°C for 10 minutes until the cured epoxy became soft. The epoxy could therefore be carefully lifted from the wafer and subsequently cut into individual chips while retaining the molded shape. Tubing and remaining Duco cement was then removed from the inlets and outlets. Devices were plasma bonded with glass slides and baked at 80°C oven for 20 mins. Clean tubing was super glued into the inlets and left to dry for >2 hours.

### 4.5.3 Cell lines

The Jurkat cell line was obtained from American Type Culture Collection (ATCC, Manassas, VA). The 697 cell line was kindly provided to us by the laboratory of Dr. Douglas Graham (Emory University, Atlanta, GA). Nalm6 and Raji cell lines were kindly provided to us by the laboratory of Dr. Krish Roy (Georgia Institute of Technology, Atlanta, GA). The primary culture media for these cell lines was RPMI (Corning, Manassas, VA) with 10% fetal bovine serum (FBS) and 1% penicillin/streptomycin.

#### *4.5.5 Expansion of primary T cells*

PBMCs from healthy consenting donors was purchased from AllCells (Alameda, CA) and cryopreserved. Upon thaw, T cells were isolated with EasySep Human T cell isolation kit (STEM CELL technologies, Vancouver, Canada) and stimulated with Dynabead Human T-Activator CD3/CD28 (Thermo Fisher Scientific, Waltham, MA) in a 1:1 ratio, according to the manufacturer protocol. T cells were expanded in X-VIVO 15 media (Lonza, Switzerland) with 10% Fetal Bovine Serum (Corning, MA), 1% penicillin/streptomycin/amphotericin B (Lonza, Greenwood, SC), 1% GlutaMAX (Gibco, Thermo Fisher Scientific, Waltham, MA) and 100 ng/mL IL-2 (PeproTech, Rocky Hill, NJ). Cells were maintained at a concentration of  $\sim 1.5 \times 10^6$  cells mL<sup>-1</sup> and incubated at 37°C with 5% CO<sub>2</sub>. 24-hour after stimulation, Dynabeads were removed by pipetting and brief incubation on DynaMag magnet before conducting a delivery experiment. For extended expansion post cell processing, the culture media was changed every 72 hours and T cells were diluted to  $1.5 \times 10^6$  cells mL<sup>-1</sup> after each media exchange. T cells were reactivated every 6 days from the last activation with a 24-hour Dynabead stimulation.

#### *4.5.6 Primary patient samples*

Viable frozen de-identified peripheral blood mononuclear cells (PBMCs) collected at the time of diagnosis from B-ALL patients were obtained from the Aflac Leukemia and Lymphoma Biorepository at Children's Healthcare of Atlanta (CHOA). Studies using human samples were conducted in accordance with relevant guidelines and regulations. Experimental protocols were approved by the Emory University Institutional Review Board (Protocol #00034535). All samples were collected after written informed consent/assent was obtained from patients and/or their legal guardian(s).

#### *4.5.7 Microfluidic cell processing setup*

In FITC-dextran delivery experiment, cells were resuspended in a cell flow media composed of serum-free media Opti-MEM™ (Gibco, Thermo Fisher Scientific, Waltham, MA) with 0.05% (w/v) methyl-cellulose at  $5 \times 10^6$  cells mL<sup>-1</sup> for FITC dextran delivery, with 0.3 mg/mL 500,000 Dalton FITC conjugated dextran.

In cas9 RNP delivery experiment, T cells were resuspended and washed in 5mL DPBS(-/-) to remove residual serum components, and resuspended in the cell flow media to  $10 \times 10^6$  cells mL<sup>-1</sup>. Purified cas9 protein with nuclear localization signal (NLS) (Aldevron, ND, USA) was complexed with 1.5X molar excess single guide RNA (sgRNA) at room temperature for 20 minutes. 5, 10, or 15 µg of cas9 was used for every 100 µL of cells.

Cell-in-media suspension was infused into the microfluidic device using a pressure controller (OB1, ElveFlow, CA, USA) at the set pressure. Following collection from the outlets, the T cells were resuspended in T cell culture media for downstream expansion and experiment. An additional wash step was added in FITC-dextran delivery experiments to

remove surface-associated dextran. Cells were washed 2X with DPBS (+/ +) to remove residual FITC-dextran. Washed cells were resuspended in flow cytometry buffer for quantification. Fluorescent data was obtained in a FACS Melody analyzer (BD Biosciences, CA, USA). Delivery efficiency is defined as the percentage of population shifting to higher intensity region compared to an unprocessed control; viability is defined as the percentage of population with negative stain when incubated with a membrane-impermeable label; intracellular cargo concentration is represented by MFI shift defined as MFI ratio of cargo positive and negative population.

#### *4.5.8 Electroporation*

T cells were prepared the same way as microfluidic-treated T cells. After the cell washing step, T cells were resuspended in the Lonza T cell Nucleofector Solution supplemented with a Supplement solution. Electroporation was conducted according to Amaxa Primary Human T cells Nucleofector Kit using manufacturer protocols for activated T cells. Cells were electroporated in an Amaxa Nucleofector II (Lonza) using Program T-020 in an 2mm cuvette.

#### *4.5.9 Flow cytometry quantification of gene knockout*

Antibodies were purchased from Biolegend (CA, USA). For CD5 expression quantification, we used a mouse anti-human CD5 conjugated to PE (catalog# 300607). For stem memory T cell phenotyping, we used a mouse anti-human CCR7 conjugated to APC (catalog# 353213), and an anti-human CD45RA conjugated to PE/Cy7 (catalog# 304125). For CD19 CAR expression, we quantified expression of EGFP that's co-expressed on the vector.

Antibody staining was carried out according to the manufacturer protocol from BioLegend.  $0.5 - 1 \times 10^6$  cells were washed and resuspended in Cell Staining Buffer (Biolegend). 200µg of antibody was incubated with 100µL cell on ice for 20 minutes. Cells were washed 2X in 2mL Cell Staining Buffer to remove residual antibodies. A cell viability marker 7-AAD or Live/Dead Aqua (Thermo Fisher Scientific) was added to the buffer before flow cytometry according to the manufacturer protocol. BD FACS Melody or Cytex Aurora was used for fluorescent analysis.

#### 4.5.10 qPCR

Genomic DNA was isolated using QuickExtract DNA Extraction Solution (Lucigen, Biosearch Technologies, United Kingdom). We performed PCR to amplify the translocation rate, using primers on different chromosomes where gRNA targeted. FAM-conjugated probes targeting the region between primer-binding loci and Bio search gRNA target loci are designed to signal amplification.

sgTRAC: 5' TGTGCTAGACATGAGGTCTA 3' PAM: TGG

Forward primer: 5' GGGCAAAGAGGGAAATGAGA 3'

Reverse primer: 5' CATTCTGAAGCAAGGAAACAG 3'

Probe: 5' TGCAAACGCCTTCAACAACAGCAT 3'

sgB2M: 5' GAGTAGCGCGAGCACAGCTA 3' PAM: AGG

Forward primer: 5' CTTGGAGACAGGTGACGGT 3'

Reverse primer: 5' GGCCACCAAGGAGAACTTG 3'

Probe: 5' TGCACCCTCTGTGGCCCTCGC 3'

TRAC-B2M translocation was defined as rate of occurrence of amplification product with TRAC-forward primer and B2M-reverse primer (B2M probe); B2M-TRAC translocation was defined as rate of occurrence of amplification product with B2M-forward primer and TRAC-reverse primer (TRAC probe). Rate was normalized to wild-type product with TRAC-forward and TRAC-reverse primers and B2M-forward and B2M-reverse primers. qPCR was done with Thermo Scientific Maxima Probe qPCR Master Mix in 96-well plate. An ABI StepOnePlus thermocycler was used to quantify amplification curve.

#### *4.5.11 Generation of CAR encoding lentiviral vector.*

High-titer, recombinant, self-inactivating (SIN) HIV lentiviral vector was produced using a four-plasmid platform. The expression plasmid encoding the CD19-41BB-3 $\zeta$  construct, along with packaging plasmids containing the gag, pol, and envelope (VSV-g) genes were transiently transfected into HEK-293 T cells by calcium phosphate transfection. Cells were cultured in DMEM (Thermo Fisher Scientific) supplemented with 10% FBS and 1% penicillin/streptomycin. Twenty-four hours after transfection, the cell culture medium was replaced with fresh medium. At 48 and 72 hours the vector supernatant was collected, filtered through a 0.22  $\mu$ m filter and stored at  $-80$  °C. After the final collection, the vector supernatant was pooled and concentrated overnight via centrifugation at 10,000 x g at 4 °C. Pelleted vector was then re-suspended in serum-free StemPro media (Thermo Fisher Scientific). Titering was performed on infected HEK-293 T cell genomic DNA using quantitative polymerase chain reaction (qPCR). Titers of the concentrated recombinant

viral vectors were  $\sim 1 \times 10^9$  TU/mL. For the CD19 CAR transduction in sequential gene editing studies, viral vector was a kind gift from Dr. Reginald Tran (Georgia Institute of Technology, Atlanta GA)

#### *4.5.12 Lentiviral vector transduction of T cells.*

For CD5KO CD19CAR: Transduction of recombinant HIV-1-based lentiviral vector particles was carried out by incubating edited T cells with vector in appropriate culture medium supplemented with 6  $\mu$ g/mL polybrene (EMD Millipore, Billerica, MA). T cells were transduced at multiplicity of index (MOI) of 20, on day 2 of T cell expansion. Twenty-four hours after transduction, culture medium was replaced with fresh media of X-VIVO 15 media (Lonza, Switzerland) with 10% Fetal Bovine Serum (Corning, MA), 1% penicillin/streptomycin/amphotericin B (Lonza, Greenwood, SC), 1% GlutaMAX (Gibco, Thermo Fisher Scientific, Waltham, MA) and 100 ng/mL IL-2 (PeproTech, Rocky Hill, NJ). Transduced T cells were maintained at a cell density of  $1.5 \times 10^6$  cells/mL with complete media exchange every 72 hours throughout the expansion. T cells were expanded for at least 9 days before assessment of downstream applications.

For TCR B2M KO CD19 CAR: transduction was done in a microfluidic device from Dr. Reginald Tran's lab [17].

#### *4.5.13 Cytotoxicity assay*

CD19 positive target cells were unstained with CellTrace Blue or CellVue Burgundy (Thermo Fisher Scientific, Waltham, MA). Effector (E) and target (T) cells were counted, and viability assessed using trypan blue exclusion or NucleoCounter NC-

200 ChemoMetec, Denmark). Target cells were mixed with effector cells in a 96 well round bottom plate at E:T ratios ranging from 0:1 to 3:1 in a total volume of 250  $\mu$ L. Target cells were added to 48 well plate along with the corresponding number of effector cells. The cell mixture was incubated for 4 hours at 37 °C in 5% CO<sub>2</sub>. After incubation, cells were washed and stained with Annexin V-APC or -PacificBlue (BioLlegend) and 7-amino-actinomycinD (7-AAD) (BD Biosciences). Flow cytometry analysis was performed to assess the total Annexin V and 7AAD positive cells. All experiments were performed in biological triplicate. To calculate specific cytotoxicity, the number of spontaneously lysed target cells in the absence of effector cells was used to normalize.

#### *4.5.14 Statistical Analysis*

GraphPad Prism and R were used to perform statistical analysis and generate plots. Tests include One-way ANOVA, Two-way ANOVA, and t-test, with or without modulation for data sets with unequal variance. All tests used an alpha value of 0.05.

## **4.6 References**

- [1] Bothmer, A., et al., Detection and Modulation of DNA Translocations During Multi-Gene Genome Editing in T Cells. *CRISPR J*, 2020. 3(3): p. 177-187.
- [2] Stadtmauer, E.A., et al., CRISPR-engineered T cells in patients with refractory cancer. *Science*, 2020.
- [3] Horii, T., et al., Efficient generation of conditional knockout mice via sequential introduction of lox sites. *Scientific Reports*, 2017. 7.
- [4] Ghassemi, S., et al., Reducing Ex Vivo Culture Improves the Antileukemic Activity of Chimeric Antigen Receptor (CAR) T Cells. *Cancer Immunology Research*, 2018. 6(9): p. 1100-1109.
- [5] Yang, J., et al., Next-day manufacture of a novel anti-CD19 CAR-T therapy for B-cell acute lymphoblastic leukemia: first-in-human clinical study. *Blood Cancer J*, 2022. 12(7): p. 104.

- [6] Tian, Y., et al., Unique phenotypes and clonal expansions of human CD4 effector memory T cells re-expressing CD45RA. *Nat Commun*, 2017. 8(1): p. 1473.
- [7] Hur, J., et al., Genetically Stable and Scalable Nanoengineering of Human Primary T Cells via Cell Mechanoporation. *Nano Letters*, 2023.
- [8] DiTommaso, T., et al., Cell engineering with microfluidic squeezing preserves functionality of primary immune cells in vivo. *Proceedings of the National Academy of Sciences of the United States of America*, 2018. 115(46): p. E10907-E10914.
- [9] Zhang, Z., et al., Optimized DNA electroporation for primary human T cell engineering. *BMC Biotechnol*, 2018. 18(1): p. 4.
- [10] Chang, C.W., et al., FT819: Translation of Off-the-Shelf TCR-Less Trac-1XX CAR-T Cells in Support of First-of-Kind Phase I Clinical Trial. *Blood*, 2019. 134.
- [11] Abou-El-Enain, M., et al., Putting a price tag on novel autologous cellular therapies. *Cytotherapy*, 2016. 18(8): p. 1056-1061.
- [12] Wang, X. and I. Riviere, Clinical manufacturing of CAR T cells: foundation of a promising therapy. *Mol Ther Oncolytics*, 2016. 3: p. 16015.
- [13] MacLeod, D.T., et al., Integration of a CD19 CAR into the TCR Alpha Chain Locus Streamlines Production of Allogeneic Gene-Edited CAR T Cells. *Molecular Therapy*, 2017. 25(4): p. 949-961.
- [14] Tsuchida, C.A., et al., Mitigation of chromosome loss in clinical CRISPR-Cas9-engineered T cells. *Cell*, 2023. 186(21): p. 4567-+.
- [15] Lemasters, J.J., et al., The mitochondrial permeability transition in cell death: a common mechanism in necrosis, apoptosis and autophagy. *Biochim Biophys Acta*, 1998. 1366(1-2): p. 177-96.
- [16] Rose, J.C., et al., Rapidly inducible Cas9 and DSB-ddPCR to probe editing kinetics. *Nature Methods*, 2017. 14(9): p. 891-+.
- [17] Tran, R. and W.A. Lam, Microfluidic Approach for Highly Efficient Viral Transduction. *Methods Mol Biol*, 2020. 2097: p. 55-65.
- [18] Huan, T., et al., Activation-induced cell death in CAR-T cell therapy. *Hum Cell*, 2022. 35(2): p. 441-447.
- [19] Tsuchida, C.A., et al., Mitigation of chromosome loss in clinical CRISPR-Cas9-engineered T cells. *bioRxiv*, 2023.



## **CHAPTER 5. CONTRIBUTIONS OF FLUID AND CELL MECHANICS TO MECHANOPORATION DELIVERY**

### **5.1 Introduction**

Prior studies have shown that mechanoporation is influenced by the degree of cell deformation induced by both shear forces and compression. Mechanical forces have been applied through a number of ways to cells and a variety of responses have been observed. For example, a study utilizing a microfluidic platform called the  $\mu$ -cell stretcher demonstrated that cells suspended in viscoelastic media exhibited significantly higher levels of deformability compared to cells in standard cell media [1]. This increased cell deformability in the presence of viscoelastic media enhances stretching forces, promotes greater cell deformation, all leading to improved mechanoporation and the internalization of external biomolecules. In addition, an investigation of ten different cell lines with different intrinsic deformability under constant fluid shear resulted in softer cells exhibiting higher delivery efficiency due to increased deformation. This finding indicated a potential correlation of the intrinsic mechanical properties of cells and mechanoporation. Other studies have found that the nucleus of cells contributed significantly to the applied shear force to facilitate high delivery [2], and concluded that nucleus size and nucleus deformability affected mechanoporation significantly. The relationship between mechanoporation and cell deformability pointed to the importance of considering cell mechanical properties in optimizing intracellular molecular delivery techniques.

Another study provided direct evidence that altering cell deformability can improve mechanoporation efficiency through modifying device design. In the study,

a method called progressive mechanoporation (PM) was tested. PM devices had narrowing neck connected to the cell squeeze region that combines shear-induced and contact-mediated membrane poration via multistage cell deformation. This design enhances delivery performance across different cell types by pre-deforming cells and potentiate the membrane and cytoskeleton for permeabilization under constriction [3]. This study showed that delivery efficiency in PM depends on cell elasticity, with stiffer cells exhibiting lower efficiency for fixed device geometries, confirming the findings by other groups that cell deformability was positively correlated to delivery efficiency.

Prior work on the VECT constriction device has also examined a mechanism of how cell mechanical properties and fluid properties synergistically affect mechanoporation [4, 5]. A simple ratio of cell viscoelastic relaxation time over cell transient time under compression predicted volume exchange [4]. Cells that adapt quickly to large strain posed by constrictions, i.e. that are viscous, are forced to lose cytosolic volume as a consequence. Fluid properties, such as flow velocity cause changes in compression rate, which in turn also impacts the effective Young's modulus, which increases with increasing flow rate due to actin network fluidization [6]. Intrinsic T cell stress relaxation rate has also been shown to change dynamic mechanical properties and likely the mechanoporation. Our aim is to explore the relation between fundamental mechanics parameters, for example as characterized by the portion Ericksen number, and delivery outcome to cells.

Furthermore, T cells naturally alter their mechanics due to physiological causes such as T cell activation and procedure through the cell cycle process. Studies on

biophysical properties using micromanipulation techniques observed changes in cell volume and mechanical strength post-activation. Specifically, an initial decrease in mechanical strength was noted at 2 days post-activation, followed by recovery at day 4, while the Young's modulus decreased at both time points, indicating increased membrane flexibility [7]. The nucleus of T lymphocytes emerges as a significant contributor to cellular strength, particularly in resisting compressive forces. These observations prompted us to study how the T cell activation process changes mechanoporation outcome.

After reviewing this evidence, we proposed to study how cell mechanics, combined with fluid mechanics that result from different microfeature designs, can be used to alter the forces acting on cells. In aim 3, we investigate the correlation between T cell biomechanics, fluid mechanics, and transfection efficiency with a goal to understand how the cell manufacturing process such as activation, and how altering device design can result in higher and more homogenous delivery by VECT. This study will utilize high-speed video analysis and atomic force microscopy (AFM) coupled with fluorescent cargo delivery to assess whether change in T cell mechanics affect the delivery outcome. We hypothesize that intrinsic cell mechanics alters the critical force ratio, represented by the Ericksen number, and in turn changes delivery efficiency by VECT. We also propose that altering device design and operational conditions can change the fluid forces cells experience, promoting delivery to hard-to-transfect T cells.

## **5.2 Contributions of Fluid Mechanics and Biomechanics to Delivery**

### 5.2.1 Strain rate and acceleration both contribute to high delivery

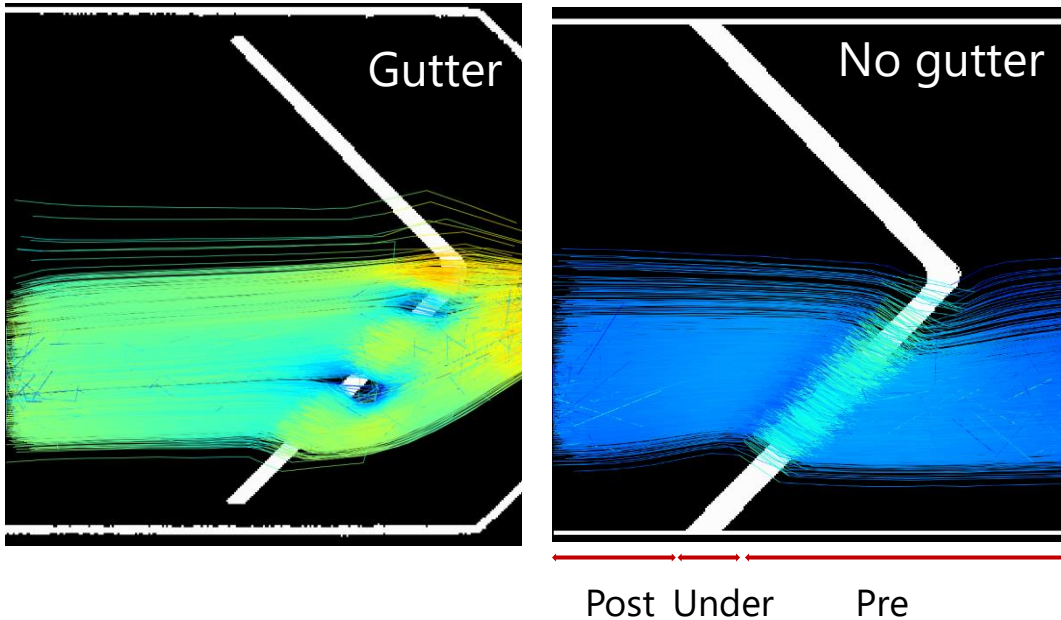


**Figure 5.1 High speed video analysis showed velocities at 3 locations relative to the ridge.** We analyzed and visualized cell velocity from high-speed videos using TrackMate on Fiji. We then calculated cell track velocity at pre-, under-, and post-ridge regions in devices with and without gutters. Cell tracks were color-coded by the velocity of links of 2 cells in adjacent frames in the same track. Images are from videos taken at 3bar (Gutter) and 2bar (No gutter)

In Chapter 2, we identified the gutter as a device feature that led to significant changes to the compression rate. Removing the gutter prompted significantly higher delivery and more uniform delivery in T cells. We rationalized that the gutter the altered fluid forces in a way as to promote delivery. To begin the study of fluid contribution to convective delivery, we took videos of 24-hour activated T cells going through devices with or without gutter at various pressures. We analyzed these videos to track the velocity of cells in positions relative to the ridge, which we termed pre-ridge, under-ridge, and post-ridge (Figure 5.1 “Pre”, “Under”, “Post”). We visualized these cell tracks with colors to indicate the velocity of cells (Figure 5.1). It is clear

that the velocity of both pre- and under-ridge velocity is higher in the no gutter devices comparing to the gutter devices. We then quantified and plotted the velocity across 3 pressures (1,2,3 bar for no gutter, 2,3,4 for gutter). Our finding confirmed the prior result from Chapter 1, that adding gutter resulted in slower compression rate. At equal pressure, gutter devices had a much lower under-ridge velocity while maintaining a relative similar or lower pre- and post-ridge velocity (Figure 5.2). The results indicate the under-ridge velocity is consistently higher in no-gutter devices at the same pressure, leading to a higher strain rate exerted on cells under a ridge with no flanking gutters. Due to this velocity difference at pre- and under-ridge locations, we noticed a difference in acceleration between the two devices, primarily due to a relatively high volumetric flow through the gutter.

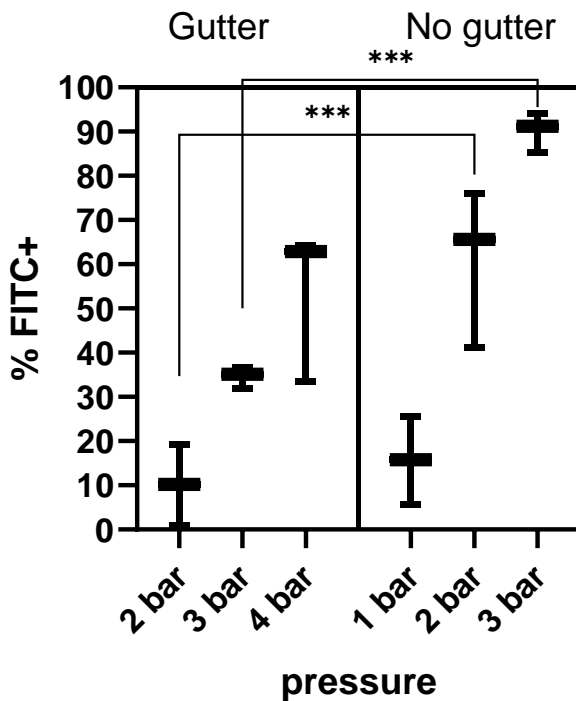


**Figure 5.2 Gutter feature reduces delivery compared to no gutter devices at equal pressure.** FITC-dextran delivery efficiency was quantified among devices with or without gutters at 3 pressures.

To test the contribution of rapid compression rate and inertial force to convective delivery, we tested dextran delivery efficiency between the two designs. We observed an increasing trend in delivery at increased pressure, and an increase in delivery in the no gutter devices at all pressures (Figure 5.3). Delivery efficiency was significantly better at equal pressure (2bar Gutter-2bar No gutter,  $p < 0.001$ ; 3bar Gutter-3bar No gutter,  $p < 0.001$ ). We hypothesized that the difference in acceleration or compression rate is a contributing factor to convective delivery. From prior studies,

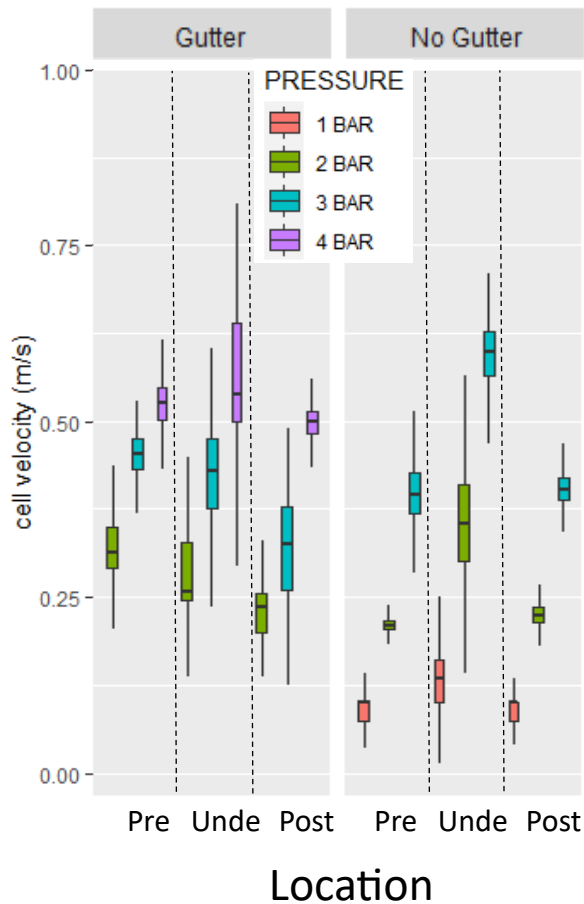


**Figure 5.3 Gutter feature reduces compression rate and reduces acceleration.** Box-whisker plots of pre-, under-, and post-ridge velocity from high-speed videos processed at 2-4 bar (gutter) or 1-3 bar (no gutter).

we identified the volume recovery time defined as cell transit time between ridges to be significantly related to delivery efficiency and intracellular concentration [4].

Therefore, we tested whether volume recovery time significantly impacted the delivery to primary T cells.

We plotted delivery efficiency as the dependent variable against compression rate defined as compressed strain over under-ridge transit time. We also plotted the

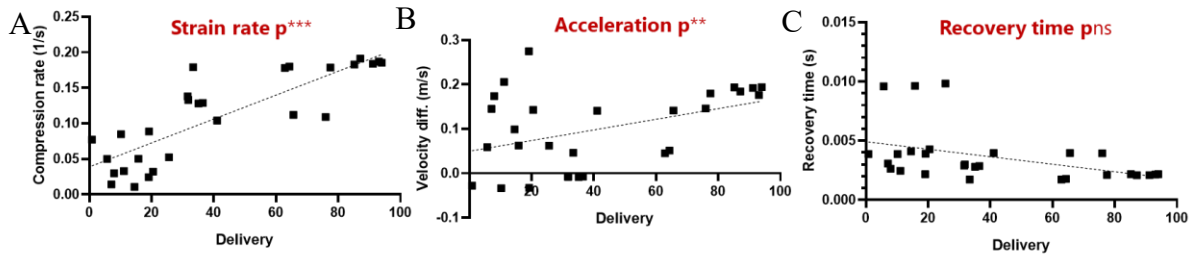


**Figure 5.4 high strain rate and acceleration significantly contributed to delivery.** Scatter plot of delivery (x-axis) with strain-rate (A), acceleration calculated as velocity difference between pre- and under-ridge cells (B), and recovery time (C). Dashed line shows linear regression fit. P-values were indicated in the title of each plot. ns  $p > 0.05$ ; \*\*  $p < 0.01$ ; \*\*\*  $p < 0.001$ . Linear regression and Pearson's correlation was used for statistical test.

acceleration, represented as the velocity difference between under-ridge and pre-ridge cells as well as the recovery time, defined as the ratio of distance between ridges and the post-ridge velocity (see Table 5.1 for definition). Shown in Figure 5.4, a clear correlation can be observed between delivery and compression rate. A positive trend was also observed between delivery and acceleration, although the data points appeared to have larger deviation from the trend line with a lower  $R^2$  value (Linear regression of individual factors revealed significant covariation between delivery and compression rate, and between delivery and acceleration. Recovery time did not show significant correlation for delivery, possibly due to a saturated recovery time is reached. We have shown in previous studies that 1 ms is sufficient for Jurkat T cells to reach full delivery [5], which is surpassed at all pressures tested.

We performed a multivariate regression on compression rate and acceleration to test their relative contribution to delivery efficiency. The regression equation included an interactive effect of compression rate and acceleration. Compression rate stood out as the primary contributor to transfection efficiency. Acceleration alone did not show significant correlation with delivery. But interaction of acceleration and compression rate (expressed as acceleration rate (m/s)  $\times$  compression rate (m/s) in the regression equation) was significantly correlated. Statistically, this means that effect of acceleration varies at different compression rate. The regression parameters are detailed in Table 5.1. This equation,  $\text{delivery \%} = -2.501 + \text{compression rate (m/s)} \times 264.7 + \text{acceleration rate (m/s)} \times 36.09 + \text{acceleration rate (m/s)} \times \text{compression rate (m/s)} \times 1080$ , suggests that cells need to reach a compression velocity of at least 0.01 m/s to enter the delivery regime without the synergistic acceleration effect. This is consistent with our previous finding that cell volume exchange happens at and beyond a cell velocity of 0.02m/s [5]. Without increasing compression rate, higher acceleration alone only marginally improve delivery. Every 0.1m/s velocity difference cells experienced improves delivery by  $\sim 5\%$ .

**Table 5.1 Multivariable regression function and statistics for delivery efficiency. Red indicates statistically significant factors impacting delivery.**

Regression equation parameters				
Parameter estimates	Variable	Definition	Estimate	Standard error
$\beta_0$	Intercept		-2.501	8.017
$\beta_1$	A : Compression rate (m/s)	$\frac{\text{cell diameter} - \text{Gap size}}{\text{Velocity (under)}}$	264.7	69.33
$\beta_2$	B : Acceleration (m/s)	Velocity(under)-Velocity(pre)	36.09	51.77
$\beta_3$	A*B		1080	440.8
P value				
Sig. diff. than zero?	Variable	Definition	P value	P value summary
$\beta_0$	Intercept		0.7578	ns
$\beta_1$	A : Compression rate (m/s)	$\frac{\text{cell diameter} - \text{Gap size}}{\text{Velocity (under)}}$	0.0008	***
$\beta_2$	B : Acceleration (m/s)	Velocity(under)-Velocity(pre)	0.4925	ns
$\beta_3$	A*B		0.0220	*

This interesting finding prompted us to develop a phase diagram for delivery that considers both compression rate and acceleration. As shown in Figure 5.5, the points on the scattered plot represented individual experiments whose acceleration and compression rate were calculated from high-speed videos. Each point is colored by their delivery efficiency of FITC-dextran. The background of the plot is colored according to the color of the points around that region. As we increase acceleration alone below a critical strain rate, we did not observe an increase in delivery efficiency as indicated by no color change along the y axis (Figure 5.5, “No improvement”). Beyond the critical strain rate, cells are promoted to the convective delivery regime. As we increase acceleration with low increase in strain rate, cells would experience a low improvement of delivery (Figure 5.5, “Low improvement”). As we increase strain rate at low acceleration, we observed a mild increase in delivery (Figure 5.5, “Intermediate improvement”). Only when we were above a threshold compression rate and move diagonally, increasing both strain rate and acceleration, did we see a rapid improvement of delivery. This finding supported our learnings from previous

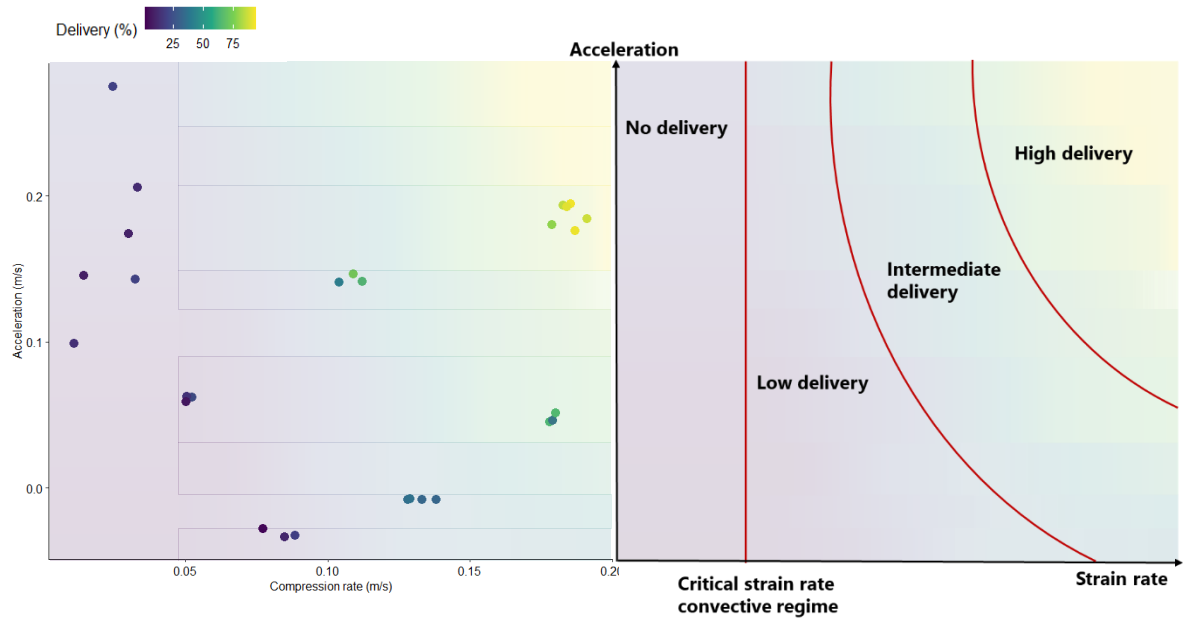


**Figure 5.5 synergistic effect of high compression and high acceleration led to rapid improvement of delivery.** Left: Each experiment is plotted as one point on a scatter plot of compression rate and acceleration (velocity difference). Data points are colored by delivery efficiency. Right: Based on delivery efficiency  $t$ , we made a phase diagram detailing how convective delivery is improved in the 4 phases on the strain rate vs. acceleration plane.

studies that convective delivery only occurs above a threshold strain rate. It also pointed to an important contribution of acceleration prior to contact with the ridge. Together, these data suggested different regimes of convective delivery with shear-force only (low strain rate, high acceleration), contact-based compression force only (high strain rate, low acceleration), and high shear force and compression force working synergistically (high strain rate, high acceleration).

However, we have also observed a drop in cell viability using the no gutter device seen in Chapter 3. We sought to understand the contribution of the three factors (strain rate, acceleration, and recovery time) on cell viability. Multivariable regression indicated that both compression rate and acceleration negatively contribute to viability, but only acceleration was strongly correlated with viability (Figure 5.6 and Table 5.2).

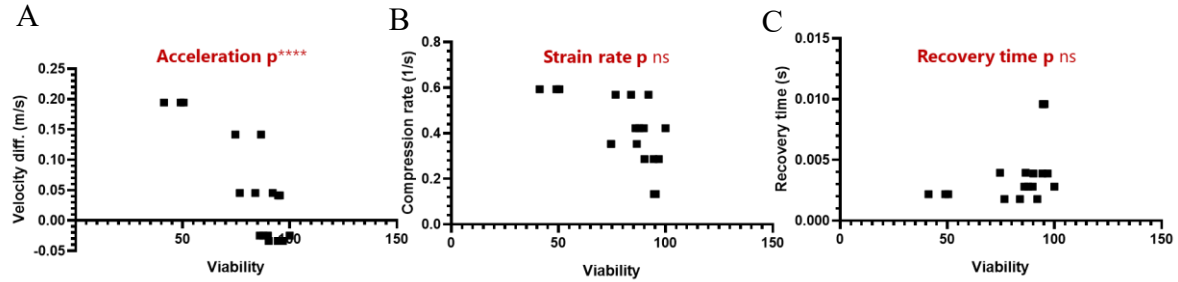


**Figure 5.6 acceleration negatively contribute to viability.** Scatter plot of viability (x-axis) with acceleration calculated as velocity difference between pre- and under-ridge cells (A), strain-rate (B), and recovery time (C).

In summary, adding features to VECT devices that enhance acceleration can improve convective delivery, but with a negative impact on viability.

### 5.2.2 Cells appear stiffer and relax faster with a high strain rate

**Table 5.2 Multivariable regression statistics for cell viability.** Red indicates statistically significant factors impacting viability.

P value			
Variable	Defination	P value	P value summary
A : Acceleration	$\frac{\text{Velocity}(\text{under}) - \text{Velocity}(\text{pre})}{\text{cell diameter} - \text{Gap size}}$	0.0003	***
B : Compression rate	$\frac{\text{Velocity}(\text{under})}{\text{spacing btw ridge}}$	0.2483	ns
C : Recovery time (s)	$\frac{1}{\text{Velocity}(\text{post})}$	0.9966	ns

We sought to understand the impact of compression rate. Since a high compression rate promotes high delivery, we hypothesize that a dimensionless number as a ratio of strain rate and cellular stress relaxation rate should positively correlate with delivery. We have previously used this ratio in a dimensionless Ericksen number.

$$Er = \frac{T_V \Delta L L}{T_C A}, \text{ where } T_V \text{ is relaxation time, the inverse of relaxation rate; and } T_C \text{ is}$$

compression time, inverse of compression rate. For a similar gap size,  $\Delta L$ ,  $L$  and  $A$  are fixed.  $Er$  therefore becomes a function of ratio of compression rate and cell relaxation rate. Thus, the Ericksen number is a useful metric to predict delivery for different device designs, for example with and without gutters. In Figure 5.7 we compare delivery in various devices with and without gutters, assessing different Ericksen number. The devices without gutters have a higher  $Er$  than counterparts with gutters, due primarily to the higher under ridge velocity. In the combination of no gutter and 3 bar condition, >90% cells experience an  $Er$  greater than or equal to 1000. In a previous study, an  $Er$  of 1000 corresponds to the maximum measured volume loss

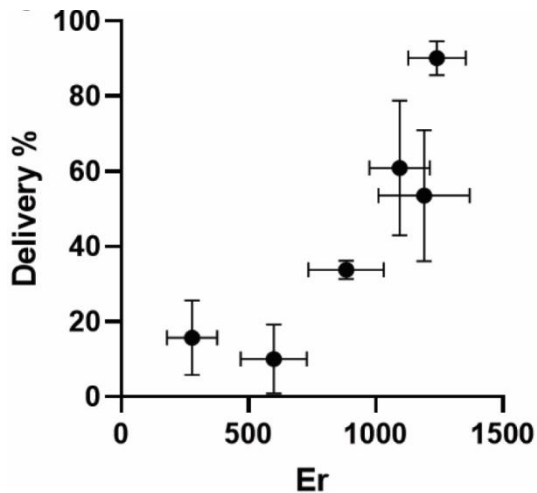


**Figure 5.7 Ericksen’s number predicts delivery efficiency for primary T cells.** Ericksen’s number from 3 no gutter devices and 3 gutter devices were calculated and plotted against delivery efficiency. Each data point has N=3 technical replicates.

[5]. In summary, these findings provided evidence for tweaking VECT designs to alter fluid forces experienced by the cells, promoting higher convective delivery.

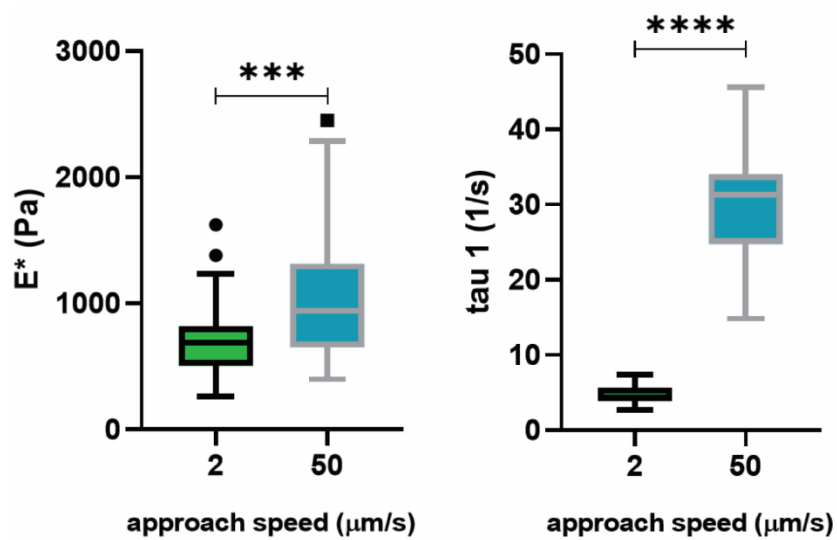


**Figure 5.8 high strain rate promote cell stiffening and fast volume recovery.** Young's modulus (left), fast relaxation constant (middle), and slow relaxation constant (right) of 24-hour activated T cells (donor ID 38321, AllCells) under slow and fast cantilever approach speed.  $N=30-40$ . Stat test= Mann-Whitney U test. Whisker = Tukey Fences. \*\*\* p-value < 0.001, \*\*\*\* p-value < 0.0001

We note that the calculation of  $E_r$  requires an estimate of cell modulus and relaxation rate. It is known that cell mechanical properties could be affected by the strain rate [8, 9]. We measured the impact of increased strain rate on cell mechanics using atomic force microscopy (AFM). While it is difficult to quantitatively measure the mechanical properties of cells at the compression rates achieved in microfluidics ( $\sim 0.1$  m/s), we did nonetheless observe a relationship between the measured mechanical properties and the compression rate by performing force-indentation at slow and fast compression rates. The cantilever approach speed was varied  $\sim 25$ -fold (maximum reliable experimental range) from the equilibrium compression rate of 2  $\mu\text{m/s}$  to a non-equilibrium rate of over 50  $\mu\text{m/s}$ .

We observed that the measured cell stiffness increased significantly when compression rate increased (Figure 5.8 left). The increase in the measured elastic modulus is consistent with a transition to a viscoelastic cytoplasm [9]. We noticed a sub-linear relation between the increase in stiffness and increase in strain rate. We also observed a linear change in cell relaxation rate with the compression rate (Figure 5.8 right) which indicates that cell volume recovery post compression can be significantly faster with a faster compression. At a 50  $\mu\text{m/s}$  approach speed, T cells require 33 ms to relax (relaxation rate  $\sim 29.68 \text{ s}^{-1}$ ). However, in microfluidics devices, the actual strain rate is closer to 0.1 m/s in the microfluidic channel and the measured time for relaxation can be faster. Given that the AFM measurement is three orders of magnitude slower strain rate compared to microfluidics, we expect the cell relaxation rate to further increase, possibly approaching relaxation speed to make the  $\sim 1\text{-}2$  ms time observed experimentally to be critical for sufficient volume influx and cargo uptake. Consistent with this speculation, our most recent study of cell mechanics in a microfluidic cell deformability device, at 0.5 m/s strain rate, cells recover their circular shape and volume in  $\sim 100 \mu\text{s}$ , about three orders of magnitude faster.

We acknowledge that under high strain rate ( $>10\text{kHz}$  deformation rate), cell cytoskeleton plays a minor role in determining apparent stiffness of cells. The cytosolic flow becomes the dominant factor in determining the shape of and the stress in cells. More specifically, for T cells, 80% of their cytosol is occupied by the nucleus. Therefore, we believe this stiffness change is more reflective of the nuclear mechanics. Due to technical limitation, we did not measure a nuclear mechanics separately from the cell mechanics. Specifically, nuclear mechanics reflects the state of nuclear

membrane, nuclear lamina, and chromatin. They are critically linked to transcription activities and mass transport through the nuclear envelope. Therefore, studying how nuclear mechanics alters delivery can provide further insight on delivery of gene reprogramming molecules directly to the nucleus by VECT. We believe additional nuclear mechanics measurements will greatly append our findings.

### *5.2.3 Stiffness is the major contributing factor to high delivery*

From the prior observation of cell stiffening under rapid compression, we hypothesized that cell stiffness is positively correlated with delivery. To test this hypothesis, we performed a FACS sorting of Jurkat T cells that have been delivered with 500 KDa FITC-dextran by VECT. E-6.1 Jurkat T cells have similar size as day 2 activated T cells. Therefore, we used the previously optimized device for day 2 activated T cells that resulted in 50% delivery efficiency. Overall, we saw 33% FITC positive Jurkat cells. These mixed populations of cells were then sorted into transfectable and non-transfectable groups based upon a threshold FITC intensity. The mechanics of each population of cells was then quantified by AFM (Figure 5.9 A). We did not observe a difference in fast or slow relaxation rate (Figure 5.9 B). We did observe a difference in cell stiffness (Figure 5.9 C). The FITC positive population was

measured to be significantly higher Young's modulus compared to the FITC negative population ( $710.57 \pm 208.231$  Pa among FITC+,  $573.60 \pm 208.231$  Pa among FITC-).

From Chapter 2, we observed a decreased knockout rate in the leukemia

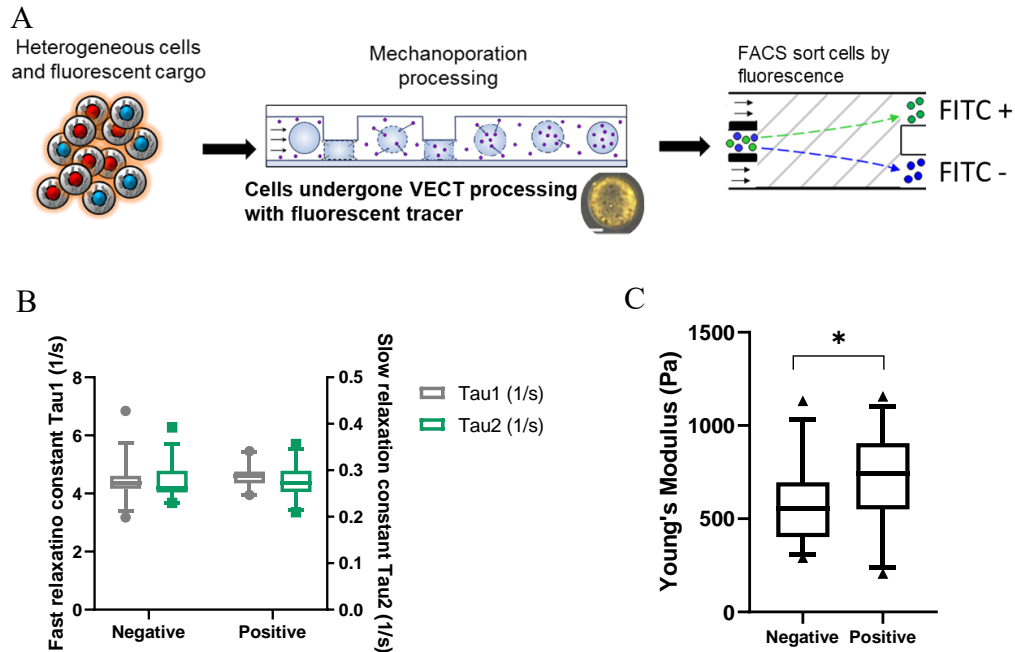


**Figure 5.9 Cell stiffness is identified in highly transfectable population.** A) schematic experiment set up. A heterogenous population of Jurkat cells were treated by VECT for FITC-dextran delivery, then sorted based on FITC intensity. Recovered cells were analyzed by AFM. B) Viscoelastic relaxation time constant, at both fast (tau 1) and slow (tau 2) time scale between FITC negative and positive Jurkat. Outliers indicated. C) Apparent Yong's modulus between negative and positive Jurkat. Outliers indicated. For all paired comparison, Wilcoxon ranked test was performed, \*  $p < 0.05$ .  $N = 35-40$ . Whiskers = Tukey Fences.

patient derived T cells compared to healthy donor T cells. We also measured the Young's modulus of cells from both populations. We used these data to hypothesize that the difference in stiffness was a contributing factor for the lower CRISPR/cas9 RNP delivery. We plot the apparent Young's modulus versus the CD5 knockout efficiency (Figure 5.10 A). They clearly follow a positively correlated relationship

with increasing delivery at increased stiffness. We also examined the relationship with cell size in the populations and found that size played a role too. Both stiffness and size correlated significantly to CD5 knockout with 0.82 and 0.75  $R^2$  value.

Given the data sets of correlation of cell stiffness with delivery observed in both the labeling experiment and the CRISPR experiments, we considered the possibility that greater cell stiffness results in greater internal forces or energy density inside the cells. The stiffer the cells are, the more stress/energy the cytoplasm exerts on the cell membrane upon deformation to the same strain. The larger the cells, the greater the strain they experience when compressed by the same constriction. And therefore, the cytoplasm experiences a greater internal force which can result in cell poration. Moreover, the internal the stress may not be dissipated with sufficient speed viscous within cell, supporting the hypothesis that cytosolic volume can be pushed out through induced pores in the cell.

During the optimization of sequential delivery, we observed that activated T cells show decreased ability to be transfected by VECT with each day post activation, even when they are compressed to the same strain at the same compression rate. Overall, unstimulated and 1-day activated T cells can show 80-90% delivery rate, while 2-day and 3-day activated T cells only showed 50% and 20% delivery. (Figure 5.11 A). We therefore hypothesized that a decrease in stiffness with activation time was a contributing reason for decreased delivery post activation. As we measured T cells on day 0-3 post activation, we indeed observed decreasing Young's modulus (Figure 5.11 B, 477.23 Pa, 403.59Pa, 364.94Pa, and 246.99Pa day 0, 1, 2, and 3 post activation). Statistically, day 0 and day 3 cells had different stiffness, while day 0, 1, and 2 cells had non-significant differences. Our study of T cell mechanics included up to 3 days post activation. It remains to be investigated whether T cells soften continuously, retain similar stiffness, or show plasticity and regain their original stiffness. We hypothesized that over a prolonged culture period, these T cells would

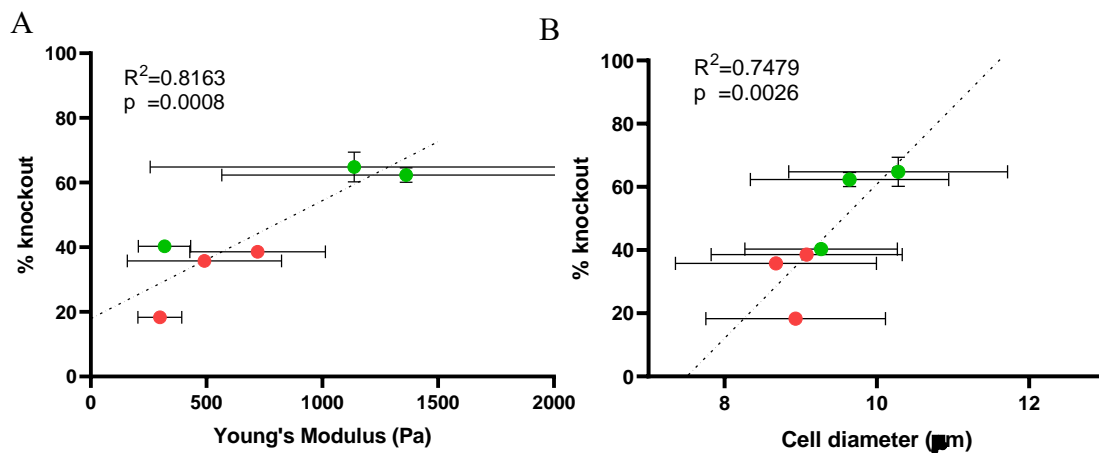


**Figure 5.10 Difference in stiffness separate T cells from healthy donors and AML patients by delivery efficacy.** A) T cell stiffness versus CD5 knockout efficiency scatter plot. Dashed line showed a smoothed trend line across 6 data points. B) T cell size versus CD5 knockout efficiency scatter plot. Linear regression was performed. Goodness of fit and p-value are shown in the graph.

return to a stiffer mechanical phenotype, due to the sequestration of the activation signaling and formation of memory phenotype. It will be important to determine the long-term T cell mechanics for future application of VECT on a range of post-activated T cells.

Comparing to previous works studies that identified cell deformability as a positive predictor to delivery, our findings supported the opposite correlation. Here,

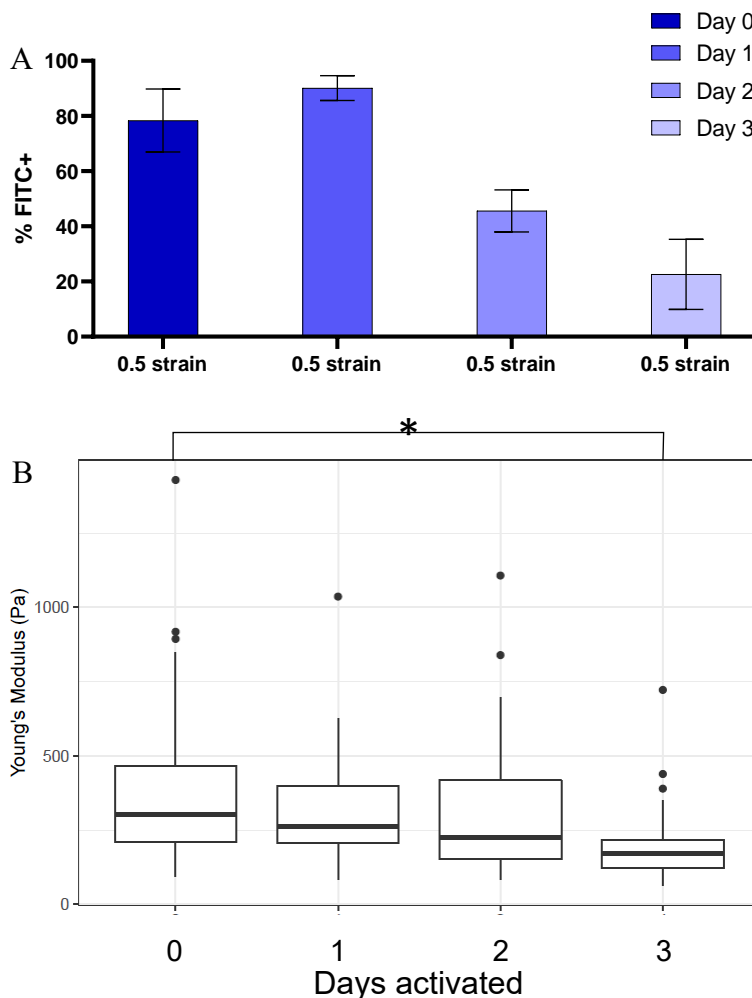


**Figure 5.11 T cell activation led to decreased cell stiffness and in turn decreased ability for T cells to be transfected.** A) bar plot showing even at the same strain and strain rate, T cells on various days post activation resulted in vastly different delivery efficiency. N=3-4. Error bar = SD. B) box-whisker plot of AFM measurement of Young's modulus indicates a softening trend among activated T cells from day 0 to 3. N=30-40. Stat = Wilcoxon ranked test. Whiskers = Tukey Fences.

we identified a positive correlation of stiffness and delivery in T cells. It is interesting to consider that this discrepancy could be the result of different mechanism of delivery that relies less on stretching the cell and more on compression of the cell with minimal stretching. In Kizer et al. (2019), cells were stretched by hydrodynamic force in a cross flow. These cells experienced similar applied stress but different cell stretching due to the uniformity of the shear stress but varying cell stiffness. Hence, the more deformable cells experienced larger strain [10]. Large strain could lead to a number of effects on the cell that lead to delivery, including greater stretching of the cell membrane. In contrast, the VECT device imposes on cells a similar strain as they progress through the constriction, yet the internal forces may be different due to different cell stiffness properties. The internal forces exerted upon the cytosol and the nucleus thus could lead to a greater poration and increased delivery correlated to stiffness instead of deformability.

### **5.3 Summary Fluid mechanics and cell mechanics**

In this chapter, we first identified acceleration in combination with strain rate to be significant contributors to delivery. We identified 3 regimes on the plane of acceleration and strain rate that correlated to no, moderate, and strong improvement in delivery. In our prior studies, we identified a threshold strain rate below which cells did not cause volume exchange. In this new study, we also identified as the threshold strain rate of  $\sim 0.04 \text{ s}^{-1}$  and confirmed the contribution of high strain rate to delivery. In addition, we concluded that acceleration, and likely the shear force that it exerts on cells, promoted delivery. Acceleration alone did not promote delivery in VECT devices; only when combined with high strain rate was strong improvement in

delivery outcome measured. However, acceleration also caused heightened cell death. Moderate to low acceleration should likely be employed for applications that required high cell viability unless a method to decouple the two parameters is discovered.

Next, we probed mechanical changes among cells when they are subjected to high strain rate, in an attempt to understand how strain rate promoted delivery. The apparent cell stiffness increases with compression rate. This observation agrees with a Maxwell model for a viscoelastic liquid-like cytoplasm where stress scales with strain rate. Under faster deformation rate, cells behave more like a viscoelastic material and takes time to deform to the size of the constriction. When cells cannot

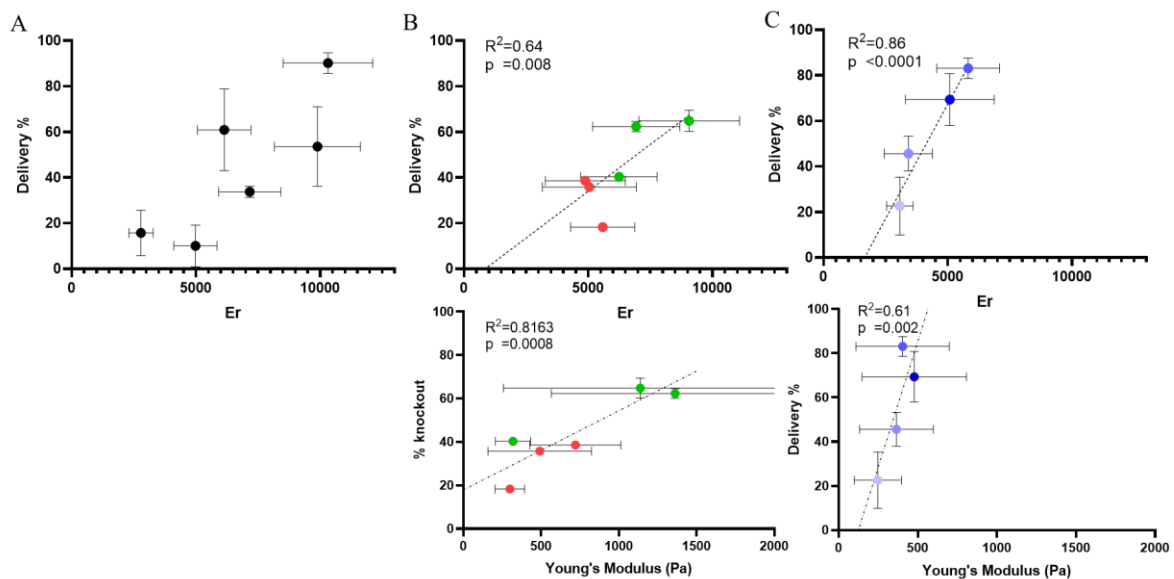


**Figure 5.12 Change in fluid mechanics and natural variation T cell mechanics cause differential Ericksen's number and Young's modulus, both are predictors of delivery by VECT.** A) varying existence of gutters and pressure cause a variation among Ericksen's number and delivery efficiency. B) T cells from healthy (green) and diseased (red) donors have natural variations in Young's modulus and led to change in Ericksen's number and delivery outcome. B) T cells from various days post activation (data from earlier days are shaded darker) have natural variations in Young's modulus and led to change in Ericksen's number and delivery outcome. N = 3-4 for Delivery % and knock %; N=30-40 for Er and Young's modulus. Error bar = SD.

creep to fit under the gap, pressure accumulates in the cytosol, increasing the energy cells experience to eventually push liquid exchange between cells and buffer.

On the other hand, there is an inverse relationship between cell relaxation rate and compression rate. This means that post compression cells can recover their volume faster if they experienced a faster compression. However, it also means the stress dissipation happens faster under compression that helps preserve cell volume. Volume exchange happens only in a regimen when the stress due to high strain rate increases faster than relaxation rate increase.

T cells are naturally heterogenous in mechanics. Their normal physiological activities such as cell cycling and activation change their actin network and mechanics [11-13]. We have identified T cell Young's modulus as a factor that contributed to delivery. Stiffer cells experience more internal pressure upon deformation, thus more likely to enter convective delivery regime. To summarize, we generalized how device design, natural variation in T cell mechanics, and physiological change in T cell mechanics impacted delivery, and how they can be predicted by Ericksen number and Young's modulus. Changing in device design, such as addition or removal of the gutter feature, and operational parameters, such as pressure, impact Like shown before, Ericksen number showed a positive correlation with delivery (Figure 5.12 A). T cell mechanics naturally varies. This could be due to health conditions. In the case of comparing T cells from healthy donors and AML patients, T cell stiffness changed without causing a huge change in cell size. This softening led to decreased delivery efficiency. This variation in delivery efficiency was also picked up by the Ericksen number (Figure 5.12 B, bottom and top), but at a lower degree of correlation. During

physiological T cell activation, we also observed changes in cell stiffness coupled with changes in cell size. The cell size change is reflected in changes in Ericksen number (Figure 5.12 C top) and correlated positively with delivery efficiency. The variation in stiffness also to some degree explained delivery outcome (Figure 5.12 C bottom), although not as accurate as Ericksen number ( $R^2=0.61$  for E,  $R^2=0.86$  for  $E_r$ ). Together, these findings suggested both fluid mechanics and cell mechanics altered delivery outcome through changing the Ericksen number or through changing cell stiffness. In summary, this is the first documentation of a biomarker that correlates to the success of mechanoporation. And it emphasized the need to incorporate biomechanics as an analytical feature in cell manufacturing.

## **5.4 Method**

### *5.4.1 PDMS-glass Composite Device Fabrication*

4 ml 10:1 PDMS: linker was mixed and spin-coated on wafer on the Laurell WS650 spin coater at 200 rpm for 90 seconds. The film (150-180  $\mu\text{m}$  thick) was cured at 80°C for 3 mins. Glass slides were cut into rectangular pieces to completely cover the microchannel. The glass pieces were plasma cleaned in an air plasma cleaner and placed over PDMS-covered channels. Additional 30ml PDMS was poured and cured at 80 °C for 1hr. Cured devices were cut, punched at inlet and outlet, and plasma bonded to glass slides.

### *5.4.2 Epoxy Device Fabrication*

Tubing (1/16" inner, 1/8" outer diameter) was cut into 1 cm pieces and glued to inlets and outlets using Duco Cement. SuperClear epoxy was mixed at 1:1 volume

and vacuum degassed. Mixture was poured and left to cure overnight at room temperature. The epoxy-covered wafer was heated at 80°C for 10 minutes until the cured epoxy became soft. The epoxy could therefore be carefully lifted from the wafer and subsequently cut into individual chips while retaining the molded shape. Tubing and remaining Duco cement was then removed from the inlets and outlets. Devices were plasma bonded with glass slides and baked at 80°C oven for 20 mins. Clean tubing was super glued into the inlets and left to dry for >2 hours.

#### *5.4.3 Video Analysis for Cell Trajectory and Speed*

To measure the cell trajectory and speed in presence and absence of gutters, we took measurements of the cell tracks from video data. Imaging was done with the VECT device on the stage of an inverted bright-field microscope (Eclipse Ti, Nikon, Japan), with a high-speed camera attachment (Phantom v7.3, Vision Research, NJ, USA). Cells were pushed through gap compression at 1 – 4bar pressure. Videos of cells were taken at 300-pixel by 300-pixel region at high speed (>10,000 fps) at the first compression ridge. 20,000 – 30,000 frames were analyzed using FIJI/ImageJ TrackMate program [14]. We calibrated the length scales of each image based on known ridge dimensions, which enabled us to translate the number of pixels into an area measurement. We also converted cell velocity from frame<sup>-1</sup> to s<sup>-1</sup> using frame rate obtained from.

#### *5.4.4 Atomic force microscopy*

To characterize the mechanical properties of primary T cells under slow and fast strain rate, we used force spectroscopy to obtain force-indentation curves with an

MFP-3D atomic force microscope (Asylum Research, CA, USA) with an integrated optical microscope (Nikon) on a vibration isolation table. Cells were attached to glass FluoroDishes (World Precision Instruments, FL, USA) using cell adhesive CellTak (Corning, NY, USA). A 5.46  $\mu\text{m}$  spherical polystyrene particle was attached to tipless silica nitride cantilevers (Bruker Probes, CA, USA) using a two-part epoxy and cured for >24 hours. The AFM was calibrated by taking a single force curve on a clean FluoroDish immersed in serum-free RPMI-1640. The Sader calibration method was used to obtain cantilever spring constants ( $k$  is approximately 10–25  $\text{pN nm}^{-1}$ ) based on the thermal vibration of the cantilever. Two groups of cells were indented at 2  $\mu\text{m s}^{-1}$  or 50  $\mu\text{m s}^{-1}$  until a force trigger of 5nN was reached. The  $z$  position of the cantilever was held in place for 10 seconds, dwelling towards the surface, allowing for viscous relaxation of the cell before the cantilever was retracted. We used custom R code to fit the dwell region of the force curve to a biexponential decay function to extract the viscous rate constant. To extract the cell Young's modulus, we used custom R code relying on the pointwise Hertzian contact model.

#### *5.4.5 Microfluidic cell processing setup*

In FITC-dextran delivery experiment, cells were resuspended in a cell flow media composed of serum-free media Opti-MEM™ (Gibco, Thermo Fisher Scientific, Waltham, MA) with 0.05% (w/v) methyl-cellulose at  $5 \times 10^6$  cells  $\text{mL}^{-1}$  for FITC dextran delivery, with 0.3 mg/mL 500,000 Dalton FITC conjugated dextran.

Cell-in-media suspension was infused into the microfluidic device using a pressure controller (OB1, ElveFlow, CA, USA) at the set pressure. Following collection from the

outlets, the T cells were resuspended in T cell culture media for downstream expansion and experiment. An additional wash step was added in FITC-dextran delivery experiments to remove surface-associated dextran. Cells were washed 2X with DPBS (+/ +) to remove residual FITC-dextran. Washed cells were resuspended in flow cytometry buffer for quantification. Fluorescent data was obtained in a FACS Melody analyzer (BD Biosciences, CA, USA). Delivery efficiency is defined as the percentage of population shifting to higher intensity region compared to an unprocessed control; viability is defined as the percentage of population with negative stain when incubated with a membrane-impermeable label; intracellular cargo concentration is represented by MFI shift defined as MFI ratio of cargo positive and negative population.

#### *5.5.6 Flow cytometry and FACS*

T cells or Jurkat processed in VECT devices with 0.3mg/mL 500KD FITC-dextran were washed to remove residual cargo in the buffer. Cells were analyzed on a BD FACS Melody, gated by FITC intensity based on the bimodal population distribution, and sorted with a “4-way purity” program. For each group, an estimated 100,000 cells were collected for downstream experiments.

#### *5.5.7 Statistical Analysis*

GraphPad Prism and R were used to perform statistical analysis and generate plots. Tests include One-way ANOVA, t-test, linear regression, and multivariable regression, with or without modulation for data set with unequal variance. All tests used an alpha value of 0.05.

## 5.5 References

- [1] Kwon, C. and A.J. Chung, Highly efficient mRNA delivery with nonlinear microfluidic cell stretching for cellular engineering. *Lab Chip*, 2023. 23(7): p. 1758-1767.
- [2] Nikfar, M., et al., Numerical simulation of intracellular drug delivery via rapid squeezing. *Biomicrofluidics*, 2021. 15(4): p. 044102.
- [3] Uvizl, A., et al., Efficient and gentle delivery of molecules into cells with different elasticity via Progressive Mechanoporation. *Lab on a Chip*, 2021. 21(12): p. 2437-2452.
- [4] Liu, A., et al., Cell Mechanical and Physiological Behavior in the Regime of Rapid Mechanical Compressions that Lead to Cell Volume Change, in *Small*. 2019. p. e1903857.
- [5] Liu, A., et al., Microfluidic generation of transient cell volume exchange for convectively driven intracellular delivery of large macromolecules. *Mater Today (Kidlington)*, 2018. 21(7): p. 703-712.
- [6] Du, M., et al., Biomechanical properties of human T cells in the process of activation based on diametric compression by micromanipulation. *Med Eng Phys*, 2017. 40: p. 20-27.
- [7] Urbanska, M., et al., A comparison of microfluidic methods for high-throughput cell deformability measurements. *Nat Methods*, 2020. 17(6): p. 587-593.
- [8] Gerum, R., et al., Viscoelastic properties of suspended cells measured with shear flow deformation cytometry. *Elife*, 2022. 11.
- [9] Burkhardt, J.K., E. Carrizosa, and M.H. Shaffer, The actin cytoskeleton in T cell activation. *Annual Review of Immunology*, 2008. 26: p. 233-259.
- [10] Thauland, T.J., et al., Cytoskeletal adaptivity regulates T cell receptor signaling. *Sci Signal*, 2017. 10(469).
- [11] Zak, A., et al., Rapid viscoelastic changes are a hallmark of early leukocyte activation. *Biophys J*, 2021. 120(9): p. 1692-1704.
- [12] Tinevez, J.Y., et al., TrackMate: An open and extensible platform for single-particle tracking. *Methods*, 2017. 115: p. 80-90.

## CHAPTER 6. CONCLUSIONS AND OUTLOOK

### 6.1 Summary of Major Findings

#### *6.1.1 Aim 1: Using Critical Design Features To Reproducibly Achieve Efficient Delivery*

Under this aim, we set the goal to identify device design and operational factors that promoted efficient and consistent delivery result to primary T cells. First, we showed that the results from cell lines did not translate to primary T cells due to differences in cell size and biomechanics. T cells, especially in early stage of cell activation, were smaller, and thus required more precision to compress with devices. We identified channel buckling as a cause of underperforming delivery at smaller gap sizes and increased operation pressures. To better understand the degree of deformation, we developed a confocal imaging method to reveal the in-situ channel geometry under flow. This method employed covalent linkage between amine and aldehyde to coat the microchannel walls with FITC-BSA, a fluorescently traceable protein. This quantification method was found to be more robust and accurate, with an easy to interpret data analytical process. It facilitates accurate assessment of deformation, thereby enhancing device performance and reproducibility. With this method, we confirmed channel deformation in PDMS devices under pressure relevant to T cell delivery. We found that at 5 bar pressure, the channel dimension can increase to almost 50% of the total channel height.

Addressing the challenge of deformation, a new fabrication method was developed. We applied a simple principle of thin-film PDMS stiffening under a stiff substrate [cite]. According to this method, we produced devices with glass substrate

on a thin layer of PDMS. We identified the glass-channel distance as one of the most important CDEs for this specific hybrid device associated with their ability to control channel deformation. It prompted us to engineer a new fabrication process using spin-coating machine for the precious control of PDMS thin film thickness. Spin coating was shown to control glass-channel distance. Through adjusting spin coating time and speed, we could control the CDE and deliver consistent performance among different devices and devices from different batches. Compared to plain PDMS devices, glass-PDMS hybrid devices significantly increased delivery to 24-hour activated T cells.

When it came to manipulating unstimulated T cells that were  $\sim 2\mu\text{m}$  smaller than 24-hour activated T cells, hybrid devices still resulted in deformation that was hard to control. We next produced a rigid device made with epoxy replica molding. We developed a fabrication method similar to PDMS replica molding, without the use of cleanroom or outsourcing to a commercial hot embossing vendor. We utilized a thermal plastic epoxy material. We confirmed the elimination of deformation in these devices that produced efficient intracellular delivery to small, unstimulated primary T cells.

Once we have identified a robust fabrication method that complied with the reproducible CDE requirement, we next focused on identifying CDEs in microfluidic channel structure design. Features such as serpentine patterns for cell focusing, clog clearing zones for viability enhancement, and specific ridge configurations are described to optimize delivery efficiency. Serpentine with both low and high curvature resulted in focusing of cells to the middle of the channel, decreasing cell flow to through the gutters. Delivery showed a plateau at 12-ridge device, suggesting

12 rounds of volume exchange was sufficient. Optimal delivery also required 880  $\mu\text{m}$  spacing between ridges. This spacing provided  $\sim 1$  ms cell recovery time between ridges, which was sufficient for cells to recover to a pre-compression volume. With 6 ridges, large spacing results in maximum delivery. However, in 12- and 24-ridge devices, 440  $\mu\text{m}$  spacing is sufficient for optimal delivery. The result suggests the number of ridges is more impactful than the ridge spacing. Delivery efficiency in the case of incomplete volume recovery can be compensated by more rounds of volume exchange. Finally, gutter as the clearing zone was how to diverge flow from under the ridge. This resulted in slower strain rate on cells. removing gutter significantly improved delivery, boosting efficiency to almost 100%. However, this design also reduced cell viability to nearly 50%. By considering both delivery efficiency and cell viability, we chose the device design to include a serpentine inlet, 12 10  $\mu\text{m}$ -wide ridges spaced 880  $\mu\text{m}$  apart, and parallel gutters to process the 24-hour activated T cells.

### *6.1.2 Aim 2: Capability to perform Sequential Gene Editing of CAR T Cells using multiplexed CRISPR/Cas9 Delivery*

In this chapter, our investigation showed functional delivery of CRISPR/Cas9 as part of a CAR T editing workflow. We also showed feasibility of a sequential gene editing process by VECT which was not feasible by electroporation. First, we demonstrated the feasibility of functionally delivering gene reprogramming molecules using VECT, using CD5 editing to generate T-cell products against T-cell leukemia that were resistant to fratricide. Through single CD5 knockout experiments, we explored VECT's impact on T-cell physiology, including viability, proliferation, and

memory phenotype. Additionally, we assessed whether VECT-treated cells retained the capacity to be transduced into cytotoxic CAR-T cells. Finally, we showcased sequential editing targeting *TRAC* and *B2M*, evaluating its effects on population heterogeneity, translocation, memory, cytotoxic efficiency.

Our findings underscore the benefits of the VECT workflow over conventional electroporation, yielding 4-fold higher quantity of edited cells over a 10-day expansion interval from experiments among 3 healthy donors in 3 technical replicates. While both methods were observed to preserve memory T cell composition, VECT showed improved cellular viability and proliferation. The increased yield not only augments operational efficiency but also supports new applications for reducing manufacturing timelines and costs and reducing CAR T cell senescence, contributing to elevated CAR T cell product quality and efficacy.

Our investigation to combine VECT and downstream CAR T transduction processes revealed the adaptability and efficacy of VECT. Integration of microfluidic mechanoporation with viral transduction did not reduce transduction efficiency or cytotoxicity of CAR T cells. To our knowledge, this study has been the first to demonstrate functional integration of mechanoporation devices with CAR T cell manufacturing. Additionally, our exploration into VECT's applicability to patient-derived T cells provided valuable insights, despite encountering challenges such as lower editing efficiency in patient-derived cells compared to healthy donor T cells. Nonetheless, the VECT process demonstrated its capability to delivery of gene-modifying cargo to patient-derived T cells, at the same time emphasizing the need for continued optimization to better suit the underlying cell biomechanics.

Lastly, our investigation into sequential gene editing highlighted the potential of VECT in enabling multiplexed gene editing for various cell engineering use cases. Reduction in translocation rate was seen in as early as 2-hour sequentially edited T cells, and reached full chromosomal repair and elimination of translocation after 24-hour DSB repair. In 2- and 6-hour sequential groups, we demonstrated the feasibility of generating proliferative, functionally edited T cell populations, emphasizing VECT's superiority over electroporation in preserving proliferative viability. Yet, among 24-hour sequentially edited cells, viability was significantly lower. This could be attributed to membrane vulnerability at this stage of T cell activation. Further optimization of the different timepoints may be needed. As another study indicated, 48-hour activated T cells had a much lower rupture strain [1]. Further investigation of membrane recovery and cytoskeleton repair should provide insight into ways to improve cell viability among 24-hour sequentially edited T cells.

An important application of sequential editing could be the processing of unstimulated T cells. We reason that if cells remain unstimulated without change in size or mechanics, then we wouldn't need to reoptimize device designs. Although we produced highly efficient delivery with rigid epoxy devices among unstimulated T cells, results led to poor proliferative capacity. Yet, we believed this was due to negative impact of cryopreservation on cell membrane integrity and further optimization of device conditions can address this deficiency. Established studies pointed out cryopreservation and thaw caused osmotic stress or ice formation that damaged the cell membrane integrity [2]. We also found out switching to T cells from

fresh blood resulted in significant viability improvement, setting a standard for cell source for the future application of VECT in naïve T cell engineering.

### *6.1.3 Aim 3: Contributions of Fluid and Cell Mechanics to Mechanoporation Delivery*

Under this aim, we highlighted the significant impact of device features, particularly the presence of gutters, on critical fluid factors and subsequent delivery efficiency. Removal of gutters led to higher delivery rates, prompting an exploration of fluid forces in delivery mechanisms. High-speed video analysis revealed distinct differences in cell velocities between devices with and without gutters, indicating altered fluid dynamics. Further investigation showed that gutter devices exhibited slower compression rates and low acceleration before impacting the ridge. To understand the contribution of compression rate and inertial force to delivery, dextran delivery efficiency was tested under various conditions. Multivariate regression analysis highlighted the combined influence of compression rate and acceleration on delivery efficiency. However, it was noted that the high acceleration led to decreased cell viability, emphasizing the need to balance delivery optimization with cell health considerations.

Next, we sought to understand changes in cells mechanics for different compression rates. We observed an increase in cell stiffness with higher compression rates. Additionally, faster compression rates were associated with faster cell relaxation rates, affecting volume recovery post-compression.

Building upon observations of cell stiffening under rapid compression, we then studied the relationship between cell stiffness and delivery efficiency. Stiffer cells

were found to exhibit higher delivery efficiency, highlighting the importance of cell biomechanics in determining delivery outcomes. Furthermore, post-activation changes in cell stiffness were observed among T cells, suggesting a potential role in modulating delivery efficiency over time. Overall, these findings underscore the significance of fluid mechanics and biomechanics in optimizing delivery strategies and improving delivery outcomes. Most importantly, this is the first documented biomarker to be correlated to mechanoporation outcome.

## **6.2 Continuing and Future Work**

The findings of this research have inspired a number of interesting research questions regarding the application and mechanism of cell VECT. As a continuation of this thesis work, we here propose multiple projects to answer these questions.

### *6.2.1 Long-term cell persistence and repeated challenge assay in sequentially edited T cells*

In this study, while both CD5-edited and sequential edited CAR T-cell therapies have been proven to be effective at eliminating target cancer cells in short-term cytotoxicity assessment, they potentially face a challenge in long-term persistence and repeated antigen challenges. For many CAR T and TCR T cell product, cells show rapid exhaustion and loss in memory phenotype after repeated antigen exposure and prolonged culture [3, 4]. In studies regarding impact of translocation on T cell persistence, they showed decreased translocation population over months after infusion to patients, and was hypothesized to be related to low persistence of multi-gene edited T cells [5]. This decrease takes weeks to months of exposure to antigen to

manifest. In the current study, we assessed the killing efficiency after a target cell exposure. This might not exert enough stress on T cells to initiate the elimination of populations carrying high translocation burden. Hence, we propose to study cell persistence and memory phenotype, comparing batch- and sequential-edited cells, after 1 to 2 weeks of repeated cancer cell challenge [6]. Not only should researchers look at the cytotoxicity, but they should also study how translocation and reduced translocation affect key gene expression, and correlate this differential gene expression to cell memory phenotype and translocation occurrence.

More importantly, sequentially knockout T cells should be tested in a *in vivo* tumor model for assessment of persistence *in vivo*. It has been shown that HLA-A-D deficient T cells could be recognized and cleared by NK cells. Therefore, choosing a mouse model with a humanized immune system can offer a systemic assessment of sequentially double KO cells in terms of their persistence under NK cell surveillance. Strategies to mitigate NK cell clearance such as knockin *HLA-E* under the B2M locus should be considered in VECT-based manufacturing of allogenic T cell product.

### *6.2.2 Gene editing homogeneity by VECT*

We have briefly mentioned the genotype heterogeneity in multiplexed gene editing by non-stochastic method. As we hypothesized that VECT relies on mechanics to delivery all types of cargo uniformly into the same cells, we believe VECT can be used to improve the homogeneity of editing outcome. In future studies where 3 or more genes are targeted, we should assess the homogeneity of editing with multicolor flow cytometry, and carefully gate all possible combination of knockout groups.

Homogeneity will be assessed by conducting Bayesian statistics, comparing to knockout efficiency calculated from multiple random independent single knockout probabilities. Since populations are likely more heterogenous for gene knockout above 3, we will consider conducting chromosomal translocation analysis on FACS sorted pure populations from each run to reduce the difficulties of multiplexed PCR.

### *6.2.3 Mechanistic study on cell death by VECT*

Under certain conditions, VECT devices fell short at preserving high cell viability. In this study, we identified a few external factors such as cell cryopreservation status and stage of cell activation. We also found a fluid mechanics property, including acceleration, to negatively alter viability. The mechanism behind cell damage due to high acceleration, or on day 2 post activation, or after sequential editing with 24-hour DSB repair time remain unclear. Abundant studies using RNA-seq, single cell seq, and metabolite analysis converged on T cell oxidative metabolism and healthy functions of the mitochondria [7-10]. Therefore, future studies on cell death post-VECT should also incorporate dysfunctional mitochondria and oxidative metabolism as a mechanism of cell damage.

### *6.2.4 Application in naïve/unstimulated T cell gene editing*

Gene editing in unstimulated T cells prior to transduction [11] was shown to reduce translocation rate compared with editing in activated T cells. The mechanism remains unknown. The finding motivated the ongoing study to apply VECT to unstimulated T cells for both sequential gene editing as well as virus-free transduction.

It is known that mechanical forces exerted to the nucleus directly change gene organization and gene accessibility [12]. Cells that undergo compression tend to downregulate histone trimethylation, a marker of inaccessible genes. Hence, we hypothesize under optimal condition, VECT can greatly increase gene editing and vector or plasmid integration rate by the mechanical regulation of epigenetic factors. Whether VECT exerts the same effect remains to be confirmed. Single-cell level studies such as ATAC-seq should be conducted on VECT-treated naïve T cells to probe gene accessibility and transgene integration rate [13]. If VECT is shown to increase gene accessibility and transgene integration, then it can replace viral vector as the primary method to engineer naïve T cells at a significantly lower cost.

#### *6.2.5 Study of T cell mechanics at fast strain rate and acceleration regime*

Mechanics study in this thesis was only done in AFM, limiting out strain rate to 50  $\mu\text{m/s}$ , However, cells in microfluidic devices experience 3-4 orders-of-magnitude faster strain rate. At different strain rate values, different parts of the cells play the determining role of mechanics. At lower strain rate, cell cytoskeletal cortex dominates cell deformation response; at higher strain rate, the viscoelastic cytosol becomes the major driver of deformation response [14, 15]. This suggests the AFM data has discrepancies from the actual cell mechanics under rapid compression. In addition, AFM only provides a normal force on cells by compressing in the vertical direction alone. The actual forces exerted on cells in VECT devices are from two directions: normal compression and tensile impact. A micropipette aspiration experiment is a better mimic of the force cells experience in VECT. But it'd require high pressure gradient to achieve the same deformation rate as in VECT. What's more, most of the

instruments measuring deformability or stiffness do not incorporate or cannot precisely control acceleration. Thus, future studies should test the combined effect of acceleration and compression rate on cell mechanics. Ongoing work in the Sulchek lab includes developing a microfluidic device that accurately reflect all forces cells experience in VECT devices. This device will provide more insight into explaining the three regimes for improving delivery identified in this thesis.

### **6.3 Conclusions**

In this comprehensive study, we identified CDEs for VECT devices, optimized Cas9 delivery for single and for sequential gene editing of CAR T cells, proved compatibility of VECT with CAR T manufacturing processes, and explored fluid mechanics and cell mechanics as drivers of variation in delivery outcome. We developed a reliable fabrication method and made robust devices suitable for CDE identification. Our understanding in device design and operational factors guided our workflow design for single gene editing and sequential gene editing in primary T cells. We achieved consistent and efficient knockout to primary T cells with superior cell yield than electroporation, demonstrated VECT devices were more suitable for T cell manufacturing pipelines. Because of the low impact on T cell physiology, VECT could be used to sequentially introduce multiple gene knockout. We proved that sequential gene editing indeed lowered chromosome translocation and potentially improved cytotoxicity. Finally, differences in knockout among healthy and patient cells, as well as among T cells at various stages post activation, prompted us to elucidate the contributions of fluid mechanics and biomechanics to delivery optimization. Our finding suggested an energy accumulation theory to drive

convective delivery. Together, this study showed the possibility of incorporating VECT in industrial manufacturing of multiplex gene edited CAR T and TCR T cells, and to consider cell mechanics during mechanoporation device design.

#### 6.4 References

- [1] Ghassemi, S., et al., Reducing Ex Vivo Culture Improves the Antileukemic Activity of Chimeric Antigen Receptor (CAR) T Cells. *Cancer Immunology Research*, 2018. 6(9): p. 1100-1109.
- [2] Ghassemi, S., et al., Rapid manufacturing of non-activated potent CAR T cells. *Nat Biomed Eng*, 2022. 6(2): p. 118-128.
- [3] Du, M., et al., Biomechanical properties of human T cells in the process of activation based on diametric compression by micromanipulation. *Med Eng Phys*, 2017. 40: p. 20-27.
- [4] Murray, K.A. and M.I. Gibson, Chemical approaches to cryopreservation. *Nature Reviews Chemistry*, 2022. 6(8): p. 579-593.
- [5] Odorizzi, P.M., et al., Genetic absence of PD-1 promotes accumulation of terminally differentiated exhausted CD8(+) T cells. *Journal of Experimental Medicine*, 2015. 212(7): p. 1125-1137.
- [6] Stadtmauer, E.A., et al., CRISPR-engineered T cells in patients with refractory cancer. *Science*, 2020.
- [7] Wei, J.S., et al., PD-1 silencing impairs the anti-tumor function of chimeric antigen receptor modified T cells by inhibiting proliferation activity. *Journal for Immunotherapy of Cancer*, 2019. 7(1).
- [8] Scharping, N.E., et al., The Tumor Microenvironment Represses T Cell Mitochondrial Biogenesis to Drive Intratumoral T Cell Metabolic Insufficiency and Dysfunction. *Immunity*, 2016. 45(2): p. 374-88.
- [9] Zhang, L., et al., Mitochondria dysfunction in CD8+T cells as an important contributing factor for cancer development and a potential target for cancer treatment: a review. *Journal of Experimental & Clinical Cancer Research*, 2022. 41(1).
- [10] Wu, H., et al., Mitochondrial dysfunction promotes the transition of precursor to terminally exhausted T cells through HIF-1 $\alpha$ -mediated glycolytic reprogramming. *Nature Communications*, 2023. 14(1).

- [11] Fraietta, J.A., et al., Determinants of response and resistance to CD19 chimeric antigen receptor (CAR) T cell therapy of chronic lymphocytic leukemia. *Nature Medicine*, 2018. 24(5): p. 563-+.
- [12] Tsuchida, C.A., et al., Mitigation of chromosome loss in clinical CRISPR-Cas9-engineered T cells. *bioRxiv*, 2023.
- [13] Song, Y., et al., Transient nuclear deformation primes epigenetic state and promotes cell reprogramming. *Nat Mater*, 2022. 21(10): p. 1191-1199.
- [14] Wang, W., et al., Joint profiling of chromatin accessibility and CAR-T integration site analysis at population and single-cell levels. *Proc Natl Acad Sci U S A*, 2020. 117(10): p. 5442-5452.
- [15] Urbanska, M., et al., A comparison of microfluidic methods for high-throughput cell deformability measurements. *Nat Methods*, 2020. 17(6): p. 587-593.
- [16] Gossett, D.R., et al., Hydrodynamic stretching of single cells for large population mechanical phenotyping. *Proc Natl Acad Sci U S A*, 2012. 109(20): p. 7630-5.